Integration of signalling in smooth muscle caveolae

Shakirova, Yulia

2010

Integration of signalling in smooth muscle caveolae

Yulia Shakirova

LUND UNIVERSITY
Faculty of Medicine

Academic dissertation

Bye due permission of the Faculty of Medicine, Lund University, Sweden. To be defended at Segerfalksalen, Biomedical Center, Sölvegatan 19, Thursday 9th of December 2010 at 09:00 for the degree of Doctor of Philosophy, Faculty of Medicine.

Faculty opponent: Dr. Ralph Peeker, Sahlgrenska University Hospital, University of Gothenburg

Organization	Document name
LUND UNIVERSITY	DOCTORAL DISSERTATION
Department of Experimental Medical Science	Date of issue 2010-10-20
	Sponsoring organization

Author(s)
Yulia Shakirova

Title and subtitle

Integration of signalling in smooth muscle caveolae

Abstract

Abstract

Caveolae and lipid rafts are plasma membrane microdomains that are considered to play a role in cellular signalling. Caveolins and cavins as well as cholesterol are required for the structure and function of caveolae. The papers summarized in this thesis examine the role of caveolae in smooth muscle function.

Ca2+ sensitization is a contractile process depending on inhibition of myosin phosphatase activity. Here I test whether protein kinase C and Rho-associated kinase-mediated Ca2+ sensitization depends on caveolae using gene disrupted (KO) mice. While the process of Ca2+-sensitization was unaffected by lack of caveolae in the intestine, •alpha-adrenergic and protein kinase C-mediated arterial contraction was increased. Arteries lacking caveolae weighed more per unit length, suggesting growth of the wall. I go on to demonstrate that small resistance arteries from KO mice are remodelled, and that these and other changes counterbalance an excessive NO production to normalize blood pressure in caveolin-1 deficient mice.

NO production is required for initiating and maintaining penile erection. Surprisingly, nerve-induced relaxation and relaxation in response carbachol and sodium nitroprusside was impaired in caveolae-deficient corpus cavernosum.

In the last two papers, I examine the role of caveolae in detrusor function. Disruption of caveolae using desorption of cholesterol was first shown to impair contraction of human bladder strips in response to muscarinic receptor activation. I then demonstrate that the membrane density of caveolae increases after bladder outlet obstruction in the rat. The latter effect was due to crowding of the same relative number of caveolin molecules on a smaller relative membrane area.

In conclusion, a considerable body of evidence has been gathered that demonstrate an important and pleiotropic physiological and pathophysiological role of caveolae in smooth muscle.

Key words: Caveola, caveolin, cavin, smooth muscle, smooth muscle contractility, remodelling, NO, vascular dysfunction, erectile dysfunction, detrusor

Classification system and/or index termes (if any):

Supplementary bibliographical information:		Language English
ISSN and key title: 1652-8220		ISBN 978-91-86671-27-3
Recipient's notes	Number of pages 114	Price
	Security classification	

Integration of signalling in smooth muscle caveolae

Yulia Shakirova

LUND UNIVERSITY
Faculty of Medicine

Department of Experimental Medical Science
Lund University
2010

Yulia Shakirova
Department of Experimental Medical Science
Lund University
BMC D12
221 84 Lund
Sweden
Yulia.Shakirova@med.lu.se

Cover image
Electron micrograph of bladder smooth muscle cells from C57Bl/6 mice. Characteristic flask shaped caveolae structures at the plasma membrane are separated by dense bands.

Lund University, Faculty of Medicine Doctoral Dissertation Series 2010:111
ISSN 1652-8220
ISBN 978-91-86671-27-3

Printed by Media-Tryck, Lund University, Sweden

The Answer to the Great Question…Of Life, the Universe and Everything …Is…Forty-two.

To my little hobbits

Table of Contents

List of Papers

I. Shakirova Y, Bonnevier J, Albinsson S, Adner M, Rippe B, Broman J, Arner A, Swärd K. **Increased Rho activation and PKC-mediated smooth muscle contractility in the absence of caveolin-1**. *Am J Physiol Cell Physiol.* 2006; 291(6):C1326-35.

II. Albinsson S*, **Shakirova Y***, Rippe A, Baumgarten M, Rosengren BI, Rippe C, Hallmann R, Hellstrand P, Rippe B, Swärd K. **Arterial remodelling and plasma volume expansion in caveolin-1 deficient mice**. *Am J Physiol Regul Integr Comp Physiol.* 2007; 293 (3):R1222-31. *These authors contributed equally.

III. Shakirova Y, Hedlund P, Swärd K. **Impaired nerve-mediated relaxation of penile tissue from caveolin-1 deficient mice**. *Eur J Pharmacol.* 2009; 602(2-3):399-405.

IV. Shakirova Y, Mori M, Ekman M, Erjefält J, Uvelius B, Swärd K. **Human urinary bladder smooth muscle is dependent on membrane cholesterol for cholinergic activation**. Eur J Pharmacol. 2010; 634(1-3):142-8.

V. Shakirova Y, Swärd K, Uvelius B, Ekman M. **Functional and biochemical correlates of an increased membrane density of caveolae in hypertrophic rat urinary bladder.** *Eur J Pharmacol. 2010 Sep 22. [Epub ahead of print]*

Abreviations and Drugs

CIRAZOLINE	α_1-adrenergic agonist
ET_1	endothelin-1
EGFR	epidermal growth factor receptor
eNOS	endothelial nitric oxide synthase
ER	endoplasmic reticulum
GPCR	G protein-coupled receptor
IR	insulin receptor
LGMD	limb-girdle muscular dystrophy
MβCD	methyl-β-cyclodextrin
MLCK	myosin light chain kinase
NO	nitric oxide
PKC	protein kinase C
ROK	Rho-kinase; a.k.a. Rho-associated coiled-coil kinase (ROCK)
RTK	receptor tyrosine kinase
SNP	sodium nitroprusside
SR	sarcoplasmic reticulum
SOC	store operated Ca^{2+} channel
VEGFR	vascular endothelial growth factor receptor

Background

Introduction to caveolae

Electron microscopic images of cell membranes reveal high densities of flask shaped invaginations with a size ranging from 50 to 100 nm in certain cells: most notably adipocytes, endothelial cells, and muscle cells. These structures have been named caveolae, from the Latin word for "small cavities". Caveolae are clathrin-free, cholesterol and sphingolipid-enriched microdomains that were first discovered by George Palade and Ken Yamada in 1950s (Palade 1953, Yamada 1955). The characteristic invaginated structure of caveolae is stabilized by proteins from the caveolin and cavin families. One caveola is considered to be generated as a membrane platform of 144 caveolin molecules (Pelkmans and Zerial, 2005) and up to 20 000 molecules of cholesterol (Ortegern et al 2004). Such platforms are assembled in the Golgi apparatus and transported *en bloc* to the plasma membrane (Hayer et al 2010). At the plasma membrane, cavins dock onto the platform (Hansen et al 2009, Hayer et al 2010). Caveolin-1 or -3 and cavin-1 and -2 are required for formation of caveolae and genetic ablation of caveolin-1, and -3, and cavin-1, respectively, causes loss of caveolae in fat, endothelia and smooth muscle (caveolin-1), skeletal muscle and heart (caveolin-3), and globally in all tissues (cavin-1) (Hnasko and Lisanti 2003, Liu et al 2009).

The caveolae-stabilizing proteins

The caveolins

There are three members of the caveolin protein family: caveolin-1, caveolin-2 and caveolin-3. In the nineteennineties two independent research teams were interested in the same small membrane-bound protein. Glenny et al had identified a 22-kDa protein as being tyrosine-phosphorylated upon infection with Rous sarcoma virus (Glenney et al 1989) and later demonstrated, using specific antibodies, that the protein was associated with the cytoplasmic surface of caveolae (Rothberg et al 1992). In parallel, Kurchalia et al (1992) described a 21-kDa membrane protein as a component of detergent-insoluble complexes derived from exocytic vesicles of epithelial cells. Cloning and sequencing showed that the proteins were identical to one another. And so, the first marker for caveolae, called caveolin or VIP21 and later caveolin-1, made its entrance.

Two isoforms of caveolin-1 (α and β) exist. The α and β isoforms are derived from different mRNAs (Fujimoto et al 2000) and have different N-termini. The α-isoform consists of residues 1-178 and the β-isoform of residues 31-178. Electron microscopic examination of isolated recombinant caveolae suggests that both α and β-isoforms of caveolin-1 give rise to morphologically similar caveolae, and the exact functional difference between the isoforms remains uncertain. Some studies suggest that caveolin-1α drives caveola biogenesis more efficiently than the β-isoform (Fujimoto et al 2000, Scherer et al 1995). A highly conserved part of caveolin-1, residues 68 to 75, known as the caveolin-signature domain, appears to be involved in trafficking of caveolin molecules to cholesterol-rich membranes (Machleidt et al 2000). The cytosolic domain of caveolin-1 including residues 82-101 directly interacts with signalling proteins harbouring the amino acid motifs ΦXΦXXXXΦ, ΦXXXXΦXXΦ, or ΦXΦXXXXΦXXΦ (where Φ = Trp, Phe, or Tyr, and X represents any amino acid) and is therefore referred to as the caveolin-scaffolding domain (Li et al 1996). Caveolin-1 is the first membrane protein described to bind cholesterol (Murata et al 1995).

Human caveolin-2 is 38% identical and 58% similar to human caveolin-1 (Scherer et al 1995). It lacks the N-terminus of caveolin-1, and three distinct isoforms have been identified: full-length caveolin-2α, and two truncated variants, caveolin-2β and caveolin-2γ (Kogo et al 2002). When expressed alone caveolin-2 does stimulate the formation of caveolae and does not reach beyond the Golgi complex where it accumulates in the absence of caveolin-1 (Mora et al 1999). Full length caveolin-1 and its membrane-spanning domain (residues 102–132) facilitate formation of >150 kDa large mixed complexes consisting of 7-14 caveolin molecules (Das et al 1999). Typically, the ratio of caveolin-1 to caveolin-2 in such complexes is 2:1 or 4:1 (Scheiffele et al 1998).

Caveolin-3 is 65% identical and 85% similar to caveolin-1. It is the smallest protein in the family and its tissue distribution more restricted (Tang et al 1996, Way et al 1995). Caveolin-3 is found primarily in striated muscle. Limited expression is seen in smooth muscles of certain vascular beds and in the intestine and urinary bladder.

Caveolins undergo changes at the post-translational stage via palmitoylation. Covalent binding of palmitate to the cytoplasmic carboxyl-terminus of caveolin proteins secures caveolin oligomer stability and hydrophobicity (Monier et al 1996). Palmitoylation occurs on three cystein residues (Dietzen et al 1995)

The cavins

The cavins were not formally grouped as a protein family until 2009 when Bastiani et al (2009) introduced the current nomenclature and demonstrated that these proteins are related and that they co-localize in caveolae. The cavins include Polymerase I and Transcript Release Factor (PTRF, cavin-1), Serum Deprivation Response protein (SDR, cavin-2), SDR-Related protein Binding C-kinase (SRBC, cavin-3), and, finally, Muscle-Restricted Coiled-coil protein (MURC, cavin-4).

Cavin-1 originally got its name (Polymerase I and transcript release factor) because it was identified as a nuclear factor required for the termination of transcription of RNA

(Jansa et al 1998). The first indication that cavin-1 resides in caveolae was obtained in Vinten's laboratory in Copenhagen. Vinten and his collaborators raised monoclonal antibodies against immunopurified caveolae. One of these antibodies bound to a 60 kDa protein that was exclusively localized in caveolae as shown using immuno-electron microscopy of plasma membrane sheets (Vinten et al 2001). The group was unable to sequence the protein until much later (Vinten et al 2005) when it was shown that the protein was identical to cavin-1. An independent study from 2004 by Aboulaich et al demonstrated that a major part of cellular cavin-1 (75-80%) is confined to caveolae.
Cavin -2 is a ~70 kDa protein that is 20 % identical with cavin-1. It plays a direct role in caveola biogenesis through recruitment of cavin-1 to plasma membrane caveolae. HeLa cell lines transfected with short hairpin RNAs specific to different regions of the cavin-2 mRNA lose cavin-1, caveolin-1 and caveolae. Overexpression of cavin-2 affects the morphology of caveolae and leads to extensive membrane tabulation arguing for involvement of cavin-2 in membrane bending. Such tubules stain positive for caveolin-1, suggesting that the classical view of caveolae as static vesicles is oversimplified. Introduction of cavin-2 as a putative curvature-inducer is a step forward in the understanding of how caveolae may act in endocytosis (Hansen et al 2009).

Cavin-3 is a ~45 kDa protein composed of 412-amino-acid module containing a LZ-domain, a PKCδ binding site, a PKC phosphorylation site, and a phosphatidylserine-binding site. Cavin-3 is localized in caveolae and is coexpressed with caveolin-1 in blood vessels, lung, heart and connective tissue. Targeting of cavin-3 to caveolae depends both on caveolin-1. When the expression of caveolin-1 is reduced using siRNA a dramatic decline in cavin-3 levels is seen, but not vice versa. Cavin-3 has been suggested to regulate microtubule-dependent trafficking of so called cavicles, intracellular caveolae, to centrosomes (MacMahon et al 2009).

Cavin-4 is a ~43 kDa skeletal and cardiac muscle-specific protein. Interestingly, cavin-4 is more likely to have independent cellular functions than other cavins as its expression is not as profoundly affected by the absence of caveolin-1 or cavin-1 (Bastiani et al 2009). In cardiac myocytes cavin-4 plays a role in Rho/ROCK activation and hence myofibrillar organization (Ogata et al 2008).

Biogenesis of caveolae

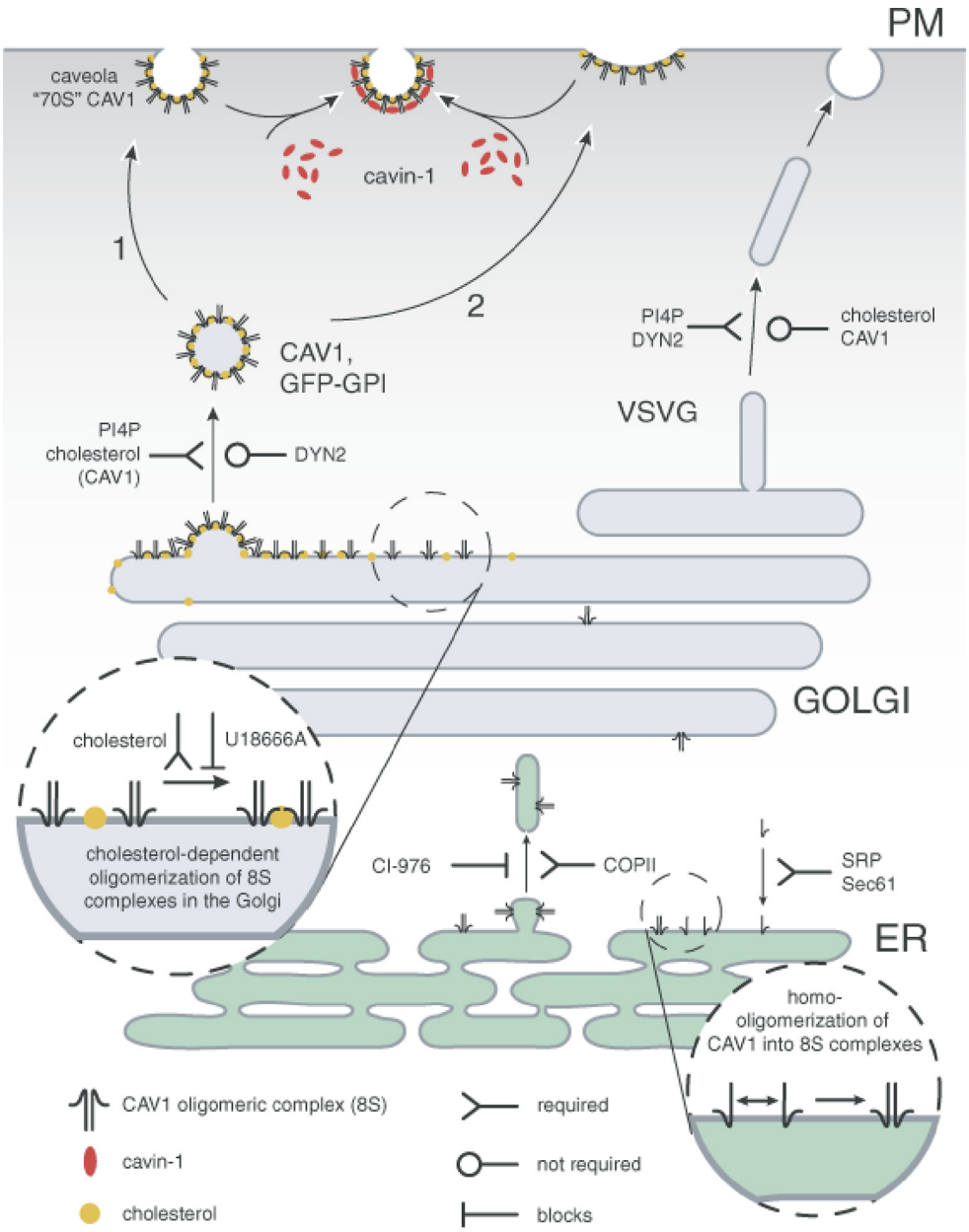

Figure 1. Caveolae assembly and biosynthetic traffic of caveolin-1 as proposed by Hayer et al. (2010). Caveolin-1 (CAV1) is transported from the endoplasmic reticulum (ER) through Golgi where it undergoes lipid dependent oligomerization prior to domain budding and transport to the membrane. Two alternative models for how cavin-1 partakes in caveola assembly exist. In model (1), formation is not induced but stabilized by cavin-1. In model (2), cavin-1 induces membrane curvature of flat CAV1 domains in the membrane. Reproduced with permission from Copyright clearance center (doi:10.1111/j.1600-0854.2009.01023.x.)

According to a recent model, assembly of caveolae starts in the endoplasmic reticulum where newly synthesized caveolins coalesce into small complexes and concentrate at ER exit sites (Figure 1). A diacidic (DXE) motif proximal to the caveolin signature domain mediates fast accumulation of highly mobile caveolin complexes at these ER sites. Mutation in the ER exit domain causes a delay in export of proteins to the Golgi complex (Hayer et al 2010). In a medial Golgi compartment, caveolins bind cholesterol, form even larger complexes and lose their diffusional mobility (Hayer et al 2010). Cholesterol is required for formation of stable supramolecular caveolin complexes but not for transport of caveolin-1 to the plasma membrane. Newly built large caveolin scaffolds undergo transportation to, and later insertion into, the plasma membrane. Cavin-1 is associated with plasma membrane caveolae but not with the Golgi pool of caveolin-1. It is diffusely distributed in a cytosol in multimeric complexes with other cavin proteins where one individual complex can contain up to 80 cavins. Cavin-1 is seldom associated with intracellular vesicles or organelles and is recruited to the cell membrane after arrival of the caveolin-1 platforms to the cell surface (Hayer et al 2010).

After its appearance on the plasma membrane, the caveolae can undergo further transformation. Caveolae can detach from the membrane and form endocytic vesicles called cavicles (Mundy et al 2002). Cavicles can carry cargo, for example a SV40 virus, to specialized endosomes called caveosomes (Pelkmans et al 2001) or proceed into recycling endosomes (Mundy et al 2002). Cavicle movement to these sites is microtubule dependent. Recent studies suggest that individual caveolae are engaged in continuous rounds of fission and fusion at the cell surface (Pelkmans and Zerial, 2005). The large majority of studies on endocytosis of caveolae have exploited cultured cells, and it remains uncertain to what extent trafficking of caveolae plays a role in highly differentiated cells such as smooth muscle cells. Indeed, evidence available from smooth muscle seem to suggest that caveolae are rather static structures, and in many cases their arrangement at the cells surface has a striking symmetry, with rows of caveolae separated by dense bands (e.g. Gabella and Blundell 1978; Fig 2).

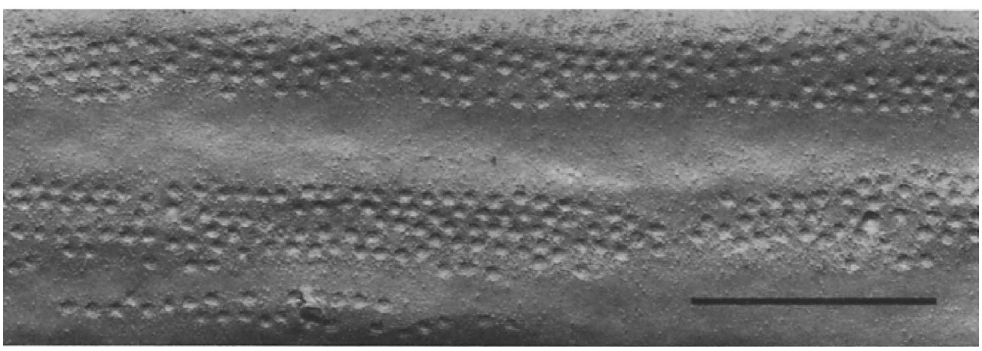

Figure 2. Electron microscopic image of freeze fractured plasma membrane of smooth muscle cell. Caveolae are fractured at their necks. The ordered rows of caveolae are separated by dense bands. Bar: 1 μm. Reproduced with permission from Copyright clearance center (Gabella and Blundell 1978, DOI: 10.1007/BF00218174).

Lipid composition of caveolae

Recently, caveolae have been proposed to represent a cellular lipid storage compartment as an alternative to lipid droplets (Parton and Simons 2007). Caveolae are enriched with free cholesterol, sphingolipids, ceramide and phosphatidylinositol diphosphate (Brown et al 1992; Pike et al 1996; Liu et al 1995, Ortegren et al 2004). Cholesterol plays a particularly important role for caveolae and after its depletion with pharmacological agents caveolae disappear (Dreja et al 2002). Cells specialized in lipid storage, such as adipocytes, are highly populated by caveolae (Ortegen et al 2004). Moreover, upon overexpression of caveolin-1, cells with low basal caveolin levels demonstrate increased fatty acid uptake and cholesterol transport (Meshulan et al 2006, Fu et al 2004, Feilding et al 2001). Consistent with the idea that caveolae constitute a lipid storage compartment, truncation of caveolin causes a decrease in surface levels of free cholesterol and increased storage of neutral lipids in lipid droplets (Pol et al 2001, Pol et al 2004).

Caveolae-associated signalling

Caveolae, as described above, are very different from the rest of the plasma membrane with regard to the protein and lipid composition. Moreover, a number of receptors and signalling molecules favour the environment in caveolae due either to their physicochemical properties or because they have so called caveolin-binding motifs in their primary sequence (Couet et al 1997, Li et al 1996). The overall concept that signalling molecules are enriched within caveolae and that this is important for their function has been referred to as the "caveolae signalling hypothesis" (Lisanti 1994). In this section the aim is to provide an overview of those signalling proteins for which evidence exists that they are associated with caveolae. A widely used method for studying the membrane distribution of signalling proteins is sucrose density fractionation. This method allows for purification of "rafts" or "detergent resistant membranes", i.e. membrane microdomains that resist the detergent Triton X-100 at 4 °C and that have a density that makes them float on 35% sucrose. While such membrane preparations invariably contain the majority of cellular caveolin-1, it is important to keep in mind that raft membranes do not equal caveolae. On the other hand, signalling proteins not recovered in rafts are not likely caveolae-associated.

G proteins and G protein-coupled receptors: Using quantitative proteomics Foster et al identified over 700 proteins in lipid rafts/caveolae (Foster et al 2003). Among the 241 proteins of those selected as authentic raft/caveolae proteins were numerous G protein subunits. Caveolin directly interacts with heterotrimeric G-proteins (Wyse et al 2003) in a manner that helps maintain Gα-proteins in an inactive, GDP-bound state (Couet et al. 1997; Li et al 1995, 1996; Murthy and Makhlouf 2000). Receptors that interact with G proteins are known as G protein-coupled receptors (GPCRs). Cholesterol plays

a role in stabilizing the conformation of specific GPCRs (Ruprecht et al. 2004, Albert and Boesze-Battaglia 2005). For example cholesterol plays a direct role in regulating the structural conformation of β_2-adrenergic receptor by influencing dimer formation (Cherezov et al. 2007). GPCRs, such as β-adrenergic receptor (β-AR), endothelin receptors (ET_A) and muscarinic receptors, all have caveolin-binding motifs in their primary sequence. These receptors have also been demonstrated to reside in or to translocate to caveolae (Rapacciuolo et al 2003, Okamoto et al 2000, Ostrom et al 2002, Feron et al 1997). Other G-protein coupled receptors that may be operating in caveolae are bradykinin receptors, adenosine A_1-receptor, the angiotensin II receptor type-1 and serotonin receptors (Patel et al 2008).

Tyrosine-kinase receptors: Growth factor receptors that belong to the receptor tyrosine kinase (RTK) family play a critical role in development and homeostasis. These receptors include vascular endothelial growth factor receptor (VEGFR), epidermal growth factor receptor (EGFR), fibroblast growth factor receptor (FGFR), platelet-derived growth factor receptor (PDGFR), insulin receptor (IR), and insulin like growth factor receptor (IGFR). The activity of RTKs can be modulated by caveolae, but the possibility also exists that some of these receptors traffic via caveolae. Many growth factor receptors carry the amino acid sequence motif that binds to the scaffolding domain of caveolin-1 (Couet et al 1997, Yomamoto et al 1999), and several RTKs have been shown to be caveolae-associated by e.g. sucrose gradient fractionation. For example, the localization of VEGFR-2 to endothelial caveolae was reported to be critical for interaction of the receptor with downstream mediators (Labercque et al 2003). It was further proposed that caveolin-1 negatively regulates VEGFR-2 keeping it in an inactive state and that ligand binding dissolved the caveolin-1 complex allowing for full ligand-dependent activation and low ligand-independent activity (Labrecque et al 2003). Similar to VEGFR-2, the EGFR is found in raft preparations made from human fibroblast in up to hundred-fold higher concentration than in the rest of the plasma membrane (Smart et al 1995). EGFR resides in caveolae in the inactive state and translocate elsewhere after ligand binding (Mineo et al 1999). Moreover, PDGFR are concentrated in caveolae together with a number of signalling molecules required for activation of mitogen-activated kinases (Liu et al 1996, Liu et al 1997).

Immunogold electron microscopy and immunofluorescence microscopy experiments have demonstrated insulin receptors (IRs) in caveolae (Gustavsson et al 1999, Smith et al 1998, Parpal et al 2001). In addition, downstream signaling molecules, including IRS-1, Shc, GRB-2, SOS, Syp, PI3-kinase, were also found in caveolae fractions, and stimulation of cells with insulin increased the content and tyrosine phosphorylation of these molecules in caveolae (Smith et al 1998). IRs directly bind to the scaffolding domain of caveolin-1 and -3 increasing the activity of IR kinase domain (Yomamoto et al 1998). In keeping with a role of caveolae in insulin signaling, adipocytes from caveolin-1 knockout mice exhibit decreased IR phosphorylation and reduced stability of the IR protein (Cohen et al. 2003). Moreover, genetic ablation of caveolin-3 leads to perturbed IR signaling in skeletal muscle (Oshikawa et al 2004).

Membrane channels and transporters: Nearly four decades ago caveolae were suggested to play a role in Ca^{2+} signalling. The first indication in this direction was electron microscopic images of muscle cells where the endoplasmic reticulum (ER) was found in a close proximity to caveolae (Gabella 1971) and X-ray spectral analysis showing a Ca^{2+} -peak in the caveola compartment (Meyer et al 1982). In 1992 Fujimoto and colleagues found an inositol 1,4,5-trisphosphate receptor-like protein in caveolae. Evidently, this protein resides on the ER membrane, and the work by Fujimoto et al must be interpreted to indicate a close proximity between ER Ca^{2+}-release sites and the plasma membrane which indirectly gates these channels. Work by the same group demonstrated that the membrane Ca^{2+}-ATPase is primarily localized in caveolae of endothelial cells, smooth muscle cells, cardiomyocytes, epidermal keratinocytes and mesothelial cells (Fujimoto et al 1992, Fujimoto et al 1993).

Ca^{2+} entry in response to depletion of ER Ca^{2+} stores is mediated by store operated Ca^{2+} channels (SOC). Candidate proteins for such channels include transit receptor potential channels (TRPC) and Orais (Feske et al 2006, Beech 2005). All functional mammalian TRPC proteins have putative caveolin-1 binding domains at both their N and C termini. TRPC1 and TRPC4 channels are involved in store operated Ca^{2+} entry and are considered to be located in caveolar microdomains (Lockwich et al 2000, Bergdahl et al 2003, Brownlow and Sage 2005, Murata et al 2007). The N-terminus of TRPC1 interacts with caveolin-1, keeping it in an inactive state (Brazer et al 2003). Interestingly TRPC1 and thus SOCE can be further regulated by STIM1, a transmembrane protein whose binding domain in TRPC1 overlaps with that for caveolin-1 (Pani and Singh 2009).

K^+ channels maintain excitable cells in a resting state serving as key regulators of membrane excitability. A body of work links caveolae and caveolin-1 to diverse K^+-channels. For example the Kv1.5 channel is colocalized with caveolin-1 on the cell surface and follows caveolin-1 after microtubule disruption in L-cells (Martens et al. 2001). Moreover, the K_{ATP} channel subunit Kir 6.1 co-precipitates with caveolin-1 in arterial homogenates and co-localizes with its upstream regulator adenylyl cyclase in caveolin enriched membrane fractions (Sampson et al 2004).

eNOS: Endothelial nitric oxide synthase (eNOS) plays a central role in regulating blood pressure and vascular tone through production of nitric oxide (NO). In endothelial cells the eNOS concentration in rafts is ten-fold higher than in other parts of the cell membrane (Shaul et al 1996). The scaffolding domains in caveolin-1 and caveolin-3 play a physiological role in inhibition of NOS activity serving as a classical example of a caveolin to signalling partner interaction (Feron et al 1998, Feron and Balligand 2006, Venema et al 1997, Garcia-Cardena et al 1997). Ablation of caveolin-1 increases eNOS activity and NO production (Drab et al 2001, Wunderlich et al 2006). Arteries from caveolin-1 knockout mice exhibit decreased steady-state tension and greater relaxation to acetylcholine (Razani et al 2001). Thus caveolin-1 serves two purposes simultaneously, it maintains eNOS in the inactive state and enriches eNOS in caveolae allowing for rapid high fidelity signaling (Sbaa et al 2005).

RhoA and PKC: Activation (neuronal or hormonal) of contraction in smooth muscle is initiated by Ca^{2+} influx into the muscle cells. The increase in Intracellular free ionized calcium leads to the binding of calcium to the 17 kDa EF hand protein calmodulin. Calmodulin with four bound Ca^{2+} ions activates myosin light chain kinase (MLCK), which catalyses the phosphorylation of the 20 kDa regulatory light chains (LC_{20}) of myosin. This in turn initiates a cyclic interaction, the cross-bridge cycle, between the molecular motor myosin and actin which leads to force production and shortening of the smooth muscle cell. Ca^{2+}-dependent activation of MLCK, and the resulting cycling of cross-bridges, represents the textbook view of how the contractile machinery is activated in smooth muscle. Data generated over the last two decades has revealed additional complexity in the activation mechanisms (Somlyo and Somlyo 2003). For example, force can increase or decrease without an associated change in the intracellular Ca^{2+} concentration. The process of force generation independently of the intracellular Ca^{2+} levels is known as calcium sensitization. Ca^{2+} desensitization is mediated by cyclic nucleotides such as cGMP. Upstream mediators of Ca^{2+} sensitization include the monomeric GTPase Rho A, the serine threonine kinase Rho-kinase (ROK or ROCK) and protein kinase C (PKC). These signaling pathways ultimately target the myosin phosphatase leading to reduced phosphatase activity and increased myosin phosphorylation. Interestingly, RhoA, ROK and PKC have all been shown to be associated with caveolae in other cells and tissues, raising the possibility that Ca^{2+} sensitization is caveola-dependent in smooth muscle.

The evidence that RhoA is localized in caveolae comes from studies using endothelial cells (Gingras et al 1998). Using electron microscopy in combination with immunogold labeling Michaely et al (1999) demonstrated that RhoA and caveolin-1 co-localize in the plasma membrane of normal human fibroblasts. Compartmentalization of signaling proteins and lipids in caveolae is moreover required for appropriate regulation of phosphoinositide turnover which precedes PKC activation (Pike and Casey 1996). PKC_{α} binds with high affinity and specificity to a binding site in caveolae membranes that has been identified as cavin-2 (Mineo et al 1998). Interestingly, cavin-3 is known to bind PKCδ directly (McMahon et al 2009). Finally, Rho kinase has been demonstrated to translocate to caveolae in a Ca^{2+}-calmodulin-dependent manner on smooth muscle depolarization. In keeping with a role of caveolae in PKC-mediated contraction, the scaffolding domain of caveolin-1 was reported to impair both membrane translocation of PKC and contraction stimulated by phorbol ester and α-agonist in the ferret aorta (Je et al 2004).

The list of signaling proteins that have been proposed to be associated with caveolae can be made much longer, and the present survey is by no means complete. Additional identified interactions between caveolae and signaling molecules can be found in recent reviews (Bergdahl and Swärd 2004, Lajoie et al 2009, Dart 2010, Balijepalli and Kamp 2008, Insel and Patel 2009, Patel et al 2008, Ostrom and Insel 2004).

The role of caveolae in transcytosis

Albumin transport has been proposed to occur through the endothelial barrier, from the luminal to the abluminal side (Schnitzer et al 1994, Tiruppathi et al 1997) in vesicles originating from caveolae. Caveolin-1 has been envisaged to regulate such vesicle trafficking through the cell by controlling the activity and localization of signalling molecules that mediate vesicle fission, endocytosis, fusion and exocytosis (Minshal and Malik 2006). Gp60, an albumin receptor found in caveolae, has further been proposed to mediate the high affinity binding of albumin in caveolae. Apart from gp60 there are other designated albumin binding-proteins with high affinity to modified or denatured albumin forms. These polypeptides have been considered to target albumin to lysosomal degradation. Conversely, binding of gp60 to albumin rescues it from transfer to an acidic lysosomal compartment (Minshall et al 2000, Vogel et al 2001).

With these facts in mind one would have expected a severe alteration in transcellular trafficking of albumin in caveolin-1 deficient mice. However, transport of albumin and other macromolecules is increased in caveolin-1 knockout mice. This is likely to be a result of increased capillary hydrostatic pressure (Rosengren et al 2006, Grände et al 2009).

Animal models for studying caveolae

Caveolin-1-deficient mice: New possibilities to investigate the role of caveolae in signal transduction appeared with the creation of mice deficient for caveolin-1 (Drab et al 2001, Razani et al 2001). Caveolin-2 was observed to be unstable in the absence of caveolin-1 so caveolin-1-deficient mice essentially represent a double knockout of caveolin-1 and -2 (Razani et al 2001). The caveolin-1-deficient mice were found to develop pulmonary defects, exercise intolerance, resistance to diet induced obesity, abnormalities in vasodilatation, high serum triglyceride levels, defects in glycosylphosphatidylinositol-anchored transport, and so on (Drab et al 2001, Sotgia et al 2002, Razani et al 2001). The list of pathologies is however still expanding.

A number of important questions regarding the phenotypes of caveolin-1 deficient mice remain unresolved. For example, these mice have a normal blood pressure despite increased NO production and they have largely normal endothelial permeability despite compromised trancytosis mechanisms (Rosengren et al 2006). Further studies are therefore required for a deeper understanding of the physiological role of caveolin-1.

Caveolin-2-deficient mice: A line of mice deficient for caveolin-2 has also been generated. In the absence of caveolin-2, caveolin-1 and caveolae still exist. At the moment the only known phenotype of the caveolin-2 deficient mice is that observed in lung tissue, in which hypercellularity and thickened alveolar septa were documented (Razani et al 2002). Tubular aggregate formation in skeletal muscle is common for patients with neuromuscular disorders and such aggregates are found in caveolin-2 deficient mice

(Schubert et al 2007). In vitro experiments with isolated pulmonary endothelial cells from caveolin-2 KO mice have demonstrated that caveolin-2 reduces cell proliferation and cell cycle progression (Xie et al 2010).

Caveolin-3-deficient mice: Caveolin-3 deficient mice (Hagiwara et al 2000, Galbiati et al 2001) lack caveolae in striated muscle as expected from its tissue distribution. Caveolin-3-deficient mice also develop muscular dystrophy, characterized by altered targeting of the dystrophin-glycoprotein complex to lipid raft microdomains and abnormalities in the organization of the T-tubule system. In work by Galbiati and colleagues (Galbiati et al 2001) it was shown that skeletal muscle fibres exhibit deformations similar to those observed in patients with limb-girdle muscular dystrophy (LGMD). In fact, mutations in caveolin-3 underlie LGMD in humans (Minetti et al 1998). Caveolin-3 deficient mice also develop a progressive cardiomyopathy with interstitial and peri-vascular fibrosis (Woodman et al 2002).

Cavin-1-deficient mice: Cavin-1-deficient mice have recently been developed. Liu et al (2008) demonstrated that cavin-1-deficient mice lack caveolae in lung epithelium, intestinal smooth muscle, endothelial cells, and skeletal muscle. Thus, both caveolin-1-driven and caveolin-3-driven caveolae depend on cavin-1. Among the notable phenotypes of the cavin-1-deficient mice were glucose intolerance and hyperinsulinemia. These knockout animals also had dramatically reduced fat mass and reduced levels of circulating adiponectin and leptin, similar to caveolin-1-deficient mice (Liu et al 2008).

Mutations in caveolae proteins in humans

Congenital generalized lipodystrophy (CGL), also known as the Berardinelli-Seip syndrome, was first described by the physicians Berardinelli from Brazil and Seip from Norway (Berardinelli 1954, Seip 1959). Over 250 patients with this disorder have been identified to date. This gives an estimate of 1 affected individual in a population of 10 million (Carg 2004). In some geographical areas that number is considerably higher and reaches ~73 in 10 million (Rego et al 2008). About 95% of individuals with BSCL have been reported to carry mutations in one of two loci: i) chromosome 9q34 encoding 1-acylglycerol-3-phosphate-O-acyltransferase 2 (AGPAT2), an enzyme that catalyzes a key intermediate step in the synthesis of triglycerides and phospholipids, and ii) chromosome 11q13, encoding the protein seipin of unknown function (BSCL2) (Magre et al 2003).

The first case with a mutation in the caveolin-1 gene, affecting the expression of both α and β isoforms, was an individual diagnosed with BSCL (Kim et al 2008). A molecular screen for caveolin-1 mutations in four patients diagnosed with BSCL that were negative for mutations in AGPAT2 and BSCL2 yielded one individual with two mutated caveolin-1-allelels. This patient, a young Brazilian woman, had homozygous mutations in exon 2 of the caveolin-1 gene. She suffered a nearly complete loss of adipose tissue since early childhood, had severe dyslipidemia and insulin resistance. She developed acantosis nigricans, hirsutism, hepatosplenomegali, hypocalcemia, hepatic

steatosis, megaesophagus and primary amenorrhea. She was diagnosed with diabetes mellitus at the age of 13 and she responded poorly to insulin therapy. Her plasma levels of leptin and adiponectin were nearly undetectable. Her height as an adult was 1.46 cm. She had no evidence of cardiomyopathy, pulmonary disease, mental retardation or cancer (Kim et al 2008).

The most widely described caveolinopathies, involving caveolin-3 mutations, are transmitted through autosomal dominant inheritance. There are at least thirty unique caveolin-3 mutations described in the human population. As mentioned above, defects in caveolin-3 lead to skeletal muscle disease classified as limb girdle muscular dystrophy 1 C (Fischer et al 2003, Sugie et al 2004, Figarella-Branger et al 2003, Fee et al 2004), rippling muscle disease (Dotti et al 2001, Bae et al 2007, Van de Bergh et al 2004, Kubisch et al 2005), distal myopathy (Fulizio et al 2005), and hyperCKemia (Carbone et al 2000, Merlini et al 2002, Alias et al 2004, Reijneveld et al 2006). In addition, mutations in caveolin-3 have been described in one case of Familial Hypertrophic Cardiomyopathy (Hayashi et al 2004), in four patients affected by Long QT Syndrome (Vatta et al 2006) and in three infants that died from Sudden Infant Death Syndrome (Cronk et al 2007). It is interesting to note that the same mutation in caveolin-3 can give rise to such a wide spectrum of clinical symptoms and phenotypes.

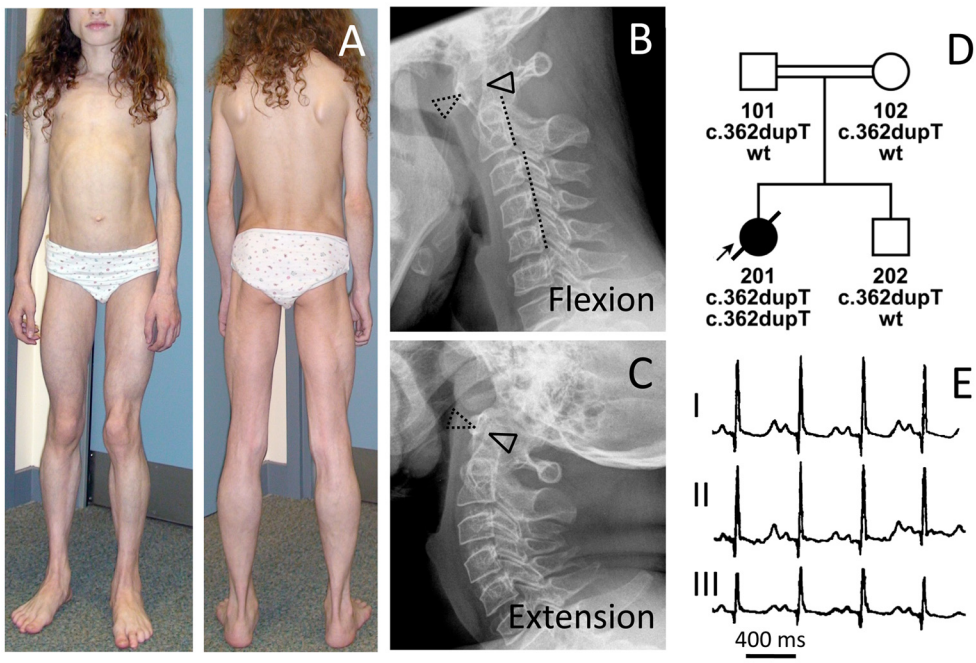

Figure 3. A 12-year-old patient with homozygous cavin-1 mutations. (A) Generalized lack of subcutaneous fat and prominent muscle hypertrophy is evident. Thickened and prominent veins (phlebomegaly) may be appreciated. X-ray images illustrate atlanto-axial instability during flexion (B), and extension (C) of the cervical spine. (D) Family pedigree and genotypes of the family members. (E) ECG recording shows a prolonged QT interval of 501 ms. Reproduced with permission from PLoS (Rejab et al 2010, doi:10.1371/journal.pgen.1000874.g002)

Mutations in the cavin-1 gene (Hayashi et al. 2009) combine generalized lipodystrophy with muscular dystrophy/myopathy. Muscles from affected individuals show a barely detectable immunoreaction to cavin-1-antibodies and no cavin-1 band is seen on Western blotting. Work by Rajab et al extended the disease panorama of individuals with mutations in cavin-1 (Rajab et al 2010). In that study the authors had access to material from eight Omani families where eleven individuals were affected, including five that died from sudden cardiac death during their teenage years. There were some patient to patient variation in symptoms, but common to all were lipodystrophy. Rajab et al unveiled a number of new diagnostic features. In controls, high cavin-1 mRNA levels were found in adipocytes, in all types of muscle tissue, osteoblasts but not in neuronal tissue. At birth patients suffered from hypertrophic pyloric stenosis, macroglossia and very small subcutaneous fat depots. In the early teens patients developed dyslipidemia, generalized lipodystrophy, tachycardia, arrhythmia, long-QT syndrome, muscle pain, stiffness and weakness, rippling muscle disease, atlantoaxial instability, skeletal and smooth muscle hypertrophy, joint contractures, rigid spine, scoliosis, and acromegaloid features (Figure 3). Patients had elevated plasma levels of creatine kinas, triglycerides and tissue damage markers such as AST and ALT. In both studies patients tested positive for insulin resistance.

In conclusion caveolin- and cavin mutations, many of which were discovered during the course of my thesis work, give rise to severe and life threatening pathologies in humans. A very crude estimate is that that there are up to 4000 individuals affected by caveolinopathies worldwide. Even if this number does not carry a significant weight by itself, the severity and the number of symptoms developed cannot be ignored. All in all, caveolopathies seen in humans serve as undeniable evidence for the physiological importance of plasma membrane caveolae.

Aims

Paper I: RhoA and protein kinase C (PKC) have been reported to be localized in caveolae and it has been suggested that this localization is functionally important. RhoA and PKC play essential roles in smooth muscle contraction. I therefore aimed to test the hypothesis that genetic ablation of caveolin-1 manifest itself in altered smooth muscle contractility and perturbed Ca^{2+} sensitization.

Paper II: Paper I demonstrated increased α_1-adrenergic contractility in caveolin-1-deficient arteries and indirectly pointed to hypertrophic arterial remodeling. Studies in the group indicated that Caveolin-1 KO mice have normal systemic arterial blood pressure despite ample evidence of increased nitric oxide (NO) production. I therefore hypothesized that increased arterial contractility and remodeling compensate for excessive NO production, leading to normalization of systemic blood pressure. The aim of study II was to test this hypothesis.

Paper III: NO is a physiological modulator of penile erection and my data in paper II was in good agreement with the general view that NO production is increased in caveolin-1 deficient mice. I therefore aimed to test how erectile mechanisms are affected in caveolin-1-deficient mice.

Paper IV: Evidence has been presented in the literature that muscarinic receptor signaling depends on caveolae. Papers I and III did not strongly support this idea. I hypothesized that the apparent contradiction could be due to species differences and set out to test this hypothesis by comparing the effect of caveolae-ablation in mouse, rat and human urinary bladders.

Paper V: Recently published work indicated that hypertrophy affects the membrane density of caveolae. I hypothesized that bladder hypertrophy leads to an increased density of caveolae which in turn affects the sensitivity to muscarinic agonists. I aimed to test this hypothesis by creating urethral obstruction in rats, which causes massive detrusor hypertrophy, and correlate the density of caveolae with sensitivity to muscarinic agonists and the expression of caveolin-1 and cavin-1.

Methods

The aim of this section is to provide a brief introduction in a manner that will ease understanding of the laboratory work presented in my papers. Specific information about protocols and reagents can be found in the original papers.

Electron microscopy

The theoretical father of electron microscopy, Reinhold Rudenberg, was a German electrical engineer and inventor who was determined to find a cure for his son that had been paralyzed by polio. The poliovirus was too small to be studied with light microscopy so Rudenberg turned his thinking into a different direction, electrons. As a scientific director of Siemens he had obtained a patent and financed the work of Ernst Ruskas to develop electron microscopy for biological specimens.

For common transmission electron microscopy a tissue sample or organism needs to be treated with fixative such as glutaraldehyde. When possible, perfusion fixation is a better alternative than simple immersion in the fixative. This is because the fixative reaches the cells with the same speed and at the same time point, providing better results. Samples are then embedded into plastics, such as epoxi resins. Ultrathin sections are cut with a diamond or glass knife and placed on a carbon coated metal grid. Specimens prepared that way have too low contrast properties so all samples have to undergo so called negative staining. Negative staining entails coating (rotary shadowing) with heavy metal salts capable of interacting with the electron beam and producing phase contrast. Placed in an EM camera, the sample is exposed to an electron beam. If electrons strike atoms in the sample they bounce back. If not, they continue to travel in a straight line. Notably, in transmission EM electrons that pass through the sample hit an image screen (whereas those that bounce do not) thus providing information on the structure of the sample. In electron microscopy, the image is often a compromise between high resolution and sharp contrast. Although modern electron microscopes are capable of considerably higher magnification then eighty years ago they remain advanced copies of Ruskas' prototype.

Western blotting

Western blotting (WB) is an analytical technique that permits detection of specific proteins in a tissue sample. Samples are first homogenized in a special buffer containing sodium dodecyl sulfate (SDS), an agent that charges and solubilizes the proteins, and

detergent. Using electrophoresis proteins are separated on a gel by charge (proportional to mass) and then transferred to e.g. nitrocellulose membranes that have a high affinity for proteins. Proteins transferred to the membrane are detected with the use of specific antibodies. The first antibody used is called the primary antibody and it is raised in live animals by inoculation of the protein of interest. After incubation with primary antibody the membrane is washed and incubated with a secondary antibody. The secondary antibody is generated against a specific fragment in the primary antibody called the Fc domain and is covalently linked to an enzyme (here horse-radish peroxidase). For example, against primary rabbit anti-protein-X antibody one can use secondary donkey anti-rabbit antibodies for detection. Finally, the membrane is incubated with a chemical substrate susceptible to enzyme cleavage and resulting in the generation of photons detectable by a specially designed camera. Within certain limits, the intensity of the signal is proportional to the amount of protein on the membrane (see Figure 2 in paper I). In this thesis I have compared the expression of a number of caveolae-associated proteins based on the intensity of the signal from samples loaded on the same membrane.

PCR

DNA polymerase is a polyfunctional enzyme responsible for replication of DNA. In 1980 Kary Mullis came up with a laboratory application, now known as the Polymerase Chain Reaction (PCR) where DNA polymerase was used for amplifying a specific DNA sequence *in vitro*. The impact of this innovation on the field of medicine and molecular biology was so big that Dr. Mullis was awarded a Nobel Prize in Chemistry in 1993. PCR can turn a few molecules of nucleic acid into sizeable, and most importantly, detectable amounts of DNA. There are three principle steps in a PCR process: denaturation, annealing and extension. The PCR cycle is repeated a number of times and each time the primer extension product is synthesized it serves as a template in the next cycle. And so, in only 20 cycles one can obtain a million copies of desired DNA target.

Advancement of PCR into Reverse Transcription PCR (RT-PCR) extended the power of amplification to RNA. RT-PCR uses reverse transcriptase to convert RNA to a cDNA and then uses DNA polymerase to amplify the cDNA to levels that are detectable.

Since the eighties PCR techniques have been under constant improvement resulting in a broadened application and higher reliability. One such advancement is monitoring of the amplification process in real time. This allows quantitative comparisons of mRNA expression (RT-qPCR) relative to a reference gene using the $2^{-\Delta\Delta Ct}$ method (Livak and Schmittgen 2001).

Isometric force recording

Isometric force recording is a plain old-school mechanical technique used in physiology for at least hundred years. I have used wire myography (I-V) and organ baths (I, III, IV) to study isometric force development. In these experiments tissue strips or vessel segments are mounted on transducers using metal wire, nylon or silk sutures. Such preparations contract upon stimulation with receptor agonists or KCl. The force of contraction is recorded by computerized software and can be analyzed in detail afterwards. Careful tissue handling and dissection is crucial for obtaining reliable result, as is appropriate stretching of the preparation prior to experimentation. Lengths and weights of the preparations can subsequently be used to calculate force per cross-sectional area (by multiplying force in mN by length in mm and density in mg/mm^3, and dividing by weight in mg). Stress measurements eliminate potential variation due to differences in size between preparations.

In many instances it is not sufficient to activate preparations with a single concentration of an agonist, as this may hide existing differences. To avoid this, concentration- or dose-response relationships are generated by cumulatively stepping up the agonist concentration. Concentration-response relations give information on the concentration of agonist that gives 50% of the full effect (EC_{50}) as well as the amplitude of the full effect (E_{max}).

Permeabilization with α-toxin

Permeabilization is a technique of removing the cell membrane barrier and yet preserving the contractile machinery of a syncytium of smooth muscle cells. The purpose of it is to study smooth muscle contraction under strict control of intracellular free ion concentration, pH, high energy phosphate levels and ionic strength. Chemical agents with detergent qualities such as Triton X-100 or β-escin can be used to achieve exactly this, but a trade-off is that the treatment is rather harsh and may lead to unwanted side effects. α-toxin is produced by the bacterium *Staphylococcus Aureus*. Under the right conditions this toxin creates pores in the plasma membrane of the cell. The advantage with this toxin over detergents is that the holes are so small (1-2 nm, Cassidy et al 1979) that they do not allow leakage of typical cytosolic proteins. Hence, receptors and their downstream signaling pathways remain intact. For experiments on permeabilized preparations solutions that closely mimic the normal intracellular ionic composition and energetic substrate content are used. Computer programs are used to calculate the exact amount of ions including Ca^{2+} and EGTA, Mg^{2+} and ATP needed for preparing a series of solutions. During the course of an experiment, permeabilized smooth muscle strips are exposed to increasing concentration of free intracellular Ca^{2+} concentration. In this manner we have determined the sensitivity of the contractile machinery to the intracellular Ca^{2+} concentration.

Electrical field stimulation

Nerve-mediated contraction or relaxation can be studied using electrical field stimulation. Electrical field stimulation is used in the organ bath set-up and pairs of electrodes are fitted close to the preparation which is submerged in the physiological buffer solution. Preparations are then stimulated by different voltages. Voltage is adjusted to optimize contraction and is applied in 0.5 s pulses. Frequency-response relationship data is recorded and later analyzed and presented in graphs. The contractile twitches generated in this manner depend on intramural nerves as shown using specific nerve blockers such as tetrodototoxin.

Pressure myography

Pressure myography is yet another method of studying arterial constriction. Arterial segments are mounted in an organ bath on small glass pipettes and perfused with physiological buffers at defined pressures. In response to addition of agonists, increased perfusion rate, or altered intraluminal pressure the diameter of the vessel changes. A digital camera captures these changes in vessel diameter.

The reason why we have used two similar techniques for studying arterial force generation is that pressure myography, despite being tedious and time consuming, has a number of advantages compared to isometric force recordings. In particular one can study pressure-induced myogenic tone and flow-induced dilation. Resistance arteries, such as small mesenteric arteries contract in response to increased intraluminal pressure. Flow exerts shear stress on the inner endothelial cell layer of the artery, leading to release of relaxing substances such as NO and prostacyclin. This process is referred to as flow-mediated dilatation.

Immunohistochemistry and confocal microscopy

I have combined confocal microscopy and immunohistochemistry to map the tissue distribution of caveolae-associated proteins. Immunohistochemistry, similar to Western blotting, exploits the specific interaction between primary antibodies and proteins of interest. The secondary antibodies are coupled to a fluorescent compound, detectable by fluorescence microscopy. Thus, instead of plain quantitative detection, as is the case in WB, immunohistochemistry provides information on where in a tissue the protein is to be found. There are many different ways of monitoring the fluorescence signal. Here I have used confocal microscopy which is a rather recent imaging technique. Its advantage is that it separates light from a thin plane, giving more accurate information on localisation than conventional fluorescence microscopy.

In practice, semithin preparations are cut from a frozen or paraffin embedded tissue. These are then placed on histological slides and permeabilized with a Triton solution. Triton is a detergent that creates holes in a plasma membrane of the cells making it

easier for antibodies to reach the antigens. Samples are further incubated (blocked) with bovine serum albumin to minimise unspecific binding of antibodies. This is followed by incubation with primary antibody, and following washing, with the secondary antibody that carries the fluorescent dye.

A number of secondary antibodies with different fluorescent dyes are available on the market. The florescent dye absorbs energy at specific wavelengths and will emit light with a certain wavelength. It is this light that is captured by the confocal microscope camera. The controls on the confocal microscope allow one to choose the wavelength for excitation and recording.

In vivo measurements of blood pressure and heart rate

Measurements of two important physiological parameters, blood pressure and heart rate in vivo were no doubt milestones in our studies of caveolin-1 deficient mice. In a blinded set of experiments mice were surgically anesthetized with isoflurane which they continued to inhale through the mask while tracheotomy was performed. A tube connected to a mechanical ventilator was placed via a small incision into the trachea. Breathing was then controlled with a respirator and the inhaled and exhaled volume set to 0.35 ml and frequency of breathing set to 98/min. A positive end-expiratory pressure of 5 mmHg was applied to prevent lungs from collapsing. A transducer was placed into the left femoral artery for blood pressure recording. Mean arterial blood pressure was recorded with low-pass filtering settings on a polygraph. Heart rate was recorded by removing low-pass filtering and increasing the chart speed for equally long periods of time repetitively through-out the experiment.

Plasma volume determination

Changes in plasma volume are one way of compensating for changes in vascular resistance or cardiac output. To measure plasma volume, a common plasma protein such as albumin carrying a radioactive isotope (in our case I-125 (^{125}I-HSA) is administered intravenously. The radioactivity of blood samples is then followed over time. After plotting the decline in radioactivity over time, plasma volume is estimated by extrapolating back to time zero. The plasma volume is then calculated by dividing the administered total radioactivity by the radioactivity in the zero sample.

Urethral obstruction

Urethral obstruction is a common complication of benign prostate hypertrophy in aging males. Affected individuals suffer from painful and frequent urination and have a higher risk of developing urinary tract infection. This condition can be mimicked in laboratory animals by bladder outlet obstruction (BOO) (Mattiasson and Uvelius 1982). In these experiments a partial surgical ligation of the urethra is performed on

anesthetized rats. After 10 days or 6 weeks the animals are euthanized and the bladders excised. The detrusor smooth muscles cells in the wall of the urinary bladder undergo hypertrophic changes in obstructed bladders (Malmgren et al 1987). The changes affect not only bladder appearance but also involve changes in agonist-induced smooth muscle contractility (Sjuve et al 2000).

Results and Discussion

The major objective of this thesis was to achieve a better understanding of the functional role of caveolae in smooth muscle. When I started my work three caveolin proteins had been identified, caveolin-deficient mice had been generated, and ample evidence suggested a role of caveolae in signal transduction. The objective of this section is to summarize and discuss the results in papers I-V.

Paper I

We started by asking the relatively simple and direct question. Is Ca^{2+}-sensitization, i.e. Rho-kinase and PKC driven changes in force at a clamped intermediate Ca^{2+} concentration, affected by genetic ablation of caveolin-1? At the time, a body of work had linked caveolae, RhoA/ROCK and PKC together (Gingras et al 1998,Michaely et al 1999, Mineo et al 1998, Je at al 2004), but the functional relevance of these interactions was uncertain.

Using an assay allowing precipitation of active, GTP-bound, Rho, we found increased activation of Rho by GTPγS in the absence of caveolae. Analysis of the precipitates of active Rho also confirmed that caveolin-1 does interact with Rho-proteins physically. Despite the increased Rho activation we were not able to detect changes in Ca^{2+}-sensitisation when we stimulated permeabilized intestinal muscle preparations from wild type and knockout mice with carbachol and GTP.

Interestingly, direct activation of PKC with phorbol ester and via stimulation of α_1-adrenergic receptors (both in the continuous presence of L-NAME to inhibit NO release) gave rise to a significantly larger contraction in KO compared to WT femoral arteries. This would seem to support the notion that protein kinase C signalling depends on caveolae, and that this is of relevance for adrenergic control of vascular tone. However, one of the reviewers asked us to also measure stress (i.e. force per cross-sectional area). We therefore weighed all preparations and measured their length. By assuming similar densities this allowed us to calculate cross-sectional area, and thus stress. To our surprise we then found that this way of expressing contractility eliminated the difference in α_1-responses between the genotypes (Figure 4) because the weight of the KO arteries was increased. This suggested two things: i) that loss of caveolae leads to thickening of the arterial wall, and ii) that PKC signalling might not actually be changed. The first suggestion is addressed in paper II. The second suggestion was tested by inhibiting protein kinase C. We predicted that if the change in α_1-induced force

was due simply to a change in arterial geometry, then the difference should withstand PKC inhibition. If, on the other hand, the difference in force between genotypes was eliminated by PKC inhibition, this would support altered PKC signalling. The result of these experiments was clear-cut; inhibition of PKC eliminated the differences between genotypes (Figure 4E), reinforcing the view that loss of caveolae disinhibits PKC and that this at least contributes to the increased α_1-responses.

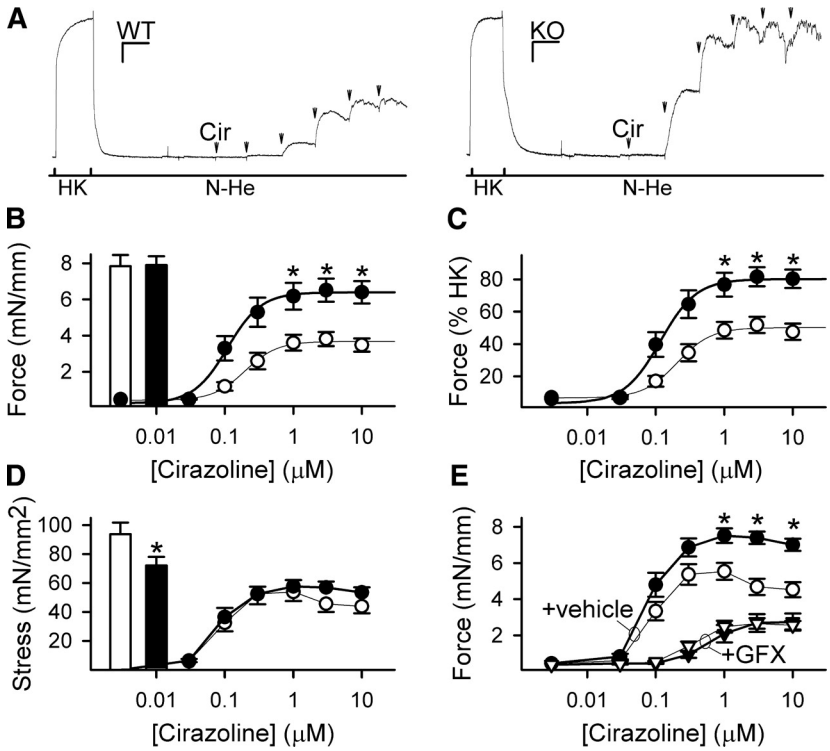

Figure 4. Dose-response relationships for the α_1-adrenergic receptor agonist cirazoline (Cir) in femoral arteries from WT and KO mice in the presence of 300 μM L-NAME (A). Horizontal and vertical calibration bars represent 1 mN/mm and 5 min, respectively. Panel B shows summarized data from panel A, expressed as absolute force (mN per unit length of artery). Bars show force in response to depolarization with 80 mM K^+ in WT (open) and KO (filled). C shows force in WT (open symbols) and KO (filled symbols) normalized to 80 mM K^+ contraction. (n=16). In panel D force is presented as stress (mN/mm^2, n=40). In panel E, dose response relations for cirazoline (triangles) with the protein kinase C inhibitor GF 109203X (5 μM) are shown. In E, controls for both genotypes were run in parallel (circles, n=8). *P<0.05 for KO vs. WT comparison. Reproduced with permission from American Physiological Society (Shakirova et al 2006).

In addition to the major findings in paper I, we made the interesting observation that the content of caveolin-3 was decreased after ablation of caveolin-1. We have later corroborated this finding using small mesenteric arteries (study II) and portal vein (study II). In study III caveolin-3 levels only tended to be reduced in corpus cavernosum, but we attribute this to insufficient statistical power. Possibly, the reduced caveolin-3 con-

tent that we have documented is a result of altered trafficking of the mature caveolin-3 protein to the membrane (Hayer et al 2010). In support of this idea the intracellular concentration of caveolin-3 observed with immunohistochemistry appeared to be increased. An indirect mechanism involving the interaction of nitric oxide with the transcription factor myogenin (Martinez-Moreno et al 2007) seems less plausible since this should have resulted in measurable changes in mRNA levels for caveolin-3.

The take home massage from paper I is that ablation of caveolae leads to an increased activity of signalling pathways coupled to activation of contraction in smooth muscle. In the case of the monomeric GTPase Rho, this is not enough to have any readily detectable effect on contraction. In the case of PKC, on the other hand, an associated and easily measurable change in contractility is noted.

Paper II

Our second paper focuses on two contradicting findings in caveolin-1-deficient mice. Normal systemic blood pressure had been reported in these mice and yet a sizeable increase of endothelial NO production had been documented by many labs. The latter effect is expected to reduce arterial tone and resistance which would lower blood pressure so how can these findings be reconciled? We hypothesized that increased smooth muscle contractility (documented in paper I) together with hypertrophic remodelling of small arteries (suggested by the stress measurements in paper I) would tend to raise blood pressure, opposing the vasodilating drive from increased NO production.

Immunofluorescence staining of small mesenteric arteries (SMA) from WT mice revealed that caveolin-1 and -2 were present in the endothelium and in the media. Caveolin-3 on the other hand was restricted to media. In SMA from KO mice, caveolin-1 and caveolin-2 were absent throughout the arterial wall. A reduction in the intensity of staining for caveolin-3 was noted, similar to our observations in paper I. A reduction of caveolin-3 by 50-60% was confirmed by Western blotting in SMA, aorta and portal vein. Detailed morphometric analysis by histology revealed that small mesenteric arteries from KO mice were remodelled with increased cross-sectional area and media thickness (Figure 5). Trichrome staining did not reveal increased connective tissue content in the arterial wall, but a small change cannot be entirely ruled out. To confirm that lumen dimensions were not affected by the fixation procedures we also examined arterial dimensions of arteries mounted in a pressure myograph at a defined physiological pressure and in the absence of extracellular Ca^{2+}. Consistent with morphometry, wall thickness (24 ±2 μm in KO vs 14±1 μm in WT, $p<0.001$) and wall area (2.2 ±0.2x10^4 μm^2 in KO vs. 1.2±0.1x10^4 μm^2) were significantly increased in SMA from KO mice. Moreover, the wall to lumen ratio was greater in KO (0.096±0.006 vs 0.063±o.006, $p<0.001$). Interestingly, an increased wall to lumen ratio is almost invariably seen in hypertension (Mulvany et al. 2002). It is debatable whether an increased wall to lumen ratio in small arteries is a cause or a consequence of hypertension, but simple geometrical considerations argue that it should increase peripheral resistance

and hence maintain or worsen the condition whatever the basic underlying mechanism would be.

The next legitimate question to ask was whether the increase in a media thickness was associated with increased force development in small mesenteric arteries. We studied responses to the selective α_1-adrenergic agonist cirazoline in SMA and aorta from WT and KO mice in the presence of L-NAME. Force was greater in a SMA from KO compared to WT with no change in potency (i.e. the EC_{50} value). Increased force was also seen on stimulation with noradrenaline, the physiological ligand for α-adrenergic receptors, and after inclusion of the K^+-channel inhibitor tetraethylammonium. In contrast, contractility was unchanged in the aorta suggesting that the increased media thickness, and the associated amplification of contractility, may be specific for small arteries.

We next studied myogenic tone and flow-induced dilation under conditions that approach the in vivo situation in a pressure myograph. Myogenic tone, when present, was decreased in KO SMAs, and this reduction was partly rescued by introduction of L-NAME which had no effect in WT. In addition, step-wise increases in flow at constant pressure of 95 mm Hg caused flow-induced dilation in WT but had no effect in KO. Introduction of L-NAME rescued flow-induced dilation in KO and had little effect in WT. The combination of pressure and α_1-adrenergic stimulation in the presence of L-NAME eliminated difference between WT and KO arguing that the increase in the α_1-adrenergic response compensates for poor myogenic tone in caveolin KO mice.

Caveolin-1 can negatively control proliferation and cellular growth (Galbiati et al. 2001, Hassan et al. 2006). One possibility therefore was that the hypertrophic remodelling was due in part to increased proliferation of vascular smooth muscle cells. We therefore measured DNA synthesis in SMA using thymidine incorporation in organ culture. Organ culture represents a defined environment where differences in pressure and flow can be ruled out. A modest increase in thymidine incorporation (by 31%) was noted in KO SMA, suggesting that changes in the rate of proliferation may well contribute.

We reasoned that increased α_1-responsiveness and hypertrophic arterial remodelling would counteract the vasodilating drive from high basal NO production in caveolin-1 knockout mice. Accordingly, we predicted that inhibition of NO synthesis would have a greater effect on blood pressure in the KO and that a higher arterial blood pressure would be unmasked after inhibition of NO synthesis. Indeed, the relative effect of L-NAME was doubled in KO mice in comparison to WT mice (17±3% increase in WT vs. 38±6% in KO, p=0.001), and the absolute blood pressure was higher in KO mice than in WT mice in the presence of L-NAME (top left panel in Figure 5).

The take home massage from paper II is that a high endothelial NO production in caveolin-1-deficient mice is neutralized by geometrical and functional changes in small arteries. Other mechanisms, such as an expanded circulating volume, likely contribute.

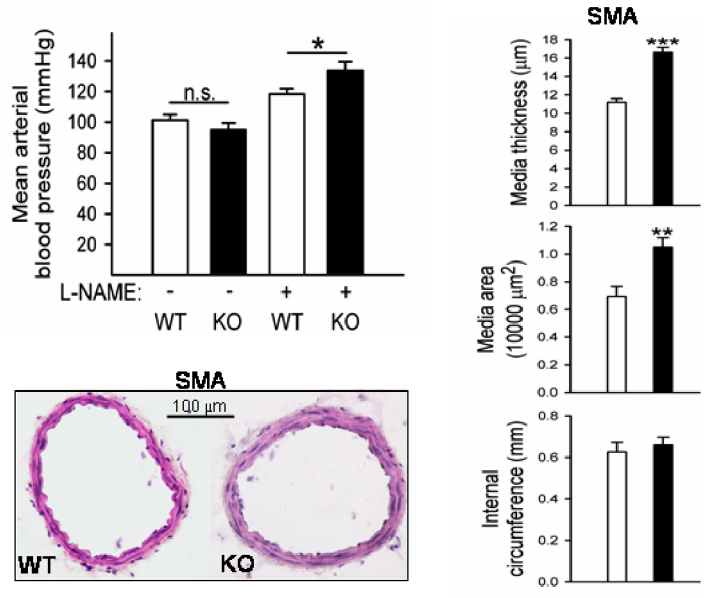

Figure 5. Top left shows mean arterial blood pressure in wild type and caveolin-1-deficient (KO) mice in the absence and presence of L-NAME. Lower left panel shows H&E stained sections of small mesenteric arteries from WT and KO, respectively. Right panels show summarized data on arterial geometry derived from histology. Reproduced with permission from American Physiological Society (Albinsson et al 2007).

Paper III

A physiological process where changes in NO production have a direct and profound effect is penile erection. The physiological mechanisms behind penile erection are relying on two steps both involving synthesis of NO, first by nNOS in nerve fibres and then by eNOS in endothelial cells of the sinusoids. Neuronal release of NO in corporal tissue causes dilatation and a rapid inflow of blood. This increases shear stress which subsequently leads to a sustained production of NO by eNOS in endothelial cells in sinusoids. As a result NO relaxes corporal smooth muscle via activation of soluble guanylyl cyclase (sGC) and protein kinase G (PKG). Increased corporal pressure compresses the veins and compromises the venous return from the penis allowing the erectile state to be maintained. The most common medication for erectile dysfunction targets the breakdown of cGMP by phosphodiesterase 5. Increased α-adrenergic contractility and increased activity of Rho kinase were suggested as pathophysiological mechanisms underling vasculogenic erectile dysfunction (Park et al 2006). We therefore reasoned that the erectile mechanisms might be affected in caveolae-ablated mice and set out to test this.

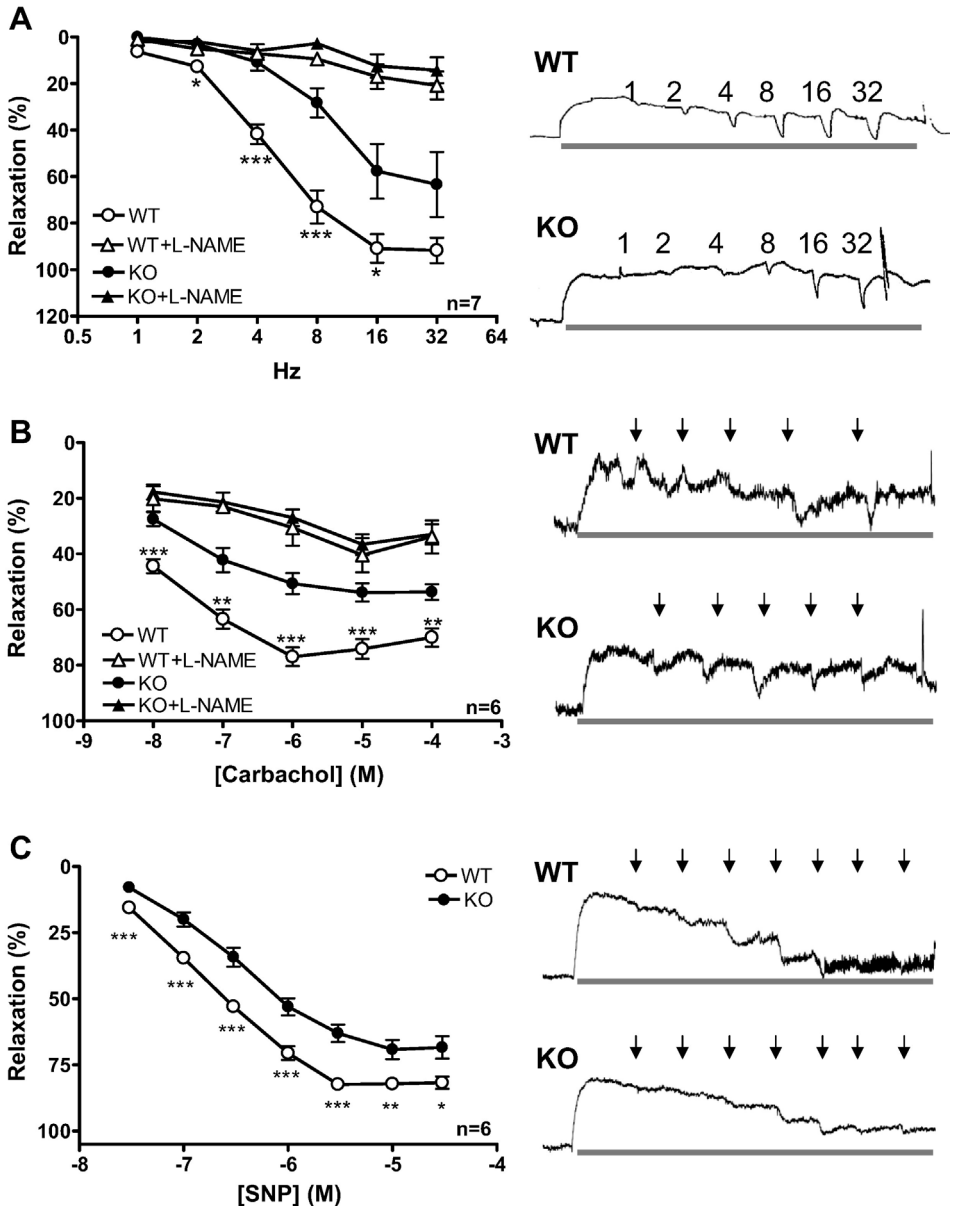

Figure 6. (**A**) Relaxation elicited by electrical field stimulation of strips of corpus cavernosum pre-contracted with 0.3 μM cirazoline. Original traces are shown to the right. (**B**) Dose response relationships for the muscarinic agonist carbachol after precontraction with 0.3 μM cirazoline. In **A** and **B** triangles represent relaxation in the presence of L-NAME (300 μM). (**C**) Relaxation in response to increasing concentrations of sodium nitroprusside (SNP) after pre-contraction with 0.3 μM cirazoline. WT: wild type; KO: knock out. *P<0.05, **P<0.01, and ***P<0.001 for WT vs. KO. Reproduced with permission from Elsevier (Shakirova et al 2009).

Caveolin-1 was present in endothelial and smooth muscle cells of the corpus cavernosum (CC) from WT mice and it was absent in KO CC as expected. Caveolin-3 was present in smooth muscle cells in the CC tissue in WT and KO. Western blotting disclosed a reduction in PTRF-cavin/cavin-1 content in KO CC. As mentioned above, no reduction in caveolin-3 in CC from KO was detected, a peculiar exception from our observations in paper I and II.

We performed a gross morphological examination of the CC to rule out fibrosis which would affect the compressibility of the tissue, but no evidence of fibrosis was found. Caveolin-1 has previously been suggested to affect collagen formation in the CC (Bakircioglu et al 2001). The overall appearance of KO CC did not differ from WT.

Corporal tissue from caveolin-1 deficient mice relaxed poorly in response to electrical field stimulation and upon stimulation with the muscarinic agonist carbachol (Figure 6). Staining for nerve fibres revealed no difference between KO and WT. Impaired relaxation on field stimulation in caveolin-1 deficient CC was not due to a reduced innervation. EFS-induced relaxation was abolished by addition of L-NAME in both strains. Inquiring if the poor relaxation in the KO was a result of decreased NO availability or reduced NO-sensitivity of the target tissue we used the NO-donor sodium nitroprusside (SNP). Relaxation in response to SNP was weaker in KO when compared to WT.

Linder et al (2006) suggested that soluble guanylylcyclase has to be located in proximity with caveolin-1 for normal erectile function in rat. The impaired relaxation to SNP that we observe seems consistent with this proposal. However, a deeper look into downstream effectors of NO is required for better understanding of impaired NO mediated relaxation in the KO.

All in all, the results of paper III point to an impairment of nerve-mediated relaxation of the penile erectile tissue in caveolin-1 deficient mice, and that this, at least in part, is due to an effect downstream of the generation of nitric oxide.

Paper IV

A number of studies have linked muscarinic M_2 and M_3 receptors to caveolae (Feron et al. 1997, Gosens et al. 2007). My own findings in paper I and III did not strongly support this view. Taking into account that interspecies differences in relation to caveolae have been observed before (Wright et all 2008, Morris et al 2006, Fujita et al. 2001) we hypothesized that decisive species differences may exist in the dependence of muscarinic signalling on caveolae and set out to compare human, rat and mouse urinary bladder.

Gene ablation on the tissue or organism level in species other than mouse is challenging, so we set out to ablate caveolae by chemical means. To this end methyl-β-cyclodextrin was used. This substance binds and removes cholesterol from the cell membrane and disrupts caveolae. It is important to keep in mind however that this treatment is not entirely specific for caveolae but also affects membrane rafts and membrane fluidity.

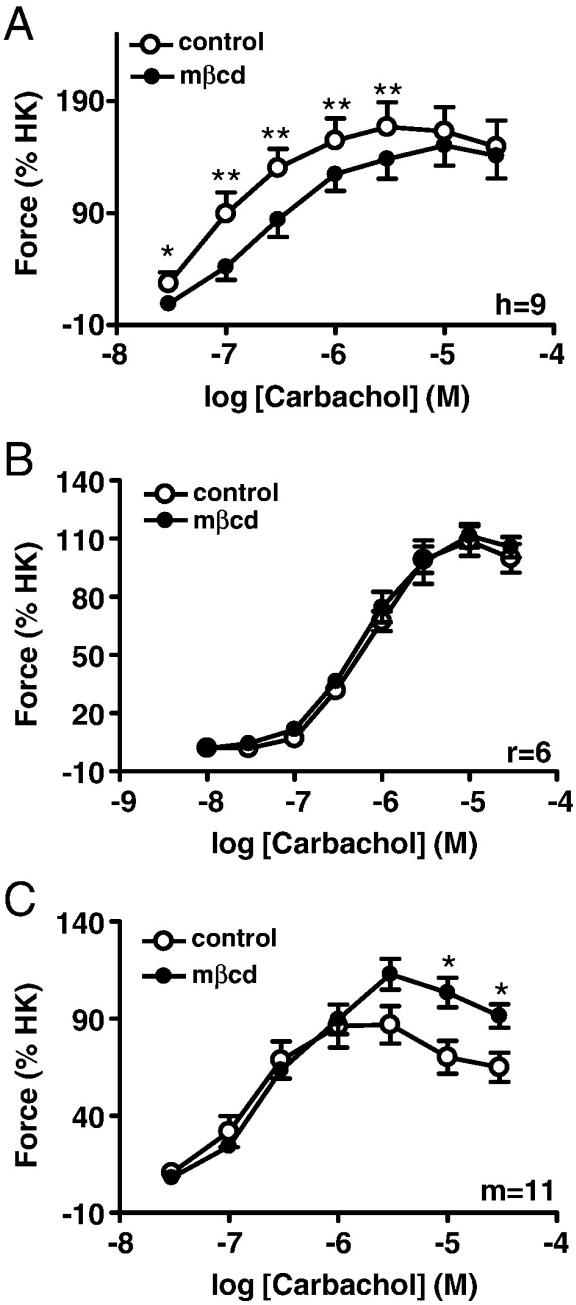

Figure 7. Dose-response relationships for the muscarinic agonist carbachol in smooth muscle preparations from human (**A**), rat (**B**), and mouse (**C**) urinary bladder. Control (white symbols) and cholesterol depleted (black symbols) where run in parallel. Force is presented as a percentage of depolarization-induced contraction (60 mM K+, HK) elicited before the depletion protocol. h, r, and m refer to the number of humans, rats, and mice. Reproduced with permission from Elsevier (Shakirova et al 2010 (a)).

Cholesterol depletion caused a right shift in the dose response curve for carbachol in human urinary bladder indicating decreased sensitivity to the agonist. Notably, no effect of caveolae disruption was seen in preparations from rat, and a slight increase in a maximum force was observed in mouse urinary bladder (Figure 7). Importantly, slight depolarisation of the membrane with K^+-high solution eliminated the effect in human urinary bladder. Moreover, pre-treatment with the L-type Ca^{2+}- channel blocker nifedipine made the effect somewhat less conspicuous. The effect of cholesterol depletion in human urinary bladder was exclusive to muscarinic signalling as neither contraction in response to purinergic stimulation nor depolarisation were affected.

No difference in the expression of caveolae proteins, muscarinic M_3 receptors or proteins involved in regulation of muscarinic signalling was noted between human and rat urinary bladder. Interestingly mouse urinary bladder expressed significantly higher levels of both M_3 and $PLC_{\beta 1}$ when compared to human and rat urinary bladder.

The novel take home massage from paper IV is that in contrast to widely used laboratory animals, such as rat and mouse, human urinary bladder requires plasma membrane cholesterol/caveolae for normal mucarinic receptor activation.

Paper V

The number of caveolae present on the plasma membrane is variable and can be affected by disease or adaptive changes (Goto et al 1990, Kikuchi et al 2005). For example, in idiopathic pulmonary hypertension, an increase in caveolin-1 expression and in the number of caveolae at the cell surface has been reported (Patel et al 2007). A study from 2009 by Polyák et al claimed that bladder outlet obstruction was associated with a decrease in the number of plasma membrane caveolae. We hypothesized that changes in the density of caveolae in association with hypertrophy might be lead to changes in contractile properties of the urinary bladder. It is important to note that paper V was initiated prior to paper IV, and at the time when we planned this work we were unaware of the species differences reported in paper IV.

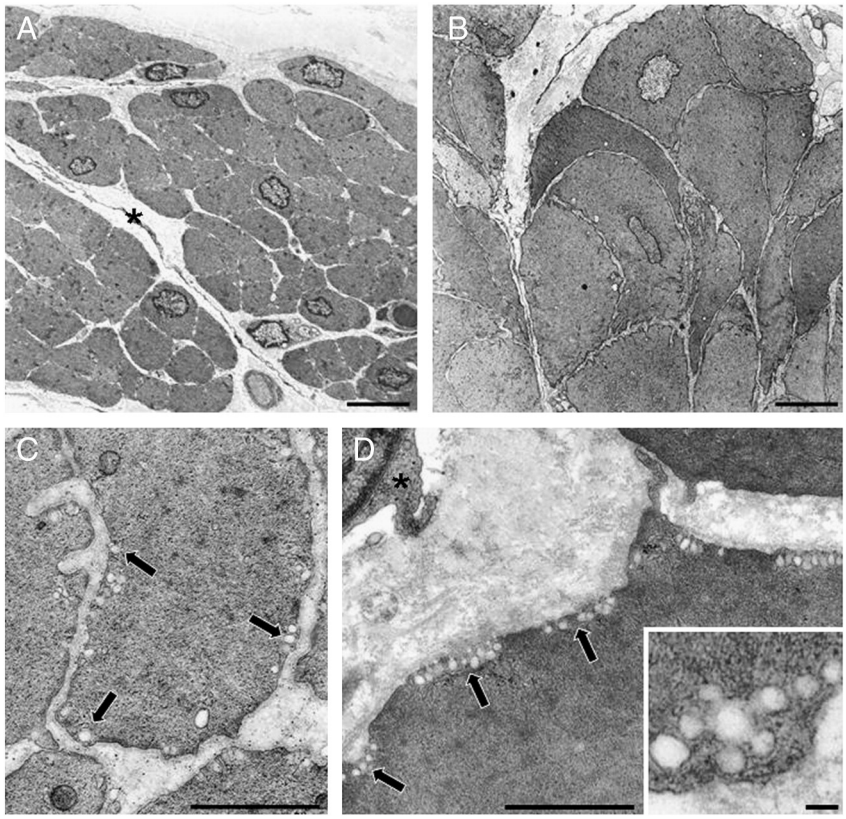

Figure 8. Electron micrographs of smooth muscle cells in control and hypertrophic rat urinary bladder (**A**-**D**). (**A**, **B**) Cross-sectioned smooth muscle cells from control and hypertrophic rat bladder, at low magnification. Fibroblasts are marked with asterisks (**A**, **D**). **C** Control (**C**) and hypertrophic (**D**) bladder smooth muscle cells at high magnification. Caveolae are highlighted with arrows in **C** and **D**. Scale bars represent 5 μm (**A** and **B**), 1 μm (**C**, **D**), and 100 nm (inset in **D**). Reproduced with permission from Elsevier (Shakirova et al 2010 (b)).

To address our hypothesis, female Sprague-Dawley rats were subjected to bladder outlet obstruction for 10 days and 6 weeks, respectively. A detailed morphometric analysis of detrusor smooth muscle cells by electron microscopy (Figure 8) revealed an increased membrane density of caveolae after 6 weeks of obstruction (3.33±0.56 caveolae per micrometer membrane) compared to the control group (1.30±0.11 caveolae per micrometer membrane (Figure 9). The estimated membrane area relative to muscle cell volume of control detrusors was 22.8±4.7 to be compared with 7.9±0.7 in obstructed bladders. Thus, obstructed bladders have 0.346 of cell membrane length per unit muscle wall cross-sectional area relative to the control group.

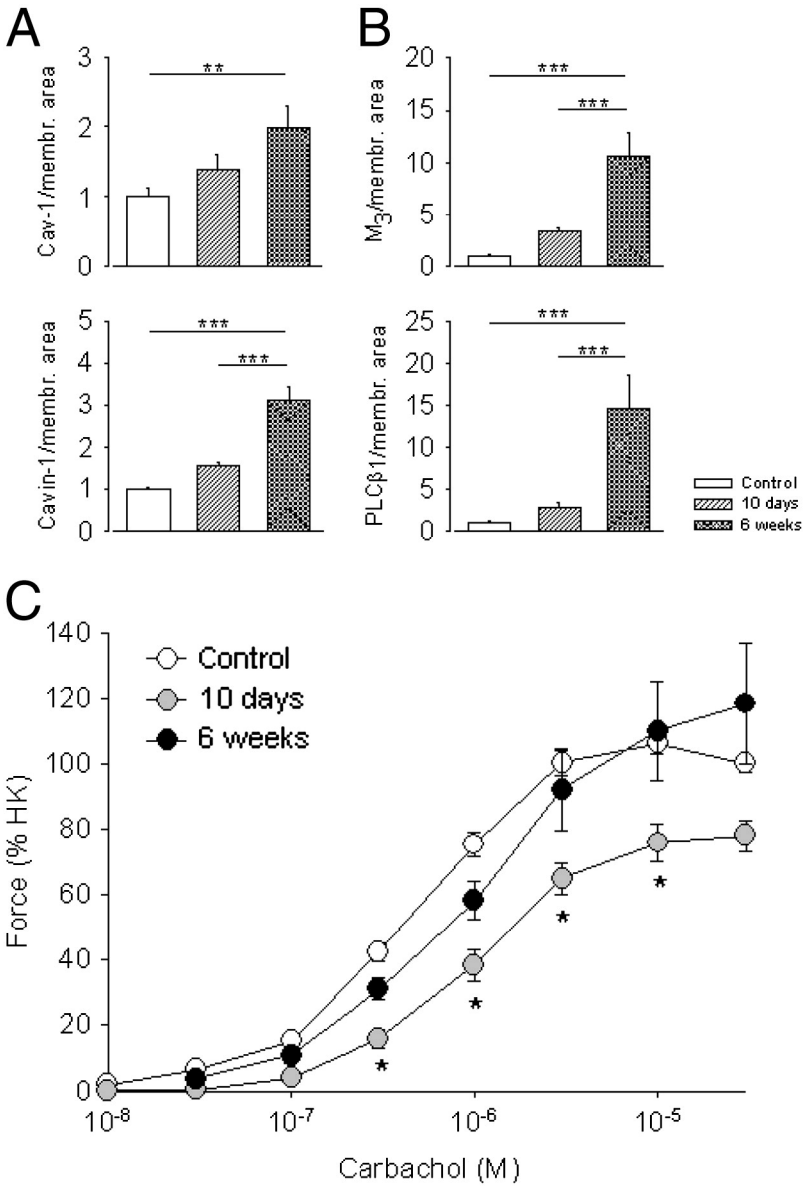

Figure 9. (**A**) Caveolin-1 and cavin-1, expression per unit membrane area (measured by electron microscopy). (**B**) Expression of M_3 and $PLC_{\beta 1}$ relative to membrane area. (**C**) Concentration-response relationships for carbachol in smooth muscle strips from control bladders and bladders obstructed for, 10 days and 6 weeks. In **C** the data is normalized to the depolarization induced contraction (HK) in the same preparations. * indicates P<0.05 vs. controls and 6 week obstructed bladders. Reproduced with permission from Elsevier (Shakirova et al 2010 (b).

Despite an increased membrane density of caveolae no difference in caveolin-1 expression relative to total protein, total actin or β-actin was noted, and immunofluorescence

imaging did not reveal any difference in the subcellular distribution of caveolin-1. Thus, the increased density of caveolae in detrusor hypertrophy is due simply to crowding of the same relative amount of caveolin-1 molecules on a smaller relative membrane area. Indeed, when caveolin-1 and cavin-1 expression was expressed relative to membrane area 2- and 3-fold increases were noted (Figure 9). This should be compared with the 2.56-fold increase in density of caveolae that we measured directly by electron microscopy. Evidently, it cannot always be taken for granted that the content of a membrane protein, measured by Western blotting and normalized to a cytosolic reference protein (as is done in hundreds of studies), says anything about its membrane density.

The response to the muscarinic agonist carbachol was increased when expressed as stress in bladders obstructed for 10 days, and reduced after 6 weeks of obstruction. Thus, the correlation between muscarinic responsiveness and the membrane density of caveolae is poor in the rat urinary bladder. To challenge our original hypothesis further we examined caveolae disruption with mβcd in control and obstructed bladders. When normalized to depolarization-induced contraction, carbachol-induced contraction was resistant to mβcd in controls, at 10 days and at 6 weeks of hypertrophy. Contraction in response to stimulation with bradykinin was insensitive to cholesterol desorption in control bladders and after 10 days of obstruction, but inhibited by it at 6 weeks.

In summary, paper V shows that bladder outflow obstruction leads to an increase in the membrane density of caveolae that is not associated with changes in caveolin-1 or cavin-1 expression relative to total protein. The effect is due to a reduced relative cell surface area and is of little importance for muscarinic signalling, at least in the rat. Caveolae-dependent changes in the response to other agonists, such as bradykinin, or in other species cannot be ruled out.

Some final reflections

I would like to think that my studies have made a difference and contributed in some way to a deeper understanding of the role of caveolae in physiology. Yet, it is very clear that major uncertainties about caveolae still exist. For example, caveolae are often seen as a static membrane structures that can be internalized in response to only a handful of agents, including viruses and cholesterol. On the completely opposite side of thinking is the suggestion that large folded and connected caveolae formations, so called ”bunches of grapes”, can fold and unfold thus affecting cell size with little energy input (Landh et all 1995). I believe that the future of the caveolae field lies in better understanding of dynamic processes involved in caveolae biogenesis and their later “membrane” and “intracellular” life.

The recent identification of mutations in caveolae proteins in humans and the association of these mutations with a variety of pathological conditions truly represent major breakthroughs. It is deeply satisfying to see that a pure preclinical topic that I started to work with six years ago has since acquired clinical relevance. A hope for new treatment approaches and better diagnostic tools seem to be within reach. Even now, one can speculate that preventive screening followed by pacemaker surgery might be helpful for a selected group of patients with long QT syndrome.

Recently an attempt to classify caveolae with respect to their mobility and protein content has been made (McMahon et al 2009). Truly caveolae can exhibit a great diversity when it comes to composition, dynamics and their associated signalling apparatus, but this must be dictated by tissue or environment rather than by stern properties of caveolae themselves. In this thesis evidence for such diversity is presented.

Populärvetenskaplig sammanfattning

Caveolae är 50-100 nm små flaskformade plasmamembranivaginationer. Särskilt många caveolae finns i endotelceller, glatta muskelceller och fettceller. Bildningen av caveolae sker med hjälp av proteinerna caveolin och cavin, men olika fetter, särskilt kolesterol, spelar även en väsentlig roll. Caveolae har föreslagits fungera som signalstationer i flera cellulära signalvägar. En klassisk caveolae-asscoierad signalmediator är endotelialt kväveoxidsyntas (eNOS). eNOS bildar gasen kväveoxid som vidgar våra kärl. Caveolin-1 binder direkt till eNOS och undertrycker proteinets enzymatiska aktivitet. Mycket av kunskapen om caveolaes roll i cellsignalering kommer från försök på caveolin knockout möss (KO). Möss som saknar caveolin-1 utvecklar defekter i lungor och hjärta och har även metabola förändringar. Sådana möss har varit centrala för flera av de studier jag sammanfattar här.

Trots att glatta muskelceller har särskilt många cavelae hade caveolae i dessa celler inte varit i centrum för detaljerade studier när jag började mitt avhandlingsarbete. Glatt muskulatur finns i luftvägarna, livmodern och kärlväggarna och spelar en livsavgörande roll för så vitt skilda saker som blodtrycksreglering och utdrivningen av barnet under förlossningen. I mitt första arbete ställde jag mig frågan om elimination av caveolae påverkar den glatta muskulaturens förmåga till sammandragning. Jag fokuserade särskilt på PKC och ROK-medierad kontraktion i kärlväggen eftersom både ROK och PKC tidigare knutits till caveolae. Mitt viktigaste fynd var att den glatta muskulaturen i kärlväggen har en ökad förmåga att utveckla kraft i frånvaro av caveolae. Detta berodde delvis på stärkt PKC-signalering, men våra data talade även för ett tjockare muskelcellslager i kärlväggen.

Möss som saknar caveolin-1 har ökad eNOS aktivitet och därför ökad produktion av kärlvidgande NO, men har trots detta visar sig ha ett normalt blodtryck. I mitt andra arbete frågade jag mig om den ökade förmåga till sammandragning som jag tidigare dokumenterat bidrar till att normalisera blodtrycket hos dessa möss. Jag ville även utreda om kärlväggen faktiskt var förtjockad. Med histologiska metoder kunde jag visa att kärlväggen var förtjockad, att detta korrelerade med en ökad förmåga till sammandragning, samt att denna (och sannolikt ytterligare) mekanismer bidrar till normaliseringen av blodtrycket hos möss som saknar caveolin-1. Jag kunde också indirekt konfirmera det andra hade rapporterat, nämligen att eNOS aktivitet är ökad i frånvaro av caveolae i kärlväggen.

NO spelar en avgörande roll för erektion av penis och läkemedel som stäker potensen verkar indirekt genom att stärka NO-signaleringen. Jag ställde mig därför frågan

om inte möss som saknar caveolin-1 borde ha lättare att få erektion. För att testa detta fripreparerade jag den erketila vävnaden från penis och studerade elektrisk inducerad relaxation medierad av NO. Till min förvåning fann jag att den erektila mekanismen var kraftigt försämrad hos möss som saknar caveolin-1.

I det fjärde delarbetet undersökte jag vilken eventuell roll caveolae spelar i urinblåsan. Jag hade unik tillgång till mänsklig blåsvävnad och ville jämföra denna med blåsvävnad från mus och råtta. Caveolae eliminerade jag på kemisk väg genom att extrahera kolesterol. Elimination av kolesterol hade mera uttalade effekter på sammandragning av mänsklig blåsa än på sammandragning av både mus och råttblåsa.

I mitt femte delarbete ville jag testa om sjukdomstillstånd i urinblåsan påverkar caveolae och om detta i sin tur har konsekvenser får blåsans förmåga till sammandragning. Jag använde en modell där urinröret knyts åt på råttor. Detta leder till en förstoring av blåsan liknande den som ses hos män med förstorad prostata. Med elektronmikroskopi kunde jag sedan visa att blåsförstoringen ledde till att antalet caveolae per yta cellmembran ökade. Till min förvåning var detta inte associerat med ändrat utryck av vare sig caveolin eller cavin utan kunde förklaras av att samma relativa mängd caveolinmolekyler trängs ihop på en mindre relativ membranyta. Jag kunde heller inte finna något som tydde på att aktivering med muskarinreceptoragonisten carbachol var förändrad som en följd av den ökade trängseln i membranet. Det verkar dock fortfarande sannolikt att blåshypertrofi hos människor skulle kunna påverka blåstömning via förändringar i caveolae.

Sammantaget bidrar min avhandling till en djupare och mera nyanserad bild av caveolaes betydelse för den glatta muskulaturens funktion och därmed blodtrycksreglering, erektion av penis och tömning av urinblåsan.

Acknowledgments

There are people that deserve to be on a front page of this thesis as much as do. I would like to thank them here instead, in a more personal and informal way.

I sincerely thank **Anna Wennerholm** for taking interest in my life and introducing me to **Per Hellstrand**.

In May 2004 I went for a job interview with Professor in physiology Per Hellstrand. The meeting was organized at the last minute before I was leaving for Russia after the rejection of my application for Biomedical research school. Needless to say I was very frustrated and sad, and had no big hopes for good fortune. I came to BMC F12 extremely determined to impress and for that reason was very stiff and impersonal, as the majority of us are on similar occasions. Per was friendly and energetic and he directly introduced me to a young…very young scientist I thought, who was **wearing shorts**, a capital crime punishable deed at a work place in Russia. The young scientist name was **Karl** and for some reason he joined us when Per showed me around and introduced me to his colleagues. I was even more surprised when Karl stayed with us during the interview and started to ask lots of questions. I was thinking hard, trying to find something clever to say to Per and was a little annoyed by questions coming from Karl. After all, my goal was to make a good impression with a potential employer and not to chat with someone who I thought was a PhD student. So more or less as I remember it I was trying to politely ignore Karl throughout the interview. As funny as it sounds for me now, that rude misconception from my side was for the best. If I knew at the time that my potential scientific advisor was Karl I probably would have been too intimidated to try to impress both him and Per at once.

In **Karl Swärd** I was fortunate to have a scientific advisor that sets a personal example. Thank you for introducing me to the caveolae field and for always setting a high standard, not only for the others, but for your self as well. I enormously respect and "envy" your ability to accumulate knowledge by extensive reading, remember all fine details and to put one and one together. Thank you for teaching me how to write scientific articles, applications and letters, it is good to learn from the best.

"I think you should ask Per…" was often said when one met a dead-end situation both in science and in practical matters. Thank you **Per Hellstrand** for being that extra-reliable source of information but also for being critical and open when I needed it. It was comforting to have a center of stability in the lab.

Patience is an exceptional virtue and patience for a fellow colleague is of a rarest kind. I thank **Ina Nordström** for being the most patient person I ever knew and thus making chaotic lab life of ours run smoothly every day. I especially thank you for fixing all presents and social events and for your lasagna.

I think I owe to **Sebastian Albinsson** a few bottles of beer. There are some that I have lost in a fair bets but also as a simple thank you for all that time you put into teaching me nearly all lab techniques I can do today. Thank you for being very helpful during these six years and for being not only a colleague but also a person to talk to.

Bengt Uvelius, thank you for introducing me to the bladder field and for giving me the unique opportunity to test our caveolae hypothesis on human tissue.

Bengt-Olof Nilsson, thank you for being a helpful, positive, kind person and a colleague.

Thank you **Maria Gomez** for your energetic attitude, clever input and for being that much needed positive example of a successful female scientist.

Thank you **Karin Jansner** for all the help with histology.

Kristina, Jenny, Lisa, Daniel, Mari, Andreas, Johan, Michiko, Maya, Anders and Cecilia all of you that made BMC F12 and then D12 not only a working place but also a pleasant place to be. Thank you for listening to my presentations at lab meetings, having fikas and lunches with me…and for occasionally sharing a gossip.

Thank you **Lisette Eklund, Gyn Nilsson** for always having time to help me and other PhD students.

Mama you are my true hero.

Frode and Saga, you support me effortlessly.

References

1. Aboulaich N, Vainonen JP, Strålfors P, Vener AV. Vectorial proteomics reveal targeting, phosphorylation and specific fragmentation of polymerase I and transcript release factor (PTRF) at the surface of caveolae in human adipocytes. *Biochem J*. 2004; 383(Pt 2):237-48.
2. Albert AD, Boesze-Battaglia K. The role of cholesterol in rod outer segment membranes. *Prog Lipid Res*. 2005; 44(2-3):99-124.
3. Albinsson S, Shakirova Y, Rippe A, Baumgarten M, Rosengren BI, Rippe C, Hallmann R, Hellstrand P, Rippe B, Swärd K. Arterial remodelling and plasma volume expansion in caveolin-1 deficient mice. *Am J Physiol Regul Integr Comp Physiol.* 2007; 293 (3):R1222-31. doi:10.1152/ajpregu.00092.2007 0363-6119/07
4. Alias L, Gallano P, Moreno D, Pujol R, Martínez-Matos JA, Baiget M, Ferrer I, Olivé M. A novel mutation in the caveolin-3 gene causingfamilial isolated hyperCKaemia. *Neuromuscul Disord*. 2004; 14: 321–324.
5. Bakircioglu ME. Sievert KD, Nunes L, Lau A, Lin CS, Lue TF. Decreased trabecular smooth muscle and caveolin-1 expression in the penile tissue of aged rats. *J. Urol*. 2001; 166, 734–738.
6. Bae JS, Ki CS, Kim JW, Suh YL, Park MS, Kim BJ, Kim SJ. A novel in-frame deletion in the CAV3 gene in a Korean patient with rippling muscle disease. *J Neurol Sci* 2007; 260: 275–278.
7. Bastiani M, Liu L, Hill MM, Jedrychowski MP, Nixon SJ, Lo HP, Abankwa D, Luetterforst R, Fernandez-Rojo M, Breen MR, Gygi SP, Vinten J, Walser PJ, North KN, Hancock JF, Pilch PF, Parton RG. MURC/Cavin-4 and cavin family members form tissue-specific caveolar complexes. *J Cell Biol.* 2009;185(7):1259-73.
8. Balijepalli RC, Kamp TJ. Caveolae, ion channels and cardiac arrhythmias. *Prog Biophys Mol Biol*. 2008;98(2-3):149-60.
9. Beech DJ. TRPC1:store-operated channel and more, *PflugersArch*. 2005; 451, 53–60.
10. Berardinelli W. Anundiagnosed endocrinometabolic syndrome: report of two cases. *J. Clin. Endocrinol. Metab*. 1954;14:193–204.
11. Bergdahl A, Gomez MF, Dreja K, Xu SZ, Adner M, Beech DJ, Broman J, Hellstrand P, Sward K. Cholesterol depletion impairs vascular reactivity to endothelin-1 by reducing store-operated Ca2+ entry dependent on TRPC1. *Circ Res.* 2003; 93, 839–847.
12. Bergdahl A, Swärd K. Caveolae-associated signalling in smooth muscle. *Can J Physiol Pharmacol*. 2004; 82(5):289-99.
13. Betz RC, Schoser BG, Kasper D, Ricker K, Ramírez A, Stein V, Torbergsen T, Lee YA, Nöthen MM, Wienker TF, Malin JP, Propping P, Reis A, Mortier W, Jentsch TJ, Vorgerd M, Kubisch C. Mutations in CAV3 cause mechanical hyperirritability of skeletal muscle in rippling muscle disease. *Nat Genet*. 2001; 28: 218–219
14. Brazer CS, Singh BB, Liu X, Swaim W, Ambudkar IS. Caveolin-1 contributes to assembly of store-operated Ca2+ influx channelsby regulating plasmamembrane localization of TRPC1. *J. Biol. Chem*. 2003; 278, 27208–27215.
15. Brown D, Rose JK. Sorting of GPI-anchored proteins to glycolipid-enriched membrane subdomains during transport to the apical cell surface. *Cell.*1992; 68, 533-544.
16. Brownlow SL, Sage SO. Transient receptor potential protein subunit assembly and membrane distribution in human platelets. *Thromb. Haemost*. 2005; 94, 839–845.
17. Carbone I, Bruno C, Sotgia F, Bado M, Broda P, Masetti E, Panella A, Zara F, Bricarelli FD, Cordone G, Lisanti MP, Minetti C. Mutation in the CAV3 gene causes partial caveolin-3 deficiency and hyperCKemia. *Neurology.* 2000; 54: 1373–1376.

18. Cassidy P, Harshman S. Characterization of detergent-solubilized iodine-125-labeled alpha-toxin bound to rabbit erythrocytes and mouse diaphragm muscle. *Biochemistry*. 1979;18(1):232-6.
19. Cherezov V, Rosenbaum DM, Hanson MA, Rasmussen SG, Thian FS, Kobilka TS, Choi HJ, Kuhn P, Weis WI, Kobilka BK, Stevens RC. High-resolution crystal structure of an engineered human beta2-adrenergic G protein-coupled receptor. *Science*. 2007; 318(5854):1258-65.
20. Cohen AW, Razani B, Wang XB, Combs TP, Williams TM, Scherer PE, Lisanti MPCaveolin-1-deficient mice show insulin resistance and defective insulin receptor protein expression in adipose tissue. *Am J Physiol Cell Physiol.* 2003; 285(1):C222-35.
21. Couet J, Sargiacomo M, Lisanti MP. Interaction of a receptor tyrosine kinase, EGF-R, with caveolins. Caveolin binding negatively regulates tyrosine and serine/threonine kinase activities. *J. Biol. Chem*. 1997; 272, 30429-38.
22. Cronk LB, Ye B, Kaku T, Tester DJ, Vatta M, Makielski JC, Ackerman MJ. Novel mechanism for sudden infant death syndrome: persistent late sodium current secondary to mutations in caveolin-3. *Heart Rhythm*. 2007; 4: 161–166.
23. Dart C. Lipid microdomains and the regulation of ion channel function. *J Physiol*. 2010; 588(17):3169-78.
24. Das K, Lewis RY, Scherer PE, Lisanti MP. The membrane- spanning domains of caveolins-1 and -2 mediate the formation of caveolin hetero-oligomers. Implications for the assembly of caveolae membranes in vivo. *J Biol Chem*. 1999; 274(26):18721-8.
25. Dietzen DJ, Hastings WR, Lublin DM. Caveolin is palmitoylated on multiple cysteine residues. Palmitoylation is not necessary for localization of caveolin to caveolae**.** *J. Biol. Chem*. 1995; 270, 6838-6842.
26. Desjardins F, Lobysheva I, Pelat M, Gallez B, Feron O, Dessy C, Balligand JL Control of blood pressure variability in caveolin-1-deficient mice: role of nitric oxide identified in vivo through spectral analysis. *Cardiovasc Res*. 2008;79(3):527-36.
27. Dotti MT, Malandrini A, Gambelli S, Salvadori C, De Stefano N, Federico A. A new missense mutation in caveolin-3 gene causes rippling muscle disease. *J Neurol Sci*. 2006; 243: 61–64.
28. Drab M, Verkade P, Elger M, Kasper M, Lohn M, Lauterbach B, Menne J, Lindschau C, Mende F, Luft FC, Schedl A, Haller H, Kurzchalia TV. Loss of caveolae, vascular dysfunction, and pulmonary defects in caveolin-1 gene-disrupted mice. *Science*. 2001; 293(5539):2449-52.
29. Dreja K, Voldstedlund M, Vinten J, Tranum-Jensen J, Hellstrand P, Swärd K.Cholesterol depletion disrupts caveolae and differentially impairs agonist-induced arterial contraction. *Arterioscler Thromb Vasc Biol*. 2002; 22: 1267-72.
30. Fee DB, So YT, Barraza C, Figueroa KP, Pulst SM: Phenotypic variability associated with Arg26Gln mutation in caveolin3. *Muscle Nerve*. 2004; 30: 375–378.
31. Feron O, Balligand JL. Caveolins and the regulation of endothelial nitric oxide synthase in the heart. *Cardiovasc Res*. 2006;69(4):788-97.
32. Feron O, Michel JB, Sase K, Michel T. Dynamic regulation of endothelial nitric oxide synthase: complementary roles of dual acylation and caveolin interactions. *Biochemistry*. 1998; 37(1):193-200.
33. Feron O, Smith TW, Michel T, Kelly RA. Dynamic targeting of the agonist-stimulated m2 muscarinic acetylcholine receptor to caveolae in cardiac myocytes. *J Biol Chem*. 1997; 272(28):17744-8.
34. Feske Y, Gwack Y, .Prakriya M, Srikanth S, Puppel SH, Tanasa B, Hogan PG, Lewis RS, Daly M, Rao A. A mutation in Orai1 causes immune deficiency by abrogating CRAC channel function. *Nature*. 2006; 441,179–185.
35. Fielding CJ, Fielding PE. Caveolae and intracellular trafficking of cholesterol. *Adv. Drug Deliv. Rev*. 2001; 49, 251–264.
36. Figarella-Branger D, Pouget J, Bernard R, Krahn M, Fernandez C, Lévy N, Pellissier JF. Limb-girdle muscular dystrophy in a 71-year-old woman with an R27Q mutation in the CAV3 gene. *Neurology*. 2003; 61:562–564.
37. Fischer D, Schroers A, Blümcke I, Urbach H, Zerres K, Mortier W, Vorgerd M, Schröder R. Consequences of a novel caveolin-3 mutation in a large German family. *Ann Neurol*. 2003;53(2):233-41.

38. Foster LJ, De Hoog CL, Mann M. Unbiased quantitative proteomics of lipid rafts reveals high specificity for signaling factors. *Proc Natl Acad Sci U S A*. 2003 ;100(10):5813-8.
39. Fu Y, Hoang A, Escher G, Parton RG, Krozowski Z, Sviridov D. Expression of caveolin-1 enhances cholesterol efflux in hepatic cells. *J Biol Chem*. 2004; 279, 14140–14146.
40. Fujimoto T. Calcium pump of the plasma membrane is localized in caveolae. *J Cell Biol*. 1993; 120, 1147–1157.
41. Fujimoto T, Kogo H, Nomura R, Une T. Isoforms of caveolin-1 and caveolar structure. *J Cell Sci.* 2000;113: 3509–3517
42. Fujimoto T, Nakade S, Miyawaki A, Mikoshiba K, Ogawa K. Localization of inositol 1,4,5-trisphosphate receptor-like protein in plasmalemmal caveolae. *J Cell Biol*. 1992; 119,1507–1513.
43. Fujita T, Toya Y, Iwatsubo K, Onda T, Kimura K, Umemura S, Ishikawa Y. Accumulation of molecules involved in alpha1-adrenergic signal within caveolae: caveolin expression and the development of cardiac hypertrophy. *Cardiovasc Res.* 2001;51:709–71
44. Fulizio L, Nascimbeni AC, Fanin M, Piluso G, Politano L, Nigro V, Angelini C. Molecular and muscle pathology in a series of caveolinopathy patients. *Hum Mutat*. 2005; 25: 82–89.
45. Gabella G. Caveolae intracellulares and sarcoplasmic reticulum in smooth muscle. *J Cell Sci*. 1971; 8, 601–609.
46. Gabella G, Blundell D. Effect of stretch and contraction on caveolae of smooth muscle cells. *Cell Tissue Res*. 1978; 190(2):255-71.
47. Galbiati F, Engelman JA, Volonte D, Zhang XL, Minetti C, Li M, Hou H Jr, Kneitz B, Edelmann W, Lisanti MP. Caveolin-3 null mice show a loss of caveolae, changes in the microdomain distribution of the dystrophin-glycoprotein complex, and t-tubule abnormalities. *J Biol Chem*. 2001;276(24):21425-33.
48. Galbiati F, Volonte D, Liu J, Capozza F, Frank PG, Zhu L, Pestell RG, Lisanti MP. Caveolin-1 negatively regulates cell cycle progression by inducing G(0)/G(1) arrest via p53/p21Waf/Cip1 dependent mechanism. *Mol Biol Cell*. 2001; 8, 2229-44.
49. Garg A. Acquired and inherited lipodystrophies. *N England Jour Med*. 2004;350(12):1220-34.
50. García-Cardeña G, Martasek P, Masters BS, Skidd PM, Couet J, Li S, Lisanti MP, Sessa WC. Dissecting the interaction between nitric oxide synthase (NOS) and caveolin. Functional significance of the nos caveolin binding domain in vivo. *J Biol Chem*. 1997;272(41):25437-40.
51. Gingras D, Gauthier F, Lamy S, Desrosiers RR, Beliveau R. Localization of RhoA GTPase to endothelial caveolae-enriched membrane domains. *Biochem Biophys Res Commun*. 1998; 247: 888-93.
52. Glenney JR. Tyrosin phosphorilation of 22-kDa protein is correlated with transformation by Rous sarcoma virus. *J Biolog Chem*. 1989; 264, 20163-20166.
53. Gosens R, Stelmack GL, Dueck G, Mutawe MM, Hinton M, McNeill KD, Paulson A, Dakshinamurti S, Gerthoffer WT, Thliveris JA, Unruh H, Zaagsma J, Halayko AJ. Caveolae facilitate muscarinic receptor-mediated intracellular Ca2+ mobilization and contraction in airway smooth muscle. *Am J Physiol Lung Cell Mol Physiol*. 2007;293(6):L1406-18.
54. Goto Y, Yoshikane H, Honda M, Morioka S, Yamori Y, Moriyama K. Three-dimensional observation on sarcoplasmic reticulum and caveolae in myocardium of spontaneously hypertensive rats. *J Submicrosc Cytol Pathol.* 1990;22(4):535-42.
55. Grände G, Rippe C, Rippe A, Rahman A, Swärd K, Rippe B. Unaltered size selectivity of the glomerular filtration barrier in caveolin-1 knockout mice. *Am J Physiol Renal Physiol*. 2009; 297(2):F257-62.
56. Gustavsson J, Parpal S, Karlsson M, Ramsing C, Thorn H, Borg M, Lindroth M, Peterson KH, Magnusson KE, Stralfors P. Localization of the insulin receptor in caveolae of adipocyte plasma membrane. *FASEB J*. 1999; 13 1961-1971.
57. Hagiwara Y, Sasaoka T, Araishi K, Imamura M, Yorifuji H, Nonaka I, Ozawa E, Kikuchi T. Caveolin-3 deficiency causes muscle degeneration in mice. *Hum Mol Genet.* 2000; 9(20):3047-54.
58. Hansen GG, Bright NA, Howard G, Nichols BJ. SDPR induces membrane curvature and functions in the formation of caveolae. *Nat Cell Biol.* 2009; 11(7): 807–814.

59. Hassan GS, Williams TM, Frank PG, Lisanti MP. Caveolin-1-deficient aortic smooth muscle cells show cell autonomous abnormalities in proliferation, migration, and endothelin-based signal transduction. *Am J Physiol Heart Circ Physiol*. 2006; 290: H2393-401.
60. Hayashi T, Arimura T, Ueda K, Shibata H, Hohda S, Takahashi M, Hori H, Koga Y, Oka N, Imaizumi T, Yasunami M, Kimura A. Identification and functional analysis of a caveolin-3 mutation associated with familial hypertrophic cardiomyopathy. *Biochem Biophys Res Commun*. 2004;313(1):178-84.
61. Hayashi YK, Matsuda C, Ogawa M, Goto K, Tominaga K, Mitsuhashi S, Park YE, Nonaka I, Hino-Fukuyo N, Haginoya K, Sugano H, Nishino I. Human PTRF mutations cause secondary deficiency of caveolins resulting in muscular dystrophy with generalized lipodystrophy. *J Clin Invest*. 2009;119(9):2623-33.
62. Hayer A, StoeberM, Bissig C, Helenius A. Biogenesis of caveolae: stepwise assembly of large caveolin and cavin complexes. *Traffic*. 2010; 11:361-368.
63. Hnasko R, Lisani MP. The biology of caveolae: lessons from caveolin knockout mice and implications for human disease. *Mol Interv*. 2003; 3(8):445-64.
64. Insel PA, Patel HH .Membrane rafts and caveolae in cardiovascular signaling. *Curr Opin Nephrol Hypertens*. 2009; 18(1):50-6.
65. Jansa, P., Mason, S. W., Hoffmann-Rohrer, U. and Grummt, I. Cloning and functional characterization of PTRF, a novel protein which induces dissociation of paused ternary transcription complexes. *EMBO J*. 1998;17, 2855–2864.
66. Je H.D, Gallant C, Leavis PC, Morgan KG. Caveolin-1 regulates contractility in differentiated vascular smooth muscle. *Am J Physiol Heart Circ Physiol*. 2004; 286: H91-8.
67. Kikuchi T, Oka N, Koga A, Miyazaki H, Ohmura H, Imaizumi T. Behavior of caveolae and caveolin-3 during the development of myocyte hypertrophy. *J Cardiovasc Pharmacol*. 2005;45(3):204-10.
68. Kim CA, Delépine M, Boutet E, El Mourabit H, Le Lay S, Meier M, Nemani M, Bridel E, Leite CC, Bertola DR, Semple RK, O'Rahilly S, Dugail I, Capeau J, Lathrop M, Magré J. Association of a homozygous nonsense caveolin-1 mutation with Berardinelli-Seip congenital lipodystrophy. *J Clin Endocrinol Metab*. 2008; 93(4):1129-34.
69. Kogo H, Ishiguro K, Kuwaki S, Fujimoto T. Identification of a splice variant of mouse caveolin-2 mRNA encoding an isoform lacking the C-terminal domain. *Arch Biochem Biophys.* 2002; 401: 108–114.
70. Kubisch C, Ketelsen UP, Goebel I, Omran H.Autosomal recessive rippling muscle disease with homozygous CAV3 mutations. *Ann Neurol*. 2005;57(2):303-4.
71. Kurzchalia TV, Dupree P, Parton RG, Kellner R, Virta H, Lehnert M, Simons K. VIP21, a 21-kD membrane protein is an integral component of trans-Golgi-network-derived transport vesicles. *J Cell Biol*. 1992;118, 1003-1014.
72. Labrecque L, Royal I, Surprenant DS, Patterson C, Gingras D, Beliveau R. Regulation of vascular endothelial growth factor receptor-2 activity by caveolin-1 and plasma membrane cholesterol. *Mol Biol Cell*. 2003; 14:334 –347.
73. Lajoie P, Goetz JG, Dennis JW, Nabi IR. Lattices, rafts, and scaffolds: domain regulation of receptor signaling at the plasma membrane. *Cell Biol.* 2009; 185(3):381-5.
74. Landh T. From entangled membranes to eclectic morphologies: cubic membranes as subcellular space organizers. *FEBS Lett*. 1995;369(1):13-7
75. Li S, Couet J, Lisanti MP. Src tyrosine kinases, Gα subunits, and H-Ras share a common membraneanchored scaffolding protein, caveolin. Caveolin binding negatively regulates the auto-activation of Src tyrosine kinases. *J Biol Chem*. 1996; 271, 29182–29190.
76. Li S, Okamoto T, Chun M, Sargiacomo M, Casanova JE, Hansen SH, Nishimoto I, Lisanti MP. Evidence for a regulated interaction between heterotrimeric G proteins and caveolin. *J Biol Chem*. 1995; 270(26):15693-701.
77. Linder AE, Leite R, Lauria K, Mills TM, Webb RC. Penile erection requires association of soluble guanylyl cyclase with endothelial caveolin-1 in rat corpus cavernosum. *Am J Physiol, Regul Integr Comp. Physiol*. 2006; 290, R1302–R1308.
78. Lisanti MP, Scherer PE, Tang Z, Sargiacomo M. Caveolae, caveolin and caveolin-rich membrane domains: a signalling hypothesis. *Trends Cell Biol*. 1994;4(7):231-5.

79. Liu P, Anderson RG. Compartmentalized production of ceramide at the cell surface, *J Biol Chem*. 1995; 270 (45)27179-85.
80. Liu P, Ying Y, Anderson RG. Platelet-derived growth factor activates mitogen-activated protein kinase in isolated caveolae. *Proc Natl Acad Sci U S A*. 1997; 94(25):13666-70.
81. Liu P, Ying Y, Ko YG, Anderson RG. Localization of platelet-derived growth factor-stimulated phosphorylation cascade to caveolae. *J Biol Chem*. 1996;271(17):10299-303
82. Liu L, Brown D, McKee M, Lebrasseur NK, Yang D, Albrecht KH, Ravid K, Pilch PF. Deletion of cavin/PTRF causes global loss of caveolae, dyslipidemia, and glucose intolerance. *Cell Metab*. 2008; 8(4): 310–317.
83. Livak KJ, Schmittgen TD. Analysis of relative gene expression data using real-time quantitative PCR and the 2(-Delta Delta C(T)) method. *Methods*. 2001; 25:402–408
84. Lockwich TP, Liu X.,Singh BB, Jadlowiec J, Weiland S, Ambudkar IS. Assembly of Trp1 in a signaling complex associated with caveolin-scaffolding lipid raft domains. *J Biol Chem*. 2000; 275, 11934–11942.
85. Magre´ J, Dele´pine M, Van Maldergem L, Robert JJ, Maassen JA, Meier M, Panz VR,AKC, Tubiana-Rufi N, Czernichow P, Seemanova E, Buchanan CR, Lacombe D, Vigouroux C, Lascols O, Kahn CR, Capeau J, Lathrop M. Prevalence of mutations in AGPAT2 among human lipodystrophies. *Diabetes*. 2003; 52:1573–1578.
86. Malmgren A, Sjögren C, Uvelius B, Mattiasson A, Andersson KE, Andersson PO. Cystometrical evaluation of bladder instability in rats with infravesical outflow obstruction. *J. Urol.* 1987; 137, 1291-1294.
87. Martens JR, Sakamoto N, Sullivan SA, Grobaski TD, Tamkun MM. Isoform-specific localization of voltage-gated K+ channels to distinct lipid raft populations. Targeting of Kv1.5 to caveolae. *J Biol Chem*. 2001; 276(11):8409-14.
88. Machleidt T, Li WP, Liu P, Anderson RG. Multiple domains in caveolin-1 control its intracellular traffic. *J Cell Biol*. 2000; 148(1):17-28.
89. Martens JR, Sakamoto N, Sullivan SA, Grobaski TD, Tamkun MM. Isoform-specific localization of voltage-gated K+ channels to distinct lipid raft populations. Targeting of Kv1.5 to caveolae. *J Biol Chem*. 2001;276(11):8409-14.
90. Martínez-Moreno M, Martínez-Ruiz A, Alvarez-Barrientos A, Gavilanes F, Lamas S, Rodríguez-Crespo I. Nitric oxide down-regulates caveolin-3 levels through the interaction with myogenin, its transcription factor. *J Biol Chem*. 2007; 282(32):23044-54.
91. Mattiasson, A., Uvelius, B. Changes in contractile properties in hypertrophic rat urinary bladder. *J Urol*. 1982; 128, 1340-1342.
92. Merlini L, Carbone I, Capanni C, Sabatelli P, Tortorelli S, Sotgia F, Lisanti MP, Bruno C, Minetti C. Familial isolated hyperCKaemia associated with a new mutation in the caveolin-3 (CAV-3) gene. *J Neurol Neurosurg Psychiatry.* 2002; 73:65–67.
93. Meshulam T, Simard JR, Wharton J, Hamilton JA, Pilch PF. Role of caveolin-1 and cholesterol in transmembrane fatty acid movement. *Biochemistry* 2006; 45, 2882–2893.
94. Meyer R, Stockem W, Schmitz M, Haas HG. Histochemical demonstration of an ATP-dependent Ca2+-pump in bullfrog myocardial cells. *Z Naturforsch C*. 1982; 37(5-6):489-501.
95. McMahon KA, Zajicek H, Li WP, Peyton MJ, Minna JD, Hernandez VJ, Luby-Phelps K, Anderson RG. SRBC/cavin-3 is a caveolin adapter protein that regulates caveolae function. *EMBO J.* 2009; 28(8):1001-15.
96. Michaely PA, Mineo C, Ying YS, and Anderson RG. Polarized distribution of endogenous Rac1 and RhoA at the cell surface. *J Biol Chem*. 1999; 274, 21430-6,
97. Mineo C, Gill GN, Anderson RG. Regulated migration of epidermal growth factor receptor from caveolae**.** *J Biol Chem*. 1999; 274(43):30636-43.
98. Mineo C, Ying YS, Chapline C, Jaken S, and Anderson RG. Targeting of protein kinase C alpha to caveolae. *J Cell Biol*. 1998; 141: 601–610.
99. Minetti C, Sotgia F, Bruno C, Scartezzini P, Broda P, Bado M, Masetti E, Mazzocco M, Egeo A, Donati MA, Volonte D, Galbiati F, Cordone G, Bricarelli FD, Lisanti MP, Zara F. Mutations in the caveolin-3 gene cause autosomal dominant limb-girdle muscular dystrophy. *Nat Genet.* 1998; 18(4):365-8.

100. Monier S, Dietzen DJ, Hastings WR, Lublin DM, Kurzchalia TV. Oligomerization of VIP21-caveolin in vitro is stabilized by long chain fatty acylation or cholesterol. *FEBS Lett.* 1996; 388(2-3):143-9.
101. Minshall RD, Malik AB. Transport across the endothelium: regulation of endothelial permeability. *Handb Exp Pharmacol*. 2006;176 (1):107-44.
102. Minshall RD, Niles WD, Tiruppathi C, Vogel SM, Gilchrist A, Hamm HE, Malik AB. Endothelial cell-surface gp60 activates vesicle formation and trafficking viaG(i)-coupled Src kinase signaling pathway. *J Cell Biol* .2000; 150, 1057–1069.
103. Morris JB, Huynh H, Vasilevski O, Woodcock EA. alpha(1)-Adrenergic receptor signaling is localized to caveolae in neonatal rat cardiomyocytes. *J Mol Cell Cardiol.* 2006; 41, 17–25.
104. Mulvany MJ. Small artery remodeling in hypertension. *Curr Hypertens Rep*. 2002; 4(1):49-55.
105. Mundy DI, Machleidt T, Ying YS, Anderson RG, Bloom GS. Dual control of caveolar membrane traffic by microtubules and the actin cytoskeleton. *J Cell Sci*. 2002; 115: 4327–4339
106. Murata T, Lin MI, Stan RV, Bauer PM, Yu J, Sessa WC. Genetic evidence supporting caveolae microdomain regulation of calcium entry in endothelial cells, *J Biol Chem*. 2007; 282, 16631–16643.
107. Murata M, Peränen J, Schreiner R, Wieland F, Kurzchalia TV, Simons K. VIP21/caveolin is a cholesterol-binding protein. *Proc Natl Acad Sci U S A*. 1995; 92(22):10339-43.
108. Murthy KS, Makhlouf GM. Heterologous desensitization mediated by G protein-specific binding to caveolin. *J Biol Chem*. 2000; 275(39):30211-9.
109. Ogata T, Ueyama T, Isodono K, Tagawa M, Takehara N, Kawashima T, Harada K, Takahashi T, Shioi T, Matsubara H, Oh H. MURC, a muscle-restricted coiled-coil protein that modulates the Rho/ROCK pathway, induces cardiac dysfunction and conduction disturbance. *Mol Cell Biol*. 2008: 28(10):3424-36.
110. Okamoto Y, Ninomiya H, Miwa S, Masaki T. Cholesterol oxidation switches the internalization pathway of endothelin receptor type A from caveolae to clathrin-coated pits in Chinese hamster ovary cells. *J Biol Chem*. 2000; 275(9):6439-46.
111. Ortegren U, Karlsson M, Blazic N, Blomqvist M, Nystrom FH, Gustavsson J, Fredman P, Strålfors P. Lipids and glycosphingolipids in caveolae and surrounding plasma membrane of rat primary adipocytes. *Eur,J. Biochemistry*. 2004; 271, 2028-2036.
112. Oshikawa J, Otsu K, Toya Y, Tsunematsu T, Hankins R, Kawabe J, Minamisawa S, Umemura S, Hagiwara Y, Ishikawa YInsulin resistance in skeletal muscles of caveolin-3-null mice. *Proc Natl Acad Sci U S A*. 2004;101(34):12670-5.
113. Ostrom RS, Insel PA. The evolving role of lipid rafts and caveolae in G protein-coupled receptor signaling: implications for molecular pharmacology. *Br J Pharmacol.* 2004;143(2):235-45
114. Ostrom RS, Liu X, Head BP, Gregorian C, Seasholtz TM, Insel PA. Localization of adenylyl cyclase isoforms and G protein-coupled receptors in vascular smooth muscle cells: expression in caveolin-rich and noncaveolin domains. *Mol Pharmacol*. 2002; 62(5):983-92.
115. Palade G.E. Fine structure of blood capillaries. *J Appl Phys.* 1953; 24,1424.
116. Pani B, Singh BB. Lipid rafts/caveolae as microdomains of calcium signaling. *Cell Calcium*. 2009;45(6):625
117. Park K, Kim SW, Rhu KS, Paick JS. Chronic administration of an oral Rho kinase inhibitor prevents the development of vasculogenic erectile dysfunction in a rat model. *J Sex Med*. 2006;3, 996–1003.
118. Parpal S, Karlsson M, Thorn H, Stralfors P. Cholesterol depletion disrupts caveolae and insulin receptor signaling for metabolic control via insulin receptor substrate-1, but not for mitogen-activated protein kinase control. *J Biol Chem*. 2001; 276, 9670-8.
119. Parton RG, Way M, Zorzi N, Stang E. Caveolin-3 associates with developing T-tubules during muscle differentiation. *J Cell Biol.* 1997; 136: 137–154.
120. Patel HH, Murray F, Insel PA. G-protein-coupled receptor-signaling components in membrane raft and caveolae microdomains. *Handb Exp Pharmacol*. 2008;(186):167-84.
121. Pelkmans L, Zerial M. Kinase-regulated quantal assemblies and kiss-and-run recycling of caveolae. *Nature.* 2005*;* 436:128–133.

122. Pelkmans L, Kartenbeck J, Helenius A. Caveolar endocytosis of simian virus 40 reveals a new two-step vesicular-transport pathway to the ER. *Nat Cell Biol*. 2001; 3(5):473-83.
123. Pike LJ, Casey L. Localization and turnover of phosphatidylinositol 4,5-bipohosphate in caveolin-enriched membrane domains. *J Biol Chem* . 1996;271; 26453-26456.
124. Pol A, Luetterforst R, Lindsay M, Heino S, Ikonen E, Parton RG.. A caveolin dominant negative mutant associates with lipid bodies and induces intracellular cholesterol imbalance. *J Cell Biol* 2001; 152, 1057–1070.
125. Pol A, Martin S, Fernandez MA, Ferguson C, Carozzi A, Luetterforst R, Enrich C, Parton RG. Dynamic and regulated association of caveolin with lipid bodies: modulation of lipid body motility and function by a dominant negative mutant. *Mol Biol Cell*. 2004; 15, 99–110.
126. Polyák E, Boopathi E, Mohanan S, Deng M, Zderic SA, Wein AJ, Chacko S. Alterations in Caveolin Expression and Ultrastructure After Bladder Smooth Muscle Hypertrophy. *J Urol*. 2009;182(5):2497-503
127. Rajab A, Straub V, McCann LJ, Seelow D, Varon R, Barresi R, Schulze A, Lucke B, Lützkendorf S, Karbasiyan M, Bachmann S, Spuler S, Schuelke M.Fatal cardiac arrhythmia and long-QT syndrome in a new form of congenital generalized lipodystrophy with muscle rippling (CGL4) due to PTRF-CAVIN mutations. *PLoS Genet.* 2010; 6(3):e1000874.
128. Rapacciuolo A, Suvarna S, Barki-Harrington L, Luttrell LM, Cong M, Lefkowitz RJ, Rockman HA. Protein kinase A and G protein-coupled receptor kinase phosphorylation mediates beta-1 adrenergic receptor endocytosis through different pathways. *J Biol Chem*. 2003; 278(37):35403-11.
129. Razani B, Engelman JA, Wang XB, Schubert W, Zhang XL, Marks CB, Macaluso F, Russell RG, Li M, Pestell RG, Di Vizio D, Hou H Jr, Kneitz B, Lagaud G, Christ GJ, Edelmann W, Lisanti MP. Caveolin-1 null mice are viable but show evidence of hyperproliferative and vascular abnormalities. *J Biol Chem*. 2001; 276(41):38121-38.
130. Razani B, Wang XB, Engelman JA, Battista M, Lagaud G, Zhang XL, Kneitz B, Hou H Jr, Christ GJ, Edelmann W, Lisanti MP. Caveolin-2-deficient mice show evidence of severe pulmonary dysfunction without disruption of caveolae. *Mol Cell Biol.* 2002; 22(7):2329-44.
131. Rêgo AG, Mesquita ET, Faria CA, Rêgo MA, Baracho Mde F, Santos MG, Egito ES, Brandão Neto J. Cardiometabolic Abnormalities in Patients with Berardinelli-Seip Syndrome. *Arq Bras Cardiol*. 2010;94(1):109-18.
132. Reijneveld JC, Ginjaar IB, Frankhuizen WS, Notermans NC: CAV3 gene mutation analysis in patients with idiopathic hyper-CK-emia. Muscle Nerve. 2006; 34: 656–658.
133. Rodrigues GJ, Restini CB, Lunardi CN, Neto Mdos A, Moreira JE, Bendhack LM. Eur J Pharmacol Decreased number of caveolae in endothelial cells impairs the relaxation induced by acetylcholine in hypertensive rat aortas. *Eur J Pharmacol*. 2010; 627(1-3):251-7.
134. Rosengren BI, Rippe A, Rippe C, Venturoli D, Swärd K, Rippe B. Transvascular protein transport in mice lacking endothelial caveolae. *Am J Physiol Heart Circ Physiol*. 2006; 291: H1371–H1377.
135. Rothberg KG, Heuser JE, Donzell WC, Ying YS, Glenney JR, Anderson RG. Caveolin, a protein component of caveolae membrane coats. *Cell*. 1992; 68(4):673-82.
136. Ruprecht JJ, Mielke T, Vogel R, Villa C, Schertler GF. Electron crystallography reveals the structure of metarhodopsin I. *EMBO J.* 2004; 23(18):3609-20.
137. Sbaa E, Frérart F, Feron O. The double regulation of endothelial nitric oxide synthase by caveolae and caveolin: a paradox solved through the study of angiogenesis. *Trends Cardiovasc Med*. 2005; 15(5):157-62.
138. Seip M. Lipodystrophy and gigantism with associated endocrine manifestations: a new diencephalic syndrome? *Acta Paediatr.* 1959;48:555–74
139. Sampson LJ, Hayabuchi Y, Standen NB, Dart C. Caveolae localized protein kinase A signaling to arterial ATP-sensitive potassium channels. *Circ Res*. 2004; 95, 1012– 8.
140. Shakirova Y, Bonnevier J, Albinsson S, Adner M, Rippe B, Broman J, Arner A, Swärd K. Increased Rho activation and PKC-mediated smooth muscle contractility in the absence of caveolin-1. *Am J Physiol Cell Physiol*. 2006;291(6):C1326-35. doi:10.1152/ajpcell.00046.2006.
141. Shakirova Y, Hedlund P, Swärd K. Impaired nerve-mediated relaxation of penile tissue from caveolin-1 deficient mice. *Eur J Pharmacol*. 2009; 602(2-3):399-405. doi:10.1016/j.ejphar.2008.11.033.

142. (a) Shakirova Y, Mori M, Ekman M, Erjefält J, Uvelius B, Swärd K. Human urinary bladder smooth muscle is dependent on membrane cholesterol for cholinergic activation. *Eur J Pharmacol. 2010; 634(1-3):142-8.* doi:10.1016/j.ejphar.2010.02.017.
143. (b) *Shakirova Y, Swärd K, Uvelius B, Ekman M. Functional and biochemical correlates of an increased membrane density of caveolae in hypertrophic rat urinary bladder. Eur J Pharmacol. 2010 Sep 22. [Epub ahead of print].* doi:10.1016/j.ejphar.2010.09.050
144. Shaul PW, Smart EJ, Robinson LJ, German Z, Yuhanna IS, Ying Y, Anderson RG, Michel T. Acylation targets emdothelial nitric-oxide synthase to plasmalemmal caveolae. *J Biol Chem*. 1996; 271(11):6518-22.
145. Scheiffele P, Verkade P, Fra AM, Virta H, Simons K, Ikonen E. Caveolin-1 and -2 in the exocytic pathway of MDCK cells. *J Cell Biol*. 1998; 140(4):795-806.
146. Scherer PE, Lewis RY, Volonte D, Engelman JA, Galbiati F, Couet J, Kohtz DS, van Donselaar E, Peters P, Lisanti MP. Cell-type and tissue-specific expression of caveolin-2. Caveolins 1 and 2 co-localize and form a stable hetero-oligomeric complex in vivo. *J Biol Chem*. 1997; 272(46):29337-46.
147. Scherer PE, Tang ZL, Chun MC, Sargiacomo M, Lodish HF, Lisanti, MP. Caveolin isoforms differ in their N-terminal protein sequence and subcellular distribution: identification and epitope mapping of an isoform-specific monoclonal antibody probe. *J Biol Chem*. 1997; 270: 16395–16401.
148. Schubert W, Sotgia F, Cohen AW, Capozza F, Bonuccelli G, Bruno C, Minetti C, Bonilla E, Dimauro S, Lisanti MP. Caveolin-1(-/-)- and caveolin-2(-/-)-deficient mice both display numerous skeletal muscle abnormalities, with tubular aggregate formation. *Am J Pathol*. 2007; 170(1):316-33.
149. Smart EJ, Ying YS, Mineo C, Anderson RG. A detergent-free method for purifying caveolae membrane from tissue culture cells. *Proc Natl Acad Sci U S A*. 1995; 92(22):10104-8.
150. Smith RM, Harada S, Smith JA, Zhang S, Jarett L. Insulin-Induced Protein Tyrosine Phosphorylation Cascade and Signalling Molecules Are Localized in a Caveolin-Enriched Cell Membrane Domain. *Cell Signal*.1998;10 355.
151. Schnitzer JE, Oh P, Pinney E, Allard J. Filipin-sensitive caveolae-mediated transport in endothelium: reduced transcytosis, scavenger endocytosis, and capillary permeability of select macromolecules. *J Cell Biol*. 1994; 127(5):1217-32.
152. Somlyo AP, Somlyo AV. Ca2+ sensitivity of smooth muscle and nonmuscle myosin II: modulated by G proteins, kinases, and myosin phosphatase. *Physiol Rev*. 2003; 83(4):1325-58.
153. Sotgia F, Razani B, Bonuccelli G, Schubert W, Battista M, Lee H, Capozza F, Schubert AL, Minetti C, Buckley JT, Lisanti MP. Intracellular retention of glycosylphosphatidyl inositol-linked proteins in caveolin-deficient cells. *Mol Cell Biol*. 2002; 22(11):3905-26.
154. Sjuve R, Boels PJ, Uvelius B, Arner A. Up-regulation of bradykinin response in rat and human bladder smooth muscle. *J. Urol*. 2000; 64, 1757-1763.
155. Sugie K, Murayama K, Noguchi S et al: Two novel CAV3 gene mutations in Japanese families. *Neuromuscul Disord* .2004; 14: 810–814.
156. Tang ZL, Scherer PE, Okamoto T, Song K, Chu C, Kohtz DS, Nishimoto I, Lodish HF, Lisanti MP. Molecular cloning of caveolin-3, a novel member of the caveolin gene family expressed predominantly in muscle. *J Biol Chem*. 1996;271: 2255–2261.
157. Tiruppathi C, Song W, Bergenfeldt M, Sass P, Malik AB.Gp60 activation mediates albumin transcytosis in endothelial cells by tyrosine kinase-dependent pathway. *J Biol Chem*. 1997;272(41):25968-75.
158. Van den Bergh PY, Gérard JM, Elosegi JA, Manto MU, Kubisch C, Schoser BG. Novel missense mutation in the caveolin-3 gene in a Belgian family with rippling muscle disease. *J Neurol Neurosurg Psychiatry*. 2004;75(9):1349-51.
159. Vatta M, Ackerman MJ, Ye B et al: Mutant caveolin-3 induces persistent late sodium current and is associated with long-QT syndrome. *Circulation*. 2006; 114:2104–2112.
160. Venema VJ, Ju H, Zou R, Venema RC. Interaction of neuronal nitric-oxide synthase with caveolin-3 in skeletal muscle. Identification of a novel caveolin scaffolding/inhibitory domain. *J Biol Chem*. 1997; 272(45):28187-90.
161. Vinten J, Johnsen AH, Roepstorff P, Harpøth J, Tranum-Jensen J. Identification of a major protein on the cytosolic face of caveolae. *Biochim Biophys Acta*. 2005;1717(1):34-40.

162. Vinten J, Voldstedlund M, Clausen H, Christiansen K, Carlsen J, Tranum-Jensen J. A 60-kDa protein abundant in adipocyte caveolae. *Cell Tissue Res*. 2001; 305(1):99-106.
163. Vogel SM, Minshall RD, Pilipovic M, Tiruppathi C, Malik AB. Activation of 60 kDa albumin-bindingprotein (gp60) stimulates albumintranscytosis in the intactpulmonary microvessel. *Am J Physiol*. 2001; 281,1512–1522.
164. Way M, Parton RG. M-caveolin, a muscle-specific caveolin-related protein. *FEBS Lett.* 1995;376, 108-112.
165. Woodman SE, Park DS, Cohen AW, Cheung MW, Chandra M, Shirani J, Tang B, Jelicks LA, Kitsis RN, Christ GJ, Factor SM, Tanowitz HB, Lisanti MP. Caveolin-3 knock-out mice develop a progressive cardiomyopathy and show hyperactivation of the p42/44 MAPK cascade. *J Biol Chem*. 2002;277(41):38988-97.
166. Wright CD, Chen Q, Baye NL, Huang Y, Healy CL, Kasinathan S, O'Connell TD. Nuclear alpha1-adrenergic receptors signal activated ERK localization to caveolae in adult cardiac myocytes. *Circ Res*. 2008;24;103(9):992-1000.
167. Wunderlich C, Schober K, Lange SA, Drab M, Braun-Dullaeus RC, Kasper M, Schwencke C, Schmeisser A, Strasser RH. Disruption of caveolin-1 leads to enhanced nitrosative stress and severe systolic and diastolic heart failure. *Biochem Biophys Res* Commun. 2006; 340: 702–708.
168. Wyse BD, Prior IA, Qian H, Morrow IC, Nixon S, Muncke C, Kurzchalia TV, Thomas WG, Parton RG, Hancock JF. Caveolin interacts with the angiotensin II type 1 receptor during exocytic transport but not at the plasma membrane. *J Biol Chem.* 2003; 278(26):23738-46.
169. Xie L, Frank PG, Lisanti MP, Sowa G. Endothelial cells isolated from caveolin-2 knockout mice display higher proliferation rate and cell cycle progression relative to their wild-type counterparts. *Am J Physiol Cell Physiol*. 2010; 298(3):C693-701.
170. Yamada, E. The fine structures of the gall bladder epithelium of the mouse. *J. Biophys. Biochem. Cytol*. 1995; 1, 445-458.
171. Yamamoto M, Toya Y, Jensen RA, Ishikawa Y. Caveolin is an inhibitor of platelet-derived growth factor receptor signaling. *Exp. Cell Res*. 1999; 247, 380.
172. Yamamoto M, Toya Y, Schwencke C, Lisanti MP, Myers MG, Jr , Ishikawa Y. Caveolin is an activator of insulin receptor signaling. *J Biol Chem* 1998; 273, 26962–68.
173. Zochbauer-Muller S, Fong KM, Geradts J, Xu X, Seidl S, End-Pfutzenreuter A, Lang G, Heller G, Zielinski CC, Gazdar AF, Minna JD. Expression of the candidate tumor suppressor gene hSRBC is frequently lost in primary lung cancers with and without DNA methylation. *Oncogene* 2005; 24: 6249–6255.

Paper I

Am J Physiol Cell Physiol 291: C1326–C1335, 2006;
doi:10.1152/ajpcell.00046.2006.

Increased Rho activation and PKC-mediated smooth muscle contractility in the absence of caveolin-1

Yulia Shakirova,[1] Johan Bonnevier,[1] Sebastian Albinsson,[1] Mikael Adner,[2] Bengt Rippe,[1] Jonas Broman,[1] Anders Arner,[3] and Karl Swärd[1]

[1]*Department of Experimental Medical Science, Lund University,* [2]*Department of Otorhinolaryngology, Malmö University Hospital, and* [3]*Department of Physiology and Pharmacology, Karolinska Institute, Stockholm*

Submitted 1 February 2006; accepted in final form 18 July 2006

Shakirova, Yulia, Johan Bonnevier, Sebastian Albinsson, Mikael Adner, Bengt Rippe, Jonas Broman, Anders Arner, and Karl Swärd. Increased Rho activation and PKC-mediated smooth muscle contractility in the absence of caveolin-1. *Am J Physiol Cell Physiol* 291: C1326–C1335, 2006; doi:10.1152/ajpcell.00046.2006.—Caveolae are omega-shaped membrane invaginations that are abundant in smooth muscle cells. Since many receptors and signaling proteins co-localize with caveolae, these have been proposed to integrate important signaling pathways. The aim of this study was to test whether RhoA/Rho-kinase and protein kinase C (PKC)-mediated Ca^{2+} sensitization depends on caveolae using caveolin (Cav)-1-deficient (KO) and wild-type (WT) mice. In WT smooth muscle, caveolae were detected and Cav-1, -2 and -3 proteins were expressed. Relative mRNA expression levels were ~15:1:1 for Cav-1, -2, and -3, respectively. Caveolae were absent in KO and reduced levels of Cav-2 and Cav-3 proteins were seen. In intact ileum longitudinal muscle, no differences in the responses to 5-HT or the muscarinic agonist carbachol were found, whereas contraction elicited by endothelin-1 was reduced. Rho activation by GTPγS was increased in KO compared with WT as shown using a pull-down assay. Following α-toxin permeabilization, no difference in Ca^{2+} sensitivity or in Ca^{2+} sensitization was detected. In KO femoral arteries, phorbol 12,13-dibutyrate (PDBu)-induced and PKC-mediated contraction was increased. This was associated with increased α_1-adrenergic contraction. Following inhibition of PKC, α_1-adrenergic contraction was normalized. PDBu-induced Ca^{2+} sensitization was not increased in permeabilized femoral arteries. In conclusion, Rho activation, but not Ca^{2+} sensitization, depends on caveolae in the ileum. Moreover, PKC driven arterial contraction is increased in the absence of caveolin-1. This depends on an intact plasma membrane and is not associated with altered Ca^{2+} sensitivity.

Ca^{2+} sensitization; Rho-associated kinase; myosin phosphatase target protein; lipid rafts; CPI-17; G protein-coupled receptor

CAVEOLAE are 50–100 nm flask-shaped membrane invaginations that are abundant in endothelial cells, adipocytes, and smooth muscle cells. Caveolae are characterized by high cholesterol and sphingolipid content, and a light buoyant density. They are stabilized by the caveolin proteins (9). Specific G protein-coupled and tyrosine kinase receptors, as well as downstream signaling intermediaries, have been shown to be caveolae associated (26, 30). Such clustering has been envisioned to facilitate receptor signaling and has been proposed to play a role in receptor internalization. The scaffolding domain of caveolin-1 (Cav-1) may also function as a broad-spectrum kinase inhibitor (9).

Compared with endothelial and adipocyte caveolae, smooth muscle caveolae have received relatively little attention. With the use of cholesterol depletion to disrupt caveolae in denuded caudal arteries from the rat, we demonstrated that serotonin ($5\text{-}HT_{2A}$) as well as endothelin-1 (ET-1) receptor signaling was impaired by cholesterol depletion. Moreover, restoration of caveolae by cholesterol replenishment recovered signaling from both receptors (3, 11). Cholesterol depletion was also shown to affect phasic but not tonic contraction in ureteric muscle (2), suggesting that raft/caveolae associated signaling influences specific steps in excitation-contraction coupling. Impaired contractile responses to ET-1, ANG II, and phorbol ester were found in arteries from Cav-1-deficient (KO) mice (10). The vessels did however, have intact endothelium, and the reduced contractility was interpreted to be secondary to enhanced nitric oxide synthase activity (29). In the urinary bladder, a general reduction of force on receptor stimulation was reported (37).

Downstream of receptor activation, RhoA, as well as Rho-kinase and protein kinase C (PKC) play key roles in regulation of contractility in smooth muscle (32). RhoA (15, 22, 34) and PKC (22, 32) have been shown to reside in or to translocate to caveolae on receptor stimulation. The scaffolding domain of Cav-1 was reported to impair both membrane translocation of PKC (34) and contraction stimulated by phorbol ester and α-agonist in the ferret aorta (16). Further support for a role of caveolae in PKC signaling is the finding that phosphoinositide turnover is compartmentalized in this membrane microdomain as shown using biochemical fractionation (27). Finally, Rho-kinase has been demonstrated to translocate to caveolae in a Ca^{2+}-calmodulin-dependent manner on smooth muscle depolarization (36). Taken together, these results suggest that caveolae may play a role in contractility and in regulation of Ca^{2+} sensitivity of contraction in smooth muscle (4).

In the present study, using KO mice, we investigate whether PKC and RhoA/Rho-kinase-mediated contractile mechanisms depend on caveolae. We have used longitudinal smooth muscle from the small intestine, which shows robust RhoA/Rho-kinase-mediated Ca^{2+} sensitization, but weak sensitization in response to PKC activation with phorbol ester (8, 21, 33), and femoral artery, which displays prominent Ca^{2+} sensitization in response to phorbol ester (8, 38).

MATERIALS AND METHODS

KO mice. Male KO mice were obtained from the Jackson Laboratory (Bar Harbor, ME), back-crossed six times onto the C57BL/6

Address for reprint requests and other correspondence: K. Swärd, Dept. of Experimental Medical Science, Lund Univ., BMC F12, SE-221 84 Lund, Sweden (e-mail: karl.sward@med.lu.se).

The costs of publication of this article were defrayed in part by the payment of page charges. The article must therefore be hereby marked "*advertisement*" in accordance with 18 U.S.C. Section 1734 solely to indicate this fact.

background, and genotyped as described by Razani et al. (28). Age-matched (10–15 wk) male C57BL/6 (Möllegard, Copenhagen, Denmark) were used as controls and are referred to as wild type (WT). Weights of KO and WT mice were 27.4 ± 0.9 and 27.3 ± 0.7 g, respectively. Mice were anesthetized with isoflurane and euthanized by cervical dislocation. The experiments were performed according to European guidelines for animal research and approved by the local animal ethics committee.

Preparation of intestine and femoral artery. The intestine and femoral artery were removed and placed in cold HEPES-buffered physiological saline solution (for composition, see below). Strips from the outer longitudinal small intestinal muscle layer were obtained by tearing the longitudinal layer off from the underlying circular layer (8).

Electron microscopy. Preparations were fixed in 2% glutaraldehyde and 1% paraformaldehyde in phosphate-buffered saline (PBS; pH 7.4, 300 mosM), postfixed in OsO_4, dehydrated, and embedded in Durcupan ACM (Fluka, Buchs, Switzerland). Ultrathin sections were examined with the use of transmission electron microscopy (3, 11).

Western blot analysis. Tissue preparations were frozen using clamps precooled in liquid N_2. Frozen tissue was pulverized and mixed with cold (4°C) SDS sample buffer, boiled, briefly centrifuged, and loaded on 15% polyacrylamide gels after the protein concentration using the Bio-Rad BC protein assay was determined. The SDS sample buffer contained 25 mM Tris·HCl (pH 6.8), 10% glycerol, 5% mercaptoethanol, 1 mg/ml bromophenol blue, 2% SDS, 30 mM DTT. Proteins were transferred to nitrocellulose membranes (Bio-Rad, Hercules, CA). After blocking, membranes were incubated with monoclonal antibodies against Cav-1, -2 or -3 (clones 2297, 65, and 26; BD Biosciences, Stockholm, Sweden). The β-actin antibody (1:5,000 dilution) was from Sigma (St. Louis, MO). ET-1 was detected using a monoclonal antibody from BD Biosciences (1:1,000). The PKC-α antibody (ab11723) was from Abcam. Anti-CPI-17 and anti-phosphorylated CPI-17 antibodies were from Santa Cruz Biotechnology (Santa Cruz, CA). P-CPI-17 was normalized to total CPI-17 in the same homogenate, and then, in each experiment, to the average CPI-17-P/CPI-17 ratio for all WT mice. Horseradish peroxidase-conjugated secondary antibodies were detected using enhanced chemiluminescence (the West Pico reagent for Cav-1, and the West Femto for Cav-2 and Cav-3; Pierce, Rockford, IL). For caveolins, identical exposure times were used to allow expression levels in the different tissues to be roughly compared.

mRNA study. Longitudinal muscle and lung parenchyma (for primer testing, see below) were rinsed with cold PBS and stored in RNAlater (QIAGEN, Hilden, Germany) at −20°C until homogenization and extraction of the total RNA using the RNeasy Mini kit (QIAGEN). The purity of total RNA was checked by a spectrophotometer and the wavelength absorption ratio (260/280 nm) was between 1.6 and 2.0 in all preparations. Reverse transcription of total RNA to cDNA was carried out using Omniscript reverse transcriptase kit (QIAGEN) in a 20-μl reaction volume at 37°C for 1 h by using Mastercycler personal PCR machine (Eppendorf, Hamburg, Germany).

Specific primers were designed by using Prime Express 2.0 software (Applied Biosystems, Foster City, CA) and synthesized by DNA Technology (Aarhus, Denmark). The sequences for Cav-1 (forward 5′-TGT ATG ACG CGC ACA CCA A-3′ and reverse 5′-TCC CTT CTG GTT CTG CAA TCA-3′), Cav-2 (forward 5′-GGC GTT GAC TAC GCA GAT CC-3′ and reverse 5′-GCA ATC AGA TCC TCG AAG CCT A-3′), Cav-3 (forward 5′-CCC AAG AAC ATC AAT GAG GAC A-3′and reverse 5′-GTG GTG AAG CTC ACC TTC CAT AC-3′) and β-actin (forward 5′-TGG GTC AGA AGG ACT CCT ATG TG-3′ and reverse 5′-CGT CCC AGT TGG TAA CAA TGC-3′) were all spanning over an intron.

Real-time PCR was performed on a Smart Cycler (Cepheid, Sunnyvale, CA) using QuantiTectTM SYBR Green PCR kit (QIAGEN). The thermal cycler was programmed to start with heating to 95°C for 15 min, followed by touchdown PCR, i.e., denature at 94°C for 30 sec and annealing at 66°C for 1 min for the first PCR cycle; thereafter, a decrease of 2°C for the annealing temperature in every cycle until 56°C was reached. Finally, 40 thermal cycles with 94°C for 30 s and 55°C for 1 min were performed. For primer testing, cDNA from lung parenchyma was diluted in half ^{10}log concentrations and the primers showed that the amplification was close to 2 (1.89–1.93).

Quantification of the gene expression was assessed with the comparative cycle threshold (C_t) method (http://docs.appliedbiosystems.com/pebiodocs/04303859.pdf). The relative amounts of mRNA for the caveolins were determined by subtracting the C_t values for these genes from the C_t value for the housekeeping gene β-actin (ΔC_t). Data are depicted as $2^{\Delta C_t} \times 10^5$.

Immunofluorescence staining of Cav-1 and -3. Tubular ileum segments were pulled over 20-μl plastic pipette tips, which were immersed in Histochoice (Amresco) for at least 4 h. After incubation in fixative, tissues were thoroughly washed in 70% ethanol and maintained therein at 4°C for at least 3 days, with three solution changes, until further processing. Following incubation in 96% (2 h) and 100% ethanol (1 h), 1:1 ethanol:xylene (30 min) and xylene (1 h), tissues were immersed in paraffin (2 × 1 h) and embedded. Sections measuring 10 μm were cut and deparaffinized. The sections were washed (2 × 30 min in PBS), permeabilized with 0.2% Triton X-100 for 15 min, blocked with 2% bovine serum albumin in PBS for 2 h, and incubated with primary antibodies in the same solution overnight at 4°C. Cav-1 and -3 antibodies (identical to those used for Western blot analysis) were used at dilutions of 1:125, and 1:1,000, respectively. After being washed in PBS, the sections were incubated with Cy5-labeled anti-mouse IgG for 1 h at room temperature. Nuclei were stained with DNA dye Sytox Green (1:3,000, Molecular Probes) after a brief washing in PBS. Pictures were obtained in a Zeiss LSM 510 confocal microscope. Caveolin proteins were detected by monitoring Cy5 fluorescence upon excitation at 633 nm. Sytox Green fluorescence was monitored upon excitation at 488 nm. Primary and secondary antibody omission controls verified specificity of staining (Fig. 3).

RhoA activation assay. RhoA activation was assayed using a kit from Upstate Biotechnology. Longitudinal ileum strips were homogenized in ice-cold lysis buffer containing 25 mM HEPES (pH 7.5), 150 mM NaCl, 10 mM $MgCl_2$, 1 mM EDTA, 1% Igepal CA-630, and 10% glycerol. After centrifugation at 14,000 *g* for 15 min, a small portion of the supernatant was removed for protein determination. The remaining supernatant was divided in two equal aliquots and 100 μM GTPγS was added to one of them. Activated RhoA was precipitated using the Rho-binding domain from Rhotekin coupled via GST to GSH beads. Loads and precipitates were analyzed by Western blotting using the antibody against Rho (A-C) supplied with the kit, or the Cav-1 and ET-1 antibodies described above.

Force recording, intact small intestinal preparations. Strips from the longitudinal muscle of the small intestine (7 mm long, 1.5 mm wide, and ~50 μm thick) were mounted in organ baths with the use of a thin silk thread between a stainless steel pin on an adjustable stand and a transducer (model FT03, Grass Instruments, Freeport, IL). Preparations were equilibrated in Krebs solution (for composition, see below) with 2.5 mM Ca^{2+} for 1 h at the optimal length for active force. The Krebs solution, pH of 7.4 at 37°C, was gassed with 95% O_2-5% CO_2. Force responses were expressed relative to the peak force of the high-K^+ (80 mM) contraction, recorded at the beginning of the experiment.

Force recording, intact femoral artery preparations. Intact femoral arteries were mounted in four-channel wire myographs (model 610M, Danish Myotechnology, Aarhus, Denmark), as described previously (3). A human hair was pulled through the arterial lumen to remove the endothelium and 300 μM N^{ω}-nitro-L-arginine methyl ester (L-NAME) was included in all solutions. Force was normalized to the tube length of the arterial segment. To get an estimate of the force per cross-sectional area (stress), force was multiplied by length (wire distance) and divided by wet weight. A complication was that the individual

preparations weighed too little (~60 μg) to weigh reliably with standard equipment. We therefore recorded force and length from four preparations and weighed them pooled together for one stress determination. Wet weight was obtained using a Mettler M3 balance after gentle blotting of the tissue on a filter paper.

Force recording, α-toxin-permeabilized preparations. Intestinal strips, 4-mm long, 1-mm wide, and 50-μm thick, were wrapped at both ends with aluminum foil. Femoral artery segments (2 mm long, cut as spiral strips from the media) were mounted on two 30 μm steel wires (31). All preparations were mounted horizontally between two tungsten wires, one of which was attached to a force transducer (model AE 801, SensoNor, Horten, Norway) and the other to a micrometer screw (8). Experiments were performed on "bubble plates" (140 μl solution) with stirring. Preparations were equilibrated in HEPES-buffered physiological saline solution and a high-K^+ (80 mM) test contraction was induced. Following relaxation, preparations were permeabilized with *Staphylococcus aureus* α-toxin (10,000 U/ml, Calbiochem-EMD Biosciences, San Diego, CA) for 60 min. Permeabilized preparations were treated with 10 μM A23187 for 20 min to deplete intracellular Ca^{2+} stores. Experiments were run at room temperature (22°C).

Solutions. The HEPES-buffered physiological saline solution for dissection contained (in mM) 135.5 NaCl, 5.9 KCl, 1.2 $MgCl_2$, 11.6 glucose, and 11.6 HEPES, pH 7.4. The Krebs solution, for experiments on intact small intestinal muscle tissue, contained (in mM) 122 NaCl, 4.7 KCl, 1.2 $MgCl_2$, 2.5 $CaCl_2$, 25 $NaHCO_3$, 1.2 KH_2PO_4, and 11.5 glucose. For permeabilized preparations, the relaxation solution (pCa 9) contained (in mM) 30 N-tris[hydroxymethyl]methyl-2-aminoethanesulfonic acid, 10 phosphocreatine, 5.14 Na_2ATP, 7.92 Mg-acetate, 46.6 K^+-methanesulfonate, 10 EGTA, and 1 DTE. The contraction solution (pCa 4.5) was made by replacing EGTA with Ca-EGTA. Ionic strength (0.15 M) and free [Mg^{2+}] (2 mM) were held constant by adjusting [K^+-methanesulfonate] and [Mg-acetate]. pH was adjusted to 7.1. Fixed free Ca^{2+} concentrations were obtained by mixing relaxation and contraction solutions.

Drugs. Y-27632 and microcystin-LR was obtained from Calbiochem-EMD Biosciences. All other drugs used were obtained from Sigma.

Statistics. Values are means ± SE. Unless stated otherwise, *n* refers to the number of mice. Statistical significance was determined using Student's *t*-test for unpaired data.

RESULTS

Caveolae. Caveolae were seen by electron microscopy in longitudinal smooth muscle from the WT mouse ileum (Fig. 1, *top left*, note arrowheads) and femoral artery (Fig. 1, *bottom left*). Caveolae were not found in longitudinal smooth muscle from KO mice (Fig. 1, *top right*). No caveolae were found in femoral artery smooth muscle cells from KO (Fig. 1, *bottom right*).

Caveolin detection by Western blot analysis. Cav-1 (α and β), Cav-2 (α and β), and Cav-3 were detected by Western blot analysis in WT longitudinal smooth muscle from the ileum (Fig. 2*A*). Cav-1 and Cav-2 were not detected in KO ileum (Fig. 2*A*). Reduced Cav-2 content in Cav-$1^{-/-}$ tissues has been reported previously (10, 28). In the KO ileum, expression of Cav-3 was also reduced (by 76 ± 6% vs. WT, $n = 7$, $P < 0.001$; Fig. 2*A*). Cav-1, Cav-2, and Cav-3 were absent, or exhibited considerably reduced expression, in the denuded femoral artery from KO (Fig. 2*B*). To verify reduced expression of Cav-3, which was unexpected, Cav-3 expression in the ileum was normalized to β-actin (Fig. 2*C*). This confirmed reduced contents in relation to a housekeeping protein in KO relative to WT ($n = 4$, $P < 0.05$). Dilutions of extracts, blotted

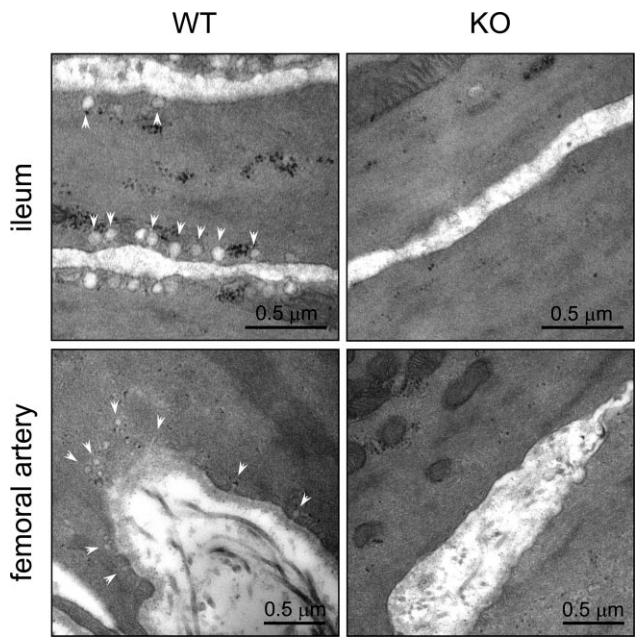

Fig. 1. Electron micrographs of small intestinal smooth muscle cells (longitudinal layer) and femoral artery smooth muscle cells from wild-type (WT) and caveolin-1 (Cav-1)-deficient (KO) mice. Arrows indicate caveolae.

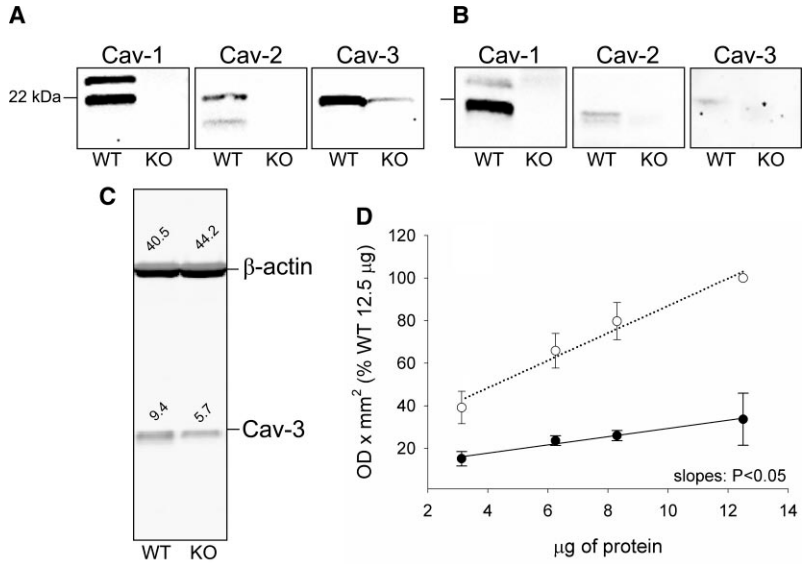

Fig. 2. *A*: Western blots of samples from WT and KO longitudinal smooth muscle from ileum, using antibodies against Cav-1, -2, and -3. Identical amounts of protein (20 μg) were loaded in all lanes ($n = 7$). *B*: blots using femoral artery homogenates ($n = 4$). *C*: to confirm reduced Cav-3 expression in the longitudinal smooth muscle from ileum and verify equal loading, Cav-3 and β-actin antibodies were used together ($n = 4$, $P < 0.05$ for Cav-3/β-actin ratio). Numbers above bands indicate optical density × mm^2 for the respective bands. *D*: regression lines of optical density × mm^2 for Cav-3 vs. micrograms of loaded protein in WT (○) and KO (●). Slopes were significantly reduced in KO vs. WT ($P < 0.05$, $n = 4$) verifying reduced Cav-3 in Cav-1-deficient smooth muscle.

for Cav-3, also verified reduced Cav-3 expression in the longitudinal smooth muscle from ileum (Fig. 2*D*).

Immunofluorescence staining of Cav-1 and Cav-3 in ileum. Cav-1 and Cav-3 were visualized by immunofluorescence. Cav-1 staining revealed 7–15 clusters per cell membrane profile (red in Fig. 3, *top left*) in ileum longitudinal smooth muscle. Cav-3 staining showed some degree of clustering along cell membrane profiles in WT muscle (Fig. 3). In KO, Cav-3 clustering was lost and staining appeared inside cells (Fig. 3).

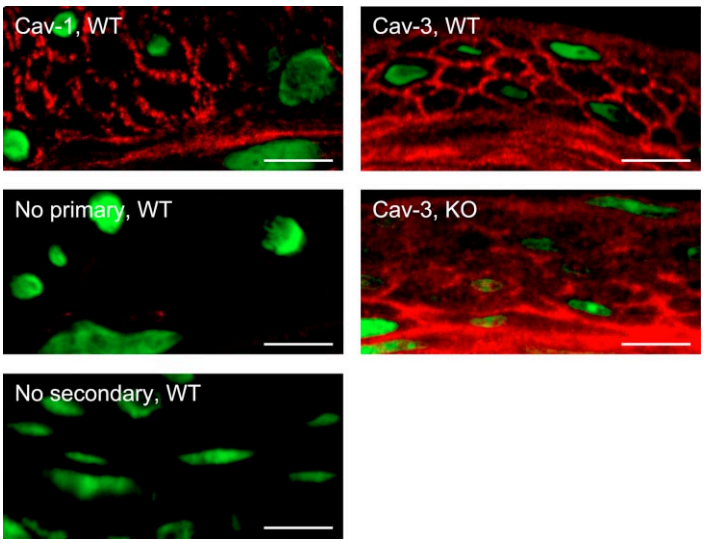

Fig. 3. Immunofluorescence staining of Cav-1 and Cav-3 (red) and nuclei (green) in paraffin embedded longitudinal ileum muscle from WT and KO mice. Visceral peritoneum is oriented upward and the longitudinal smooth muscle cells are cross-sectioned. *Top left*: caveolin-1 staining in WT. *Left middle and bottom*: omission controls. *Top right*: caveolin-3 staining in WT. *Right bottom*: Cav-3 staining in KO mice. Scale bars = 10 μm.

Quantitative real-time PCR. In WT longitudinal muscle Cav-1 mRNA levels were ~15-fold higher than those of Cav-2 and Cav-3 (Fig. 4). No differences in mRNA between WT and KO tissues were obtained for Cav-2. The mRNA levels for Cav-3 were lower in KO compared with WT longitudinal smooth muscle preparations but this difference did not reach significance ($P = 0.091$). The tissues used for PCR (Fig. 4) correspond with that used for blotting in Fig. 2*A*.

Contractile properties of intact longitudinal smooth muscle from the ileum. High-K^+ induced contractions were similar in WT and KO ileum longitudinal muscle (WT: 8.6 ± 0.4, KO 8.1 ± 0.9 mN, Krebs solution, 37°C, $n = 12$). Since WT and KO preparations were of similar sizes, these results suggest that active force generation in response to membrane depolarization is unchanged in KO.

Force responses to receptor agonists were examined in intact ileum strips. Original records are shown in Fig. 5*A*. Amplitudes of the carbachol and 5-HT responses were unchanged in the KO preparations (Fig. 5*B*). The EC_{50} values for carbachol in KO and WT ileum were not different (WT: 0.35 ± 0.08; KO: 0.34 ± 0.03 μM, $n = 8$), and contractions exhibited a rapid phase followed by sustained contraction in both KO and WT. Contractions in response to 10 nM ET-1 were reduced by 50% in small intestinal tissue from KO compared with WT mice (Fig. 5).

Rho activation in longitudinal smooth muscle from the ileum. RhoA plays an important role in the sustained phase of muscarinic contraction in the ileum (21). To assess activation of Rho in WT and KO ileum, a pull-down assay exploiting the specific GTP dependent association of Rho with the Rho-binding domain in Rhotekin coupled via GST to glutathione beads, was used (Fig. 6). Homogenates and precipitates were blotted for Rho, Cav-1, and ET-1 receptor A (ET_A). Rho was activated by GTPγS (Fig. 6*A*). Basal Rho-activity was below the detection limit (Fig. 6*B*). The Rho-activation level was increased in KO vs. WT muscle after incubation with GTPγS ($n = 5$, $P < 0.05$). Moreover, Cav-1 was precipitated together with Rho in WT but not in KO. Some ET_A receptor also coprecipitated with Rho. The amount of Rho (A, B, C) and ET_A was similar in WT and KO homogenates (Fig. 6*A*, *left lanes*). In six experiments on independent homogenates, ET_A receptor expression was 114 ± 13% in KO relative to WT ($P > 0.05$).

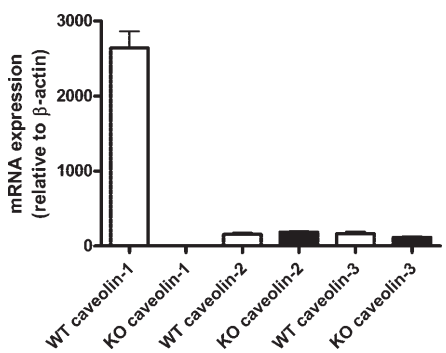

Fig. 4. Real-time PCR to assess the mRNA levels for Cav-1, -2, and -3 in dissected longitudinal smooth muscle from the mouse small intestine from WT and KO mice. mRNA is expressed in relation to the internal control gene β-actin as $2^{\Delta C_t} \times 10^5$ and presented as means ± SE ($n = 7$–8). C_t, cycle threshold.

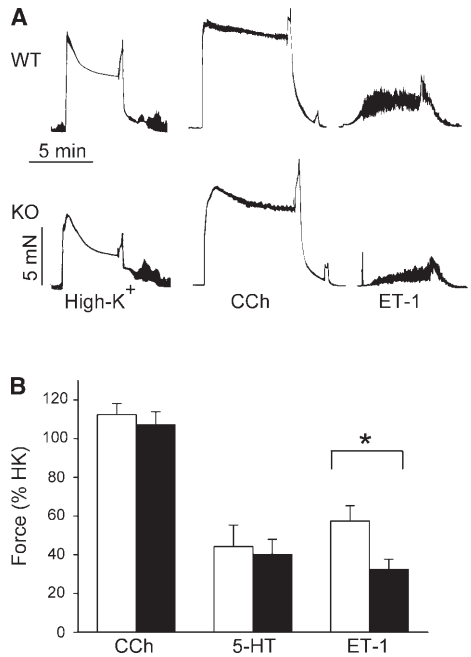

Fig. 5. *A*: original traces of force in longitudinal ileum muscle preparations from WT and KO animals. The preparations were activated with high-K^+ (80 mM KCl), 10 μM carbachol (CCh), and 10 nM endothelin-1 (ET-1). ET-1 gave rise to phasic contractions superimposed on a sustained contraction. *B*: mean values of the maximal force responses to 10 μM CCh, 1 μM 5-HT, and 10 nM ET-1 in intact longitudinal smooth muscle from the ileum of WT (open bars) and KO (solid bars) mice. Force is expressed relative to the peak of the high-K^+ responses. *$P < 0.05$, $n = 8$.

Force responses of α-toxin permeabilized longitudinal smooth muscle from the ileum. To examine whether Ca^{2+} sensitization might be affected in the absence of caveolae, we used α-toxin permeabilized smooth muscle. In the ileum, Rho/Rho-kinase mediated modulation of Ca^{2+} sensitivity is prominent and well characterized (8, 18, 33). The pCa-force relationships were identical in α-toxin permeabilized strips from WT and KO (Fig. 7*A*). Following a submaximal Ca^{2+} concentration (pCa 6.0), strips were stimulated with carbachol (10 μM; in the presence of 30 μM GTP) and GTPγS (10 μM). A maximal contraction was finally achieved by inhibiting the myosin phosphatase with 1 μM microcystin-LR. Ca^{2+} sensitization was not affected in KO compared with WT, irrespective of stimulus (Fig. 7*B*). Separate experiments showed that ET-1 (10 nM following 30 μM GTP) induced little or no Ca^{2+} sensitization in the mouse ileum (not shown).

To address the possibility that dependence of Ca^{2+} sensitization on Rho-kinase might be different in KO vs. WT, 30 μM of specific Rho-kinase inhibitor Y27632 was used. Y27632

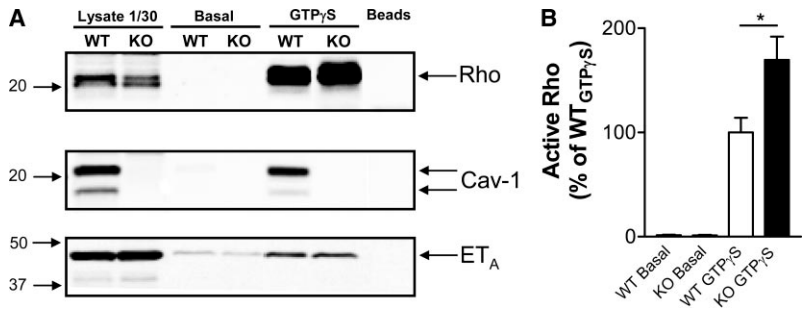

Fig. 6. Rho activation by GTPγS in ileum longitudinal smooth muscle assessed using a pulldown assay. *A*: equal amounts of protein from lysates of WT and KO longitudinal smooth muscle were loaded in the first two lanes. Lysates were then adjusted to contain identical amounts of protein and 30-fold more protein was used for precipitation. Precipitates after incubation with Rhotekin RBD beads and resuspended in identical volumes were loaded in the next four lanes. The last lane was loaded with Rhotekin RBD beads as a negative control. Top membrane was probed with an antibody against Rho (A, B, and C), middle membrane with an antibody vs. Cav-1, and bottom membrane with an antibody vs. the ET_A receptor. *B*: active Rho expressed as % of $WT_{GTP\gamma S}$. $^*P < 0.05$, $n = 5$.

inhibited GTPγS-induced contraction completely in both WT and KO mice (not shown).

PKC-mediated contraction in intact femoral arteries. Since PKC responses have been shown to depend on CPI-17 (19, 38), and the CPI-17 content is low in longitudinal smooth muscle from the ileum, we investigated whether PKC-mediated contraction was different using femoral arteries. In the femoral artery, the CPI-17 content is high and phorbol 12,13-dibutyrate (PDBu), which activates PKC, gives rise to a sizeable contraction (8). Experiments on denuded, but otherwise intact, ring preparations of the femoral artery were made in the continuous presence of 300 μM L-NAME to avoid residual nitric oxide synthesis. Following relaxation from contraction induced by 80 mM K^+ (HK), 1 μM PDBu was added (Fig. 8*A*). The time course of contraction in response to PDBu was slower in KO, but the level of force reached after 30 min was increased (Fig. 8, *A* and *B*, $n = 16$ WT and 16 KO preparations from 4 WT/KO pairs of mice, $P < 0.05$). After 30 min in the PDBu solution, the PKC inhibitor GF 109203X (GFX) was added in a cumulative manner (Fig. 8, *A* and *C*). The IC_{50} value for GFX was not different in KO vs. WT (0.31 ± 0.05 μM for WT and 0.40 ± 0.07 μM for KO, $P > 0.05$). Expression of PKC-α, as assessed by Western blot analysis, was not different in KO (KO: 106 ± 12% of WT, $n = 8$).

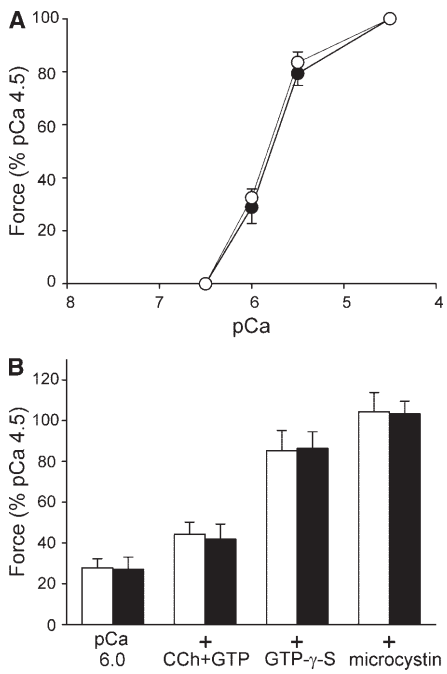

Fig. 7. Ca^{2+}-force relationships and Ca^{2+} sensitization in α-toxin-permeabilized longitudinal smooth muscle from WT (○) and KO (●) ileum. *A*: force expressed relative to force at pCa 4.5, plotted against free [Ca^{2+}] in pCa units ($n = 6$). *B*: force at pCa 6.0 (unsensitized contraction), and after Ca^{2+} sensitization induced by carbachol (10 μM CCh in the presence of 30 μM GTP), GTPγS (10 μM), and microcystin-LR (1 μM). WT (open bars) and KO (solid bars). $n = 6$.

α_1-Adrenergic responses in rabbit femoral artery are mediated in part by PKC (17). We compared the concentration response relations for the selective α_1-adrenergic receptor agonist cirazoline in WT and KO femoral arteries in the presence of L-NAME. The typical pattern was sustained contraction with little inactivation, such as that shown in Fig. 9*A*. Phasic repetitive activity sometimes occurred, and contraction often inactivated faster in WT than in KO in those cases. Force was averaged during the time that each concentration was maintained. Consistent with increased PKC-mediated contraction in KO, cirazoline responses were increased, both when expressed as absolute force (Fig. 9*B*), and following normalization to contraction induced by 80 mM K^+ (Fig. 9*C*), which was unchanged (bars in Fig. 9*B*). EC_{50} values for cirazoline were not different (0.17 ± 0.08 in KO vs. 0.36 ± 0.19 μM in WT, $n = 16$ preparations from 4 animals of each genotype; $P > 0.05$).

To measure stress, the length between attachments and the wet weight of the femoral artery preparations were determined. Wet weight per millimeter of tube length of femoral artery was greater in KO than in WT (42 ± 5 vs. 34 ± 4 μg/mm, $n =$

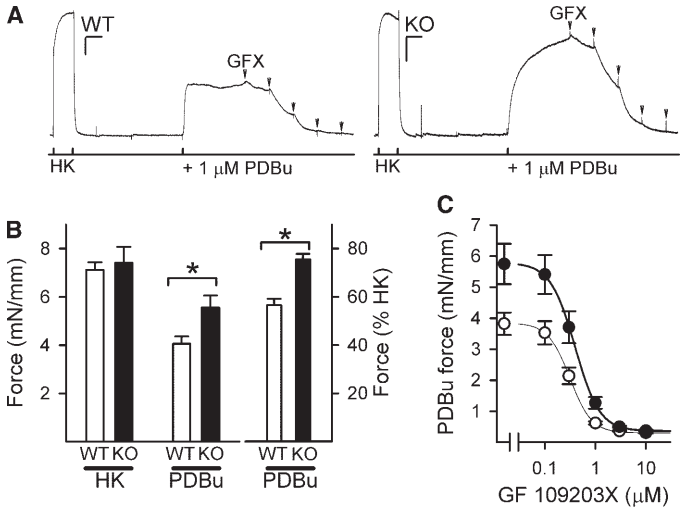

Fig. 8. *A*: original records of contraction in response to phorbol ester in intact femoral arteries from WT and KO. Following depolarization with 80 mM K^+ (HK), arteries were incubated with phorbol 12, 13-dibutyrate (PDBu; 1 μM) for 30 min. The protein kinase C inhibitor GF 109203X was subsequently added in a cumulative manner. Horizontal and vertical calibration bars represent 1 mN/mm and 5 min, respectively. 300 μM N^{ω}-nitro-L-arginine methyl ester (L-NAME) was present throughout. *B*: summarized force data, expressed as mN/mm (*left*), and as a percentage of HK (*right*) for WT (open bars) and KO (solid bars). *C*: compiled data from the concentration response experiments with GF 109203X (WT, ○; KO, ●). $n = 16$ and 16 preparations, respectively, from 4 WT/KO pairs.

10 mice of each genotype; $P < 0.001$). Consequently, stress was lower in response to depolarization in KO compared with WT, whereas the cirazoline-induced stress was unchanged (Fig. 9*D*).

α_1-Adrenergic contraction was next examined in the presence of the PKC inhibitor GFX. Cirazoline-induced force was not different following PKC inhibition ($n = 8$ preparations from 2 WT/KO pairs; Fig. 9*E*). Vehicle-treated preparations from the same animals confirmed the difference in cirazoline-induced force between WT and KO.

PKC mediated contraction in permeabilized femoral arteries. To address whether increased PDBu-induced and PKC-mediated contraction was due to increased Ca^{2+} sensitization, α-toxin-permeabilized spiral strips from the femoral artery

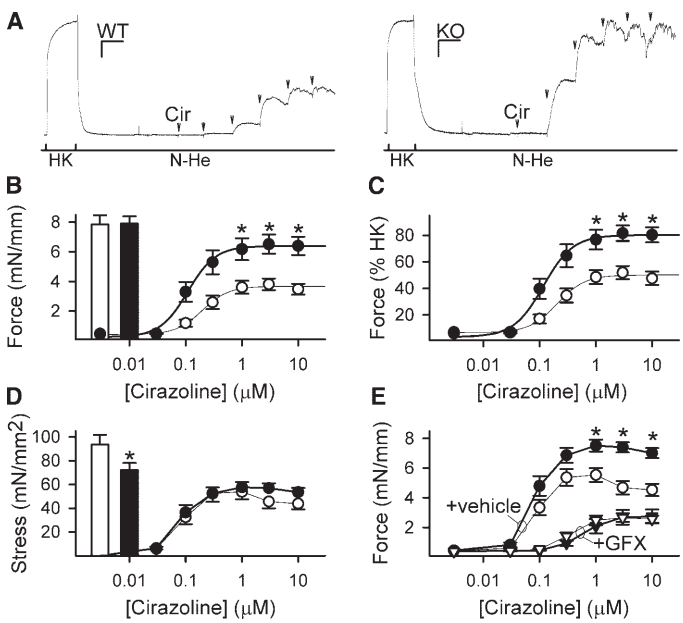

Fig. 9. *A*: concentration response relationships for the α_1 adrenergic receptor agonist cirazoline (Cir) in intact femoral arteries from WT and KO mice. Horizontal and vertical calibration bars represent 1 mN/mm and 5 min, respectively. 300 μM L-NAME was present throughout. *B*: summarized force data, expressed as mN/mm, during the concentration response experiments depicted in *A*. Bars in *B* show force in response to 80 mM K^+ in WT (open) and KO (solid). *C*: force in WT (○) and KO (●) expressed instead as a percentage of 80 mM K^+ contraction. $n = 16$ and 16 preparations, respectively, from 4 WT/KO pairs. *D*: force expressed as stress. Cross-sectional area was obtained from the weight and distance between attachments. $n = 40$ preparations pooled in 10 groups from 10 mice of each genotype. *E*: concentration response relations for cirazoline in the presence (▽) and absence (○) of the protein kinase C inhibitor GF 109203X (5 μM). $n = 8$ preparations from 2 mice of each genotype for both treatments. *$P < 0.05$ for KO vs. WT comparison.

were used. Force was normalized to a reference (pCa 4.5) contraction. The response to an intermediate Ca^{2+} concentration (pCa = 6.5) was similar in strips from WT and KO mice. Moreover, the addition of increasing amounts of PDBu caused Ca^{2+} sensitization that was identical in WT and KO (Fig. 10, *A* and *B*). Results were the same when data was normalized to depolarization-induced contraction obtained before permeabilization (not shown). Phosphorylation of CPI-17 was similar in intact preparations from WT and KO after 30-min incubation with 1 μM PDBu (WT: 100 ± 9%, KO: 102 ± 10%, $n = 4$).

DISCUSSION

In this study, we show that Rho activation and PKC mediated contraction of smooth muscle is increased in the absence of caveolae and Cav-1. Ablation of caveolae attenuated endothelin-induced contraction in the ileum, without influencing muscarinic or serotonergic force. Increased Rho activation and PKC-mediated contraction may occur in other cell types, including endothelial cells and fibroblasts.

All caveolin family members were expressed in smooth muscle. In agreement with previous studies (10, 28, 37), ablation of Cav-1 was associated with reduction of the Cav-2 protein(s). We also made the unexpected observation that the Cav-3 protein content was reduced and its distribution altered in KO mice. The relative mRNA abundance for Cav-1, -2, and -3 was found to be 15:1:1 in the ileum. This suggests that an absolute minority (7%) of caveolae in WT intestinal smooth muscle are Cav-3 driven. The relative levels of expression, the intracellular Cav-3 accumulation, and the observed reduction of Cav-3 protein, probably all explain the apparent absence of caveolae in electron micrographs from KO tissue. The basis of the reduced Cav-3 protein expression is unclear. Cav-3 mRNA levels were not different, which suggests a mechanism involving Cav-3 protein degradation. Importantly, however, the apparent absence of caveolae and the reduced membrane association of Cav-3 in the KO argue against the possibility that the remaining Cav-3 compensates for the lack of Cav-1 in smooth muscle.

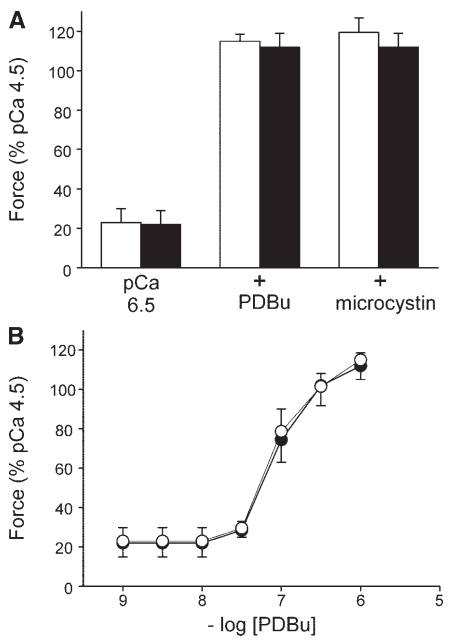

Fig. 10. Ca^{2+} sensitivity and Ca^{2+} sensitization of force in femoral arteries. *A*: α-toxin permeabilized femoral artery strips from WT (open bars) and KO (solid bars) at intermediate [Ca^{2+}] (pCa 6.5), activated with PDBu (1 μM) or the phosphatase inhibitor microcystin-LR (1 μM). Force is expressed relative to a reference (pCa 4.5) contraction. *B*: force at increasing PDBu concentrations in femoral arteries activated at pCa 6.5, $n = 4$ preparations from 4 mice of each genotype.

Caveolae have been suggested to play a role in signaling from smooth muscle ET-1 and 5-HT_{2A} receptors (3, 6, 11). M_2 muscarinic receptors have been shown to translocate to caveolae on agonist binding which was suggested to be important for downstream signaling (12). Finally, caveolae have been proposed to play a role in M_2 and M_3 receptor desensitization (25). In support of a role of caveolae in muscarinic signaling, contraction was found to be selectively impaired (by 70%) in the bladder of KO mice (20), although another study suggested a reduction of contraction elicited by both carbachol and KCl in the bladder (37). We find that contractions in response to 5-HT and the muscarinic agonist carbachol are unchanged in intestinal muscle lacking caveolae when expressed relative to a reference high-K^+ contraction. Serotonergic contractions of longitudinal smooth muscle from the small intestine have been reported to be due to 5-HT_1 and 5-HT_3 receptors (39). The contribution to contraction of 5-HT_{2A} receptors, which may be caveolae associated (6, 11, 13), could thus be small in the ileum longitudinal smooth muscle.

It may be relevant in regard to endothelin-induced contraction that both ET_A and ET_B receptors have been proposed to depend on caveolae (3, 35). The present results showed that impaired contractility in response to ET-1 in the ileum was not associated with reduced ET-1 receptor expression, nor was it due to reduced Ca^{2+} sensitization. Further studies of endothelin signaling in the absence of caveolae seem warranted.

On the basis of the reported translocation to caveolae of key components of Ca^{2+} sensitization, we formulated the hypothesis that Ca^{2+} sensitization would be affected in the absence of caveolae. Our results confirm the association between Rho and Cav-1 that was previously observed in endothelial cells and fibroblasts (15, 22). This interaction appears to be functionally inhibitory since Rho activation was greater in KO. Our data on permeabilized ileum suggest, however, that Ca^{2+}-sensitization proceeds normally in permeabilized muscle without caveolae and Cav-1. It therefore has to be assumed that GTPγS-induced Ca^{2+} sensitization is not limited by Rho activation in the mouse ileum. Alternatively, Rho activation by ligand plus GTP may not be changed. We also failed to detect a difference in the sustained phase of carbachol contraction, which is known to depend on RhoA/Rho-kinase (21, 33). This indicates that Ca^{2+} sensitization is unchanged in situ in the absence of caveolae. A modest change in stress (force per cross-sectional area) cannot be ruled out, nor can it be ruled out that Ca^{2+}-sensitization mechanisms have adapted by a fine tuning of the expression of downstream intermediaries, but caveolae and Cav-1 are clearly

not required for a functional pathway, albeit subtly affecting maximal RhoA activation.

PKC-mediated contraction in the intact femoral artery was increased in the KO relative to the WT. PKC protein expression was not changed as shown directly for PKC-α, and as suggested by the Ca^{2+}-sensitization study. The data is thus compatible with the removal of an inhibitory influence of Cav-1 similar to the situation with Rho. Moreover, α_1-adrenergic contraction was increased as expected for a response mediated partly by PKC. α_1-Adrenergic contraction was not enhanced following inhibition of PKC; thus creating a strong argument that enhanced PKC signaling in KO compared with WT indeed underlies the increased α_1-adrenergic contraction. The unchanged Ca^{2+} sensitization following permeabilization, and the unchanged phosphorylation of CPI-17, demonstrate that the increased PKC-induced contraction is due to a membrane-delimited mechanism. It seems reasonable to propose that Cav-1 is effective as a kinase inhibitor only in the sarcolemma, where it is located, and not intracellularly, where substrates such as CPI-17 are found. A variety of membrane-associated effector mechanisms, which could mediate the PKC effect, have been described. Examples include the delayed rectifier current (1), K_{ATP} channels (5), and Ca^{2+} sparks (7), all of which are bypassed in the α-toxin permeabilized preparations. It is notable that the frequency of spontaneous transient outward currents, which are activated by Ca^{2+} sparks, are reduced in cerebral arterial myocytes from Cav-1-deficient mice (10). Whether this reduction is normalized by PKC inhibition is not known.

The possible association of α_1-adrenergic receptors with caveolae is controversial. We previously examined the distribution of α_{1A}-receptors in sucrose density gradients of smooth muscle homogenates from the rat caudal artery, and found that the α_{1A}-receptors were present in the fractions of highest density, contrasting with $5HT_{2A}$ receptors which were present in the lighter caveolin-containing fractions (11). On the other hand, binding of isotope-labeled phenylephrin and prazosin to caveolin-containing sucrose gradient fractions from heart and aorta was observed by others (14, 24). The latter studies support a caveolar association of α_1-receptors in those specific cells and tissues. The present data does not distinguish between the possible α_1-receptor locales, which may be tissue and receptor subtype specific. Alleviated inhibition of PKC by caveolin at the membrane is sufficient to explain the present results in the femoral artery.

Measurements of stress (force per cross-sectional area), using traditional methodology involving weighing, showed that depolarization-induced stress was reduced in KO compared with WT femoral arteries. This was due to a significant increase in the wet weight per mm length of femoral artery rather than a change in depolarization induced force. A detailed morphometric analysis needs to be made to justify such a stress calculation, because the increased wet weight may be due to increased extracellular matrix or increased adventitial cell populations. Moreover, force per length of arterial tube, not stress, is the relevant variable for regulation of peripheral resistance. In permeabilized tissue it is notoriously difficult to minimize experimental variation in stress and absolute force determinations. This is because cutting of strips involves considerable handling that may harm the tissue, the small weight of the preparations (≈60 μg), and because the success of permeabilization varies. We can therefore not rule out changes in stress or absolute force in the permeabilized strips. Our data in intact tissue justifies normalization to a reference contraction, however, and the unchanged phosphorylation of CPI-17 independently shows that PKC-driven Ca^{2+} sensitization is unaltered in the absence of caveolae.

Our results concerning PKC-mediated contraction are fully compatible with the inhibitory effect seen after chemical loading of the scaffolding domain peptide from Cav-1 in the intact ferret aorta (16).

In conclusion, PKC mediated contraction and Rho activation but not Ca^{2+}-sensitization are increased in smooth muscle following genetic ablation of Cav-1. Increased RhoA activation and PKC-driven force generation in the absence of caveolae may play a role in contractility or motility in many cell types, including, apart from smooth muscle cells, endothelial cells and fibroblasts.

ACKNOWLEDGMENTS

We thank Ingegerd Larsson for technical assistance in the mRNA study, Gunnel Roos for genotyping, Karin Jansner for advice regarding histology, and Prof. Rupert Hallmann for advice, support, and help with establishing the Cav-1-deficient mouse colony.

GRANTS

This study was supported by Swedish Research Council Grants 71X-14955 (to K. Swärd), 04X-8268 (to A. Arner), 04X-08285–17A (to B. Rippe), funds from the Crafoord, Åke Wiberg, and Magnus Bergvall foundations (to K. Swärd), the Royal Physiographic Society (K. Swärd), and the Swedish Heart-Lung foundation (to K. Swärd and A. Arner). This study was supported by a program grant from the Ragnar Söderberg foundation to the Vascular Wall Program at Lund University.

REFERENCES

1. **Aiello EA, Clement-Chomienne O, Sontag DP, Walsh MP, and Cole WC.** Protein kinase C inhibits delayed rectifier K^+ current in rabbit vascular smooth muscle cells. *Am J Physiol Heart Circ Physiol* 271: H109–H119, 1996.
2. **Babiychuk EB, Smith RD, Burdyga T, Babiychuk VS, Wray S, and Draeger A.** Membrane cholesterol regulates smooth muscle phasic contraction. *J Membr Biol* 198: 95–101, 2004.
3. **Bergdahl A, Gomez MF, Dreja K, Xu SZ, Adner M, Beech DJ, Broman J, Hellstrand P, and Swärd K.** Cholesterol depletion impairs vascular reactivity to endothelin-1 by reducing store-operated Ca^{2+} entry dependent on TRPC1. *Circ Res* 93: 839–847, 2003.
4. **Bergdahl A and Swärd K.** Caveolae-associated signalling in smooth muscle. *Can J Physiol Pharmacol* 82: 289–299, 2004.
5. **Cole WC, Malcolm T, Walsh MP, and Light PE.** Inhibition by protein kinase C of the K(NDP) subtype of vascular smooth muscle ATP-sensitive potassium channel. *Circ Res* 87: 112–117, 2000.
6. **Bhatnagar A, Sheffler DJ, Kroeze WK, Compton-Toth B, and Roth BL.** Caveolin-1 interacts with 5-HT2A serotonin receptors and profoundly modulates the signaling of selected Gαq-coupled protein receptors. *J Biol Chem* 279: 34614–23, 2004.
7. **Bonev AD, Jaggar JH, Rubart M, and Nelson MT.** Activators of protein kinase C decrease Ca^{2+} spark frequency in smooth muscle cells from cerebral arteries. *Am J Physiol Cell Physiol* 273: C2090–C2095, 1997.
8. **Bonnevier J and Arner A.** Actions downstream of cyclic GMP/protein kinase G can reverse protein kinase C-mediated phosphorylation of CPI-17 and Ca^{2+} sensitization in smooth muscle. *J Biol Chem* 279: 28998–29003, 2004.
9. **Cohen AW, Hnasko R, Schubert W, and Lisanti MP.** Role of caveolae and caveolins in health and disease. *Physiol Rev* 84: 1341–1379, 2004.
10. **Drab M, Verkade P, Elger M, Kasper M, Löhn M, Lauterbach B, Menne J, Lindschau C, Mende F, Luft FC, Schedl A, Haller H, and Kurzchalia TV.** Loss of caveolae, vascular dysfunction, and pulmonary defects in caveolin-1 gene-disrupted mice. *Science* 293: 2449–2452, 2001.
11. **Dreja K, Voldstedlund M, Vinten J, Tranum-Jensen J, Hellstrand P, and Swärd K.** Cholesterol depletion disrupts caveolae and differentially

impairs agonist-induced arterial contraction. *Arterioscler Thromb Vasc Biol* 22: 1267–72, 2002.
12. **Feron O, Smith TW, Michel T, and Kelly RA.** Dynamic targeting of the agonist-stimulated m2 muscarinic acetylcholine receptor to caveolae in cardiac myocytes. *J Biol Chem* 272: 17744–8, 1997.
13. **Fiorica-Howells E, Hen R, Gingrich J, Li Z, and Gershon MD.** 5-HT_{2A} receptors: location and functional analysis in intestines of wild-type and 5-HT_{2A} knockout mice. *Am J Physiol Gastrointest Liver Physiol* 282: G877–G893, 2002.
14. **Fujita T, Toya Y, Iwatsubo K, Onda T, Kimura K, Umemura S, and Ishikawa Y.** Accumulation of molecules involved in alpha1-adrenergic signal within caveolae: caveolin expression and the development of cardiac hypertrophy. *Cardiovasc Res* 51: 709–716, 2001.
15. **Gingras D, Gauthier F, Lamy S, Desrosiers RR, and Beliveau R.** Localization of RhoA GTPase to endothelial caveolae-enriched membrane domains. *Biochem Biophys Res Commun* 247: 888–893, 1998.
16. **Je HD, Gallant C, Leavis PC, and Morgan KG.** Caveolin-1 regulates contractility in differentiated vascular smooth muscle. *Am J Physiol Heart Circ Physiol* 286: H91–H98, 2004.
17. **Kitazawa T, Eto M, Woodsome TP, and Brautigan DL.** Agonists trigger G protein-mediated activation of the CPI-17 inhibitor phosphoprotein of myosin light chain phosphatase to enhance vascular smooth muscle contractility. *J Biol Chem* 275: 9897–9900, 2000.
18. **Kitazawa T, Gaylinn BD, Denney GH, and Somlyo AP.** G-protein-mediated Ca^{2+} sensitization of smooth muscle contraction through myosin light chain phosphorylation. *J Biol Chem* 266: 1708–1715, 1991.
19. **Kitazawa T, Takizawa N, Ikebe M, and Eto M.** Reconstitution of protein kinase C-induced contractile Ca^{2+} sensitization in triton X-100-demembranated rabbit arterial smooth muscle. *J Physiol* 520: 139–152, 1999.
20. **Lai HH, Boone TB, Yang G, Smith CP, Kiss S, Thompson TC, and Somogyi GT.** Loss of caveolin-1 expression is associated with disruption of muscarinic cholinergic activities in the urinary bladder. *Neurochem Int* 45: 1185–1193, 2004.
21. **Lucius C, Arner A, Steusloff A, Troschka M, Hofmann F, Aktories K, and Pfitzer G.** Clostridium difficile toxin B inhibits carbachol-induced force and myosin light chain phosphorylation in guinea-pig smooth muscle: role of Rho proteins. *J Physiol* 506: 83–93, 1998.
22. **Michaely PA, Mineo C, Ying YS, and Anderson RG.** Polarized distribution of endogenous Rac1 and RhoA at the cell surface. *J Biol Chem* 274: 21430–21436, 1999.
23. **Mineo C, Ying YS, Chapline C, Jaken S, and Anderson RG.** Targeting of protein kinase Calpha to caveolae. *J Cell Biol* 141: 601–610, 1998.
24. **Morris JB, Huynh H, Vasilevski O, and Woodcock EA.** α_1-Adrenergic receptor signaling is localized to caveolae in neonatal rat cardiomyocytes. *J Mol Cell Cardiol* 41: 17–25, 2006.
25. **Murthy KS and Makhlouf GM.** Heterologous desensitization mediated by G protein-specific binding to caveolin. *J Biol Chem* 275: 30211–30219, 2000.
26. **Ostrom RS and Insel PA.** The evolving role of lipid rafts and caveolae in G protein-coupled receptor signaling: implications for molecular pharmacology. *Br J Pharmacol* 143: 235–245, 2004.
27. **Pike LJ and Casey L.** Localization and turnover of phosphatidylinositol 4,5-bisphosphate in caveolin-enriched membrane domains. *J Biol Chem* 271: 26453–26456, 1996.
28. **Razani B, Engelman JA, Wang XB, Schubert W, Zhang XL, Marks CB, Macaluso F, Russell RG, Li M, Pestell RG, Di Vizio D, Hou H Jr, Kneitz B, Lagaud G, Christ GJ, Edelmann W, and Lisanti MP.** Caveolin-1 null mice are viable but show evidence of hyperproliferative and vascular abnormalities. *J Biol Chem* 276: 38121–38138, 2001.
29. **Razani B and Lisanti MP.** Caveolin-deficient mice: insights into caveolar function human disease. *J Clin Invest* 108: 1553–1561, 2001.
30. **Shaul PW and Anderson RG.** Role of plasmalemmal caveolae in signal transduction. *Am J Physiol Lung Cell Mol Physiol* 275: L843–L851, 1998.
31. **Sjöblom-Widfeldt N, Arner A, and Nilsson H.** Contraction of small mesenteric arteries induced by micromolar concentrations of ATP released from caged ATP. *J Vasc Res* 30: 38–42, 1993.
32. **Somlyo AP and Somlyo AV.** Ca^{2+} sensitivity of smooth muscle and nonmuscle myosin II: modulated by G proteins, kinases, and myosin phosphatase. *Physiol Rev* 83: 1325–1358, 2003.
33. **Swärd K, Dreja K, Susnjar M, Hellstrand P, Hartshorne DJ, and Walsh MP.** Inhibition of Rho-associated kinase blocks agonist-induced Ca^{2+} sensitization of myosin phosphorylation and force in guinea-pig ileum. *J Physiol* 522: 33–49, 2000.
34. **Taggart MJ, Leavis P, Feron O, and Morgan KG.** Inhibition of PKCalpha and rhoA translocation in differentiated smooth muscle by a caveolin scaffolding domain peptide. *Exp Cell Res* 258: 72–81, 2000.
35. **Teixeira A, Chaverot N, Schroder C, Strosberg AD, Couraud PO, and Cazaubon S.** Requirement of caveolae microdomains in extracellular signal-regulated kinase and focal adhesion kinase activation induced by endothelin-1 in primary astrocytes. *J Neurochem* 72: 120–128, 1999.
36. **Urban NH, Berg KM, and Ratz PH.** K^+ depolarization induces RhoA kinase translocation to caveolae and Ca^{2+} sensitization of arterial muscle. *Am J Physiol Cell Physiol* 285: C1377–C1385, 2003.
37. **Woodman SE, Cheung MW, Tarr M, North AC, Schubert W, Lagaud G, Marks CB, Russell RG, Hassan GS, Factor SM, Christ GJ, and Lisanti MP.** Urogenital alterations in aged male caveolin-1 knockout mice. *J Urol* 171: 950–957, 2004.
38. **Woodsome TP, Eto M, Everett A, Brautigan DL, and Kitazawa T.** Expression of CPI-17 and myosin phosphatase correlates with Ca^{2+} sensitivity of protein kinase C-induced contraction in rabbit smooth muscle. *J Physiol* 535: 553–564, 2001.
39. **Yamano M, Ito H, and Miyata K.** Species differences in the 5-hydroxytryptamine-induced contraction in the isolated distal ileum. *Jpn J Pharmacol* 74: 267–274, 1997.

Paper II

Am J Physiol Regul Integr Comp Physiol 293: R1222–R1231, 2007.
First published July 11, 2007; doi:10.1152/ajpregu.00092.2007.

Arterial remodeling and plasma volume expansion in caveolin-1-deficient mice

Sebastian Albinsson,[1]* Yulia Shakirova,[1]* Anna Rippe,[2] Maria Baumgarten,[1] Bert-Inge Rosengren,[2] Catarina Rippe,[2] Rupert Hallmann,[3] Per Hellstrand,[1] Bengt Rippe,[2] and Karl Swärd[1]

[1]*Department of Experimental Medical Science, Lund University, Biomedical Centre, Lund;* [2]*Department of Nephrology, University Hospital of Lund, Lund, Sweden; and* [3]*Institute for Physiological Chemistry and Pathobiochemistry, Münster, Germany*

Submitted 8 February 2007; accepted in final form 2 July 2007

Albinsson S, Shakirova Y, Rippe A, Baumgarten M, Rosengren B-I, Rippe C, Hallmann R, Hellstrand P, Rippe B, Swärd K. Arterial remodeling and plasma volume expansion in caveolin-1-deficient mice. *Am J Physiol Regul Integr Comp Physiol* 293: R1222–R1231, 2007. First published July 11, 2007; doi:10.1152/ajpregu.00092.2007.—Caveolin-1 (Cav-1) is essential for the morphology of membrane caveolae and exerts a negative influence on a number of signaling systems, including nitric oxide (NO) production and activity of the MAP kinase cascade. In the vascular system, ablation of caveolin-1 may thus be expected to cause arterial dilatation and increased vessel wall mass (remodeling). This was tested in Cav-1 knockout (KO) mice by a detailed morphometric and functional analysis of mesenteric resistance arteries, shown to lack caveolae. Quantitative morphometry revealed increased media thickness and media-to-lumen ratio in KO. Pressure-induced myogenic tone and flow-induced dilatation were decreased in KO arteries, but both were increased toward wild-type (WT) levels following NO synthase (NOS) inhibition. Isometric force recordings following NOS inhibition showed rightward shifts of passive and active length-force relationships in KO, and the force response to α_1-adrenergic stimulation was increased. In contrast, media thickness and force response of the aorta were unaltered in KO vs. WT, whereas lumen diameter was increased. Mean arterial blood pressure during isoflurane anesthesia was not different in KO vs. WT, but greater fluctuation in blood pressure over time was noted. Following NOS inhibition, fluctuations disappeared and pressure increased twice as much in KO ($38 \pm 6\%$) compared with WT ($17 \pm 3\%$). Tracer-dilution experiments showed increased plasma volume in KO. We conclude that NO affects blood pressure more in Cav-1 KO than in WT mice and that restructuring of resistance vessels and an increased responsiveness to adrenergic stimulation compensate for a decreased tone in Cav-1 KO mice.

CAVEOLAE ARE 50- to 100-nm large membrane invaginations in which cholesterol and sphingolipids are enriched. Two caveolin protein homologs (Cav-1 and -3) are necessary for the formation of caveolae and act as scaffolds for many signaling molecules (4, 21, 28). A prototypical example of a caveolae-associated signal-transduction molecule is endothelial nitric oxide (NO) synthase (eNOS), which is targeted to caveolae via acylation (29). Cav-1 exerts a negative regulatory influence on eNOS activity, and this is of relevance for NO production (18). Accordingly, Cav-1 ablation, which blocks formation of caveolae in the vasculature, results in increased NO generation and vasodilatation ex vivo (5, 23, 32, 35). Despite increased NO release, a threefold increase in cGMP in smooth muscle cells (5), a major reduction of myogenic tone (1, 5, 7), and the development of heart failure (4, 32, 35), mean arterial blood pressure is largely normal in adult Cav-1 knockout (KO) mice (26).

Blood pressure is essential for homeostasis, and it is expected that a reduction in myogenic tone in KO arteries will be compensated, possibly via the baroreceptor reflex. This would restore blood pressure via increased sympathetic activity and thus neurogenic tone. No major difference in heart rate was, however, found in anesthetized KO relative to wild-type (WT) mice (26). On the other hand, force in response to α_1-adrenergic stimulation is increased in denuded femoral arteries from KO mice compared with WT controls (27), suggesting compensation at the level of the vascular wall. Increased contraction in response to noradrenaline was similarly found in the saphenous artery (20). An increased contractile response to α_1-adrenergic stimulation would counteract the blood pressure-lowering effect of NO in the vasculature. In addition, hypertrophic remodeling without a matching increase in lumen diameter would amplify the effect of a given vasoconstrictor's influence on arterial resistance (8).

Shear stress by blood flow has been proposed to activate both eNOS activity and the Ras-Raf-MAP kinase pathway within caveolae in the endothelium (24, 25). Accordingly, a recent study (33) demonstrated that carotid arteries from KO mice show impaired flow-mediated dilatation. Such an effect could potentially contribute to altered regulation of vascular resistance in Cav-1 KO mice. However, it should be noted that vascular resistance is also influenced by endothelium-derived hyperpolarizing factor, distinct from NO and prostacyclin (3). Thus the role of flow-dependent vasodilatation in KO mice needs to be studied also in resistance vessels. Finally, plasma volume is an important determinant of venous return to the heart and is an effector mechanism for renin-angiotensin system activation. Plasma volume is known to be expanded in heart failure (16) and may therefore be increased in KO mice, of possible importance for the control of blood pressure.

The aim of the present study was to test the following hypotheses in Cav-1 KO mice: *1*) that small mesenteric arteries (SMAs) are remodeled and have increased α_1-adrenergic contractility; *2*) that flow-mediated dilatation is impaired; and *3*) that the plasma volume is expanded. If so, a few candidate mechanisms contributing to blood pressure normalization in

* S. Albinsson and Y. Shakirova contributed equally to this work.

Address for reprint requests and other correspondence: K. Swärd, Dept. of Experimental Medical Science, Lund Univ., BMC D12, SE-221 84 Lund, Sweden (e-mail: Karl.Sward@med.lu.se).

The costs of publication of this article were defrayed in part by the payment of page charges. The article must therefore be hereby marked "*advertisement*" in accordance with 18 U.S.C. Section 1734 solely to indicate this fact.

the setting of a large constitutive NO production in these mice would have been identified.

MATERIALS AND METHODS

Cav-1 KO mice. Cav-1 KO mice on the C57BL/6 background obtained from the Jackson Laboratory (Bar Harbor, ME) were further backcrossed on the same background and were genotyped as described by Razani et al. (23). WT littermates or purchased C57BL/6 mice (Möllegard, Copenhagen, Denmark), matched for age and sex, were used as controls (all are referred to as WT); 10- to 16-wk-old mice of both sexes weighing between 20 and 30 g were used. Mice had free access to standard chow and water. For in vitro experiments, mice were euthanized by cervical dislocation. All experiments conformed to the American Physiological Society's "Guiding Principles in the Care and Use of Animals" and were approved by the local animal ethics committee.

Preparation of vessel segments. The intestine with the mesentery attached, aorta, and portal vein were removed and placed in cold (4°C) HEPES-buffered Krebs solution (composition in mM: 135.5 NaCl, 5.9 KCl, 1.2 $MgCl_2$, 11.6 glucose, 11.6 HEPES, pH 7.4), prepared by using Milli-Q water and containing 2.5 mM Ca^{2+} as indicated. First-generation SMAs, aortas, and portal veins were carefully freed from adhering tissue under a microscope.

Isometric force recording. SMA and aorta segments (1.5 mm long) were mounted in a myograph (610M; Danish MyoTechnology, Aarhus, Denmark), as previously described (2). In these experiments, all vessels were denuded of endothelium (6), and 300 μM L-NAME was included, which eliminated relaxation in response to 10 μM acetylcholine, because the objective was to determine the effects of remodeling on force generation irrespective of endothelial NO production. The exact length of each segment was determined by using a microscope with an ocular scale, and force was expressed relative to length. After determination of the passive force for optimal active force development (1.7 mN/mm in both KO and WT, see Fig. 5 and *Flow-induced dilatation and combined tone*), SMAs were routinely stretched to 2.5 mN (=1.7 mN/mm). The same basal force was applied to the aorta, because pilot experiments had shown that this was close to L_0, the circumference resulting in the greatest active (total minus passive) force in each preparation. Circumference-tension relationships were generated by increasing wire distance in a stepwise fashion. At each wire distance, preparations were allowed to equilibrate for 5 min. High-K^+ solution, obtained by exchanging 60 mM NaCl for KCl, was then applied for 7 min. Depolarization was used, rather than noradrenaline, because it generates highly reproducible contraction for repeated challenges. At the end of each cycle, passive force was obtained by relaxing the preparations for 10 min in Ca^{2+}-free solution, which was shown in control experiments to give complete relaxation. Thereafter, wire distance was increased and the cycle was repeated.

Pressure myograph recording. SMAs with intact endothelium were mounted on glass cannulae (diameter = 100 μm) in a pressure myograph chamber (Living Systems Instrumentation, Burlington, VT) and were secured with silk sutures. The myograph chamber was placed on a Nikon Diaphot 200 inverted microscope equipped with a charge-coupled device (CCD) camera. VediView 1.2 software (Danish MyoTechnology) was used to monitor lumen and vessel diameter and was also used to determine wall thickness and cross-sectional area after full dilatation. The edges chosen by the software were examined critically in all experiments. The vessel was superfused with HEPES-buffered Krebs solution gassed with O_2, and temperature and pH (7.4) were monitored. Intraluminal pressure was applied by gravity via the cannula from a solution reservoir mounted at an adjustable height. Pressure was monitored by two pressure transducers mounted at the inflow and outflow line. Flow was applied by using a peristaltic pump, and intraluminal pressure was maintained during this procedure. An expandable rubber tube was mounted at the inflow line to reduce pulsations from the pump.

Before experimentation, intraluminal pressure was gradually increased to 95 mmHg. At this pressure, the vessel was stretched manually in the longitudinal direction to 115% of its unstretched length. Preparations were subsequently equilibrated at 36°C during 1 h at 45 mmHg. Arteries that showed signs of leakage, identified by using a drop chamber mounted on the inflow line, were discarded.

Myogenic tone was provoked by raising intraluminal pressure from 20 to 120 mmHg in 25-mmHg steps. Each pressure level was maintained for 5 min, and the vessel diameter was then measured. Intraluminal flow (25–125 μl/min, corresponding to shear stresses of 9–45 dyn/cm^2 in WT and 4–20 dyn/cm^2 in KO) was applied at a pressure of 95 mmHg. Shear stress was calculated by using the formula $SS = 4\mu Q/\pi r^3$, where SS is the sheer stress, μ is the viscosity (taken to be 0.007 Poise), Q is the flow (cm^3/s), and r is the radius (cm). Flow was maintained for 5 min, and the mean relaxation during this time was measured. Control experiments showed that prolonged application of flow did not give further dilatation. This procedure was repeated with the same vessel after 45 min of incubation with 300 μM N^{ω}-nitro-L-arginine methyl ester (L-NAME). At the end of each experiment, the vessel was relaxed by using Ca^{2+}-free buffer supplemented with 2 mM EGTA. In control experiments, sodium nitroprusside (1 μM) was added to the Ca^{2+}-free buffer. This did not cause additional dilatation, showing that Ca^{2+}-free buffer is sufficient to eliminate tone. Myogenic tone (%) was expressed as $[(D_1 - D_2)/D_1] \cdot 100$, where D_1 is the passive diameter in Ca^{2+}-free buffer and D_2 is the active diameter.

In separate experiments, SMAs were preconstricted with the selective α_1-adrenergic agonist cirazoline (0.03 μM) applied both intraluminally and in the superfusate at 95 mmHg. In these experiments, flow rates were calculated for each vessel to give a shear stress of 25 dyn/cm^2, because this resulted in robust dilatation. Flow was applied in the absence of inhibitors, in the presence of L-NAME (300 μM), and in the presence of indomethacin (10 μM). Inhibitors were prepared on the day of the experiment.

Morphometry and immunofluorescence. Following relaxation in Ca^{2+}-free solution for 30 min, aortic segments and SMAs, adjacent to those used in the mechanical experiments, were fixed with 2% formaldehyde in PBS (pH 7.4) for 30 min. In a subset of experiments, 20 ml fixative was infused through the femoral artery (see *In vivo experiments*, below) while blood was allowed to leave through the jugular vein. This was done following full arterial dilatation with sodium nitroprusside, which was given as bolus doses (10 nmol in 10 μl) until the blood pressure reduction saturated. Blood pressure was 40 ± 2 mmHg in WT and 34 ± 3 mmHg in KO following nitroprusside saturation ($P = 0.08$; $n = 7$ for both). Arteries were then removed and maintained in fixative for another 30 min. Fixed specimens were washed in PBS containing 10% sucrose and methylene blue (2 × 10 min) followed by embedding in Tissue-Tek (Sakura, Zoeterwoude, Netherlands). After freezing, 10 μm cross-sections were obtained in a cryostat. For morphometry, sections were stained with hematoxylin and eosin (Merck, Darmstadt, Germany) or Masson's Trichrome (Biocare Medical, Concord, CA), following the manufacturers instructions, and media thickness, area, and internal circumference were determined by using a computerized image-analysis system (Leica Q500MC). At least four glasses from each mouse were used. Media thickness was obtained from four averaged measurements in positions defined by two perpendicular diameters.

For immunofluorescence, tissue sections were washed (2 × 30 min in PBS), permeabilized with 0.2% Triton-X-100 for 15 min, blocked with 2% bovine serum albumin in PBS for 2 h, and incubated with primary antibodies in the same solution overnight at 4°C. Cav-1 (clone 2297), -2 (clone 65), and -3 (clone 26) antibodies were obtained from BD Biosciences (San Jose, CA) and were used at dilutions of 1:125, 1:200, and 1:1,000, respectively. After being washed in PBS, sections were incubated with Cy5-labeled anti-mouse

IgG in PBS with 2% bovine serum albumin for 1 h at room temperature. Nuclei were stained with SYTOX Green (1:3,000; Molecular Probes, Carlsbad, CA). Sections were examined in a Zeiss LSM 510 confocal microscope. Caveolin proteins were detected by monitoring Cy5 fluorescence on excitation at 633 nm. SYTOX Green fluorescence was monitored on excitation at 488 nm.

Transmission electron microscopy. First-generation SMAs were dissected in Ca^{2+}-free HEPES-buffered Krebs solution, cut into small pieces (~30, <0.3-mm length), and opened in the longitudinal direction to minimize diffusion distances for the fixative. Following transfer to 1.5-ml Eppendorf tubes, preparations were allowed to settle at the bottom, and the physiological buffer was aspirated and exchanged for fixative containing 2.5% glutaraldehyde in 0.15M sodium cacodylate, pH 7.4. This was repeated once to remove all physiological buffer, and fixation was allowed to proceed overnight. Samples were washed with sodium cacodylate, postfixed for 1 h in 1% osmium tetroxide in sodium cacodylate, and finally washed with sodium cacodylate. They were dehydrated with an ascending ethanol series and were embedded in Agar 100 Resin R1031 medium with acetone as an intermediate solvent. Specimens were sectioned into 50-nm ultrathin sections and were stained with uranyl acetate and lead citrate. Specimens were observed in a Philips CM10 electron microscope operated at 60 kV. Images were recorded on Kodak SO-163 plates without preirradiation at a dose of 2,000 electrons/nm^2.

Western blotting. Western blotting using the Cav-3 antibody (see above) was performed as described (27), with dilutions recommended by the manufacturer. SMAs from one mouse gave insufficient protein for reliable quantification. Therefore, SMAs from three mice were combined for each homogenate ($n = 1$), whereas single aortas and portal veins were used for individual homogenates. Protein concentration was determined with a Bio-Rad protein assay (Bio-Rad, Hercules, CA), and equal amounts of protein were loaded in all lanes. To illustrate equal loading, nontransferred proteins were stained with Coomassie blue, and a section around the actin band is shown.

Organ culture. To assess DNA synthesis independently of hemodynamic conditions in vivo, whole mesenteric arterial trees were subjected to organ culture. SMA trees were dissected under sterile conditions, and blood was removed from the lumen by gentle stroking with a rubber policeman. Following weighing, preparations were cultured in DMEM:Ham's F-12 medium (1:1) with 2% dialyzed fetal calf serum and 10 nM insulin and with the addition of 50 U/ml penicillin and 50 μg/ml streptomycin for 4 days. [^{3}H]thymidine (10 μCi; Amersham Biosciences Europe, Uppsala, Sweden) was added during the last 24 h of culture. On harvesting, preparations were washed in ice-cold PBS and were frozen in liquid nitrogen. Following freeze crushing, preparations were dissolved in 400 μl 0.2 M NaOH and were sonicated twice, and 300 μl was removed. Following two cycles of precipitation with trichloroacetic acid (5% TCA), centrifugation (13,200 *g*), and washing (5% TCA), the supernatant was discarded and the pellet was resuspended in Soluene. After 2 h, 8 ml of liquid scintillation cocktail was added, and preparations were subjected to scintillation counting (Beckman LS6500, Beckman Instruments, Fullerton, CA). Protein concentration was determined in the remaining homogenate (100 μl) by using the Bio-Rad protein assay. Radioactive counts were divided by the amount of protein and were normalized to WT (100%) in each experiment.

In vivo experiments. Mice were placed in a small container, and surgical anesthesia was induced with 4% isoflurane (Isoflurane Forene; Abbot Scandinavia, Solna, Sweden) in room air. After mice were transferred to a heating pad, keeping body temperature at 37 ± 1°C with a rectal probe (Temperature Control Unit HB 101/2; Panlab, Barcelona, Spain), anesthesia was temporarily maintained with a small mask. The animals were tracheostomized, and anesthesia was controlled and maintained by mechanical ventilation with air containing 2% isoflurane by using a mouse ventilator (28025; Ugo Basile, Comerio, Italy). Tidal volume was set at 0.35 ml, frequency was set to 98/min, and a positive end-expiratory pressure of 5 mmHg was applied. The right jugular vein was cannulated for infusion purposes. The left femoral artery was cannulated for blood sampling and blood pressure monitoring on a polygraph (Model 7B; Grass Instruments, Quincy, MA).

Mean arterial blood pressure, obtained by low-pass filtering the pressure data with the polygraph, was recorded for at least 45 min before the infusion of L-NAME. L-NAME was given as a bolus (5 μmol in 50 μl), followed by continuous infusion (23 mM at a rate of 7 μl/min), to uphold a constant plasma concentration. L-NAME was infused for 1 h, but pressure stabilized at a higher level within a few minutes. Heart rate was obtained by removing the low-pass filter and increasing chart speed at regular intervals during the experiment.

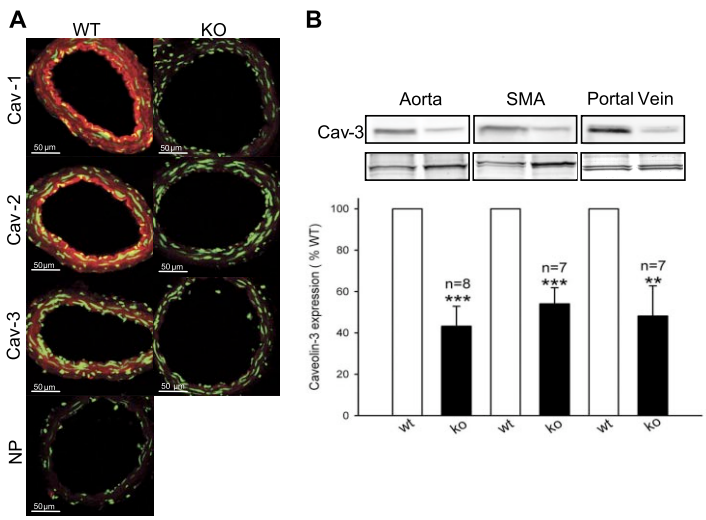

Fig. 1. *A*: immunofluorescence staining of caveolin (Cav)-1, -2, and -3 (red) in small mesenteric arteries (SMAs) from wild-type (WT) and Cav-1 knockout (KO) mice. Nuclei are stained green. Note that Cav-1 and -2 proteins are expressed in endothelium, i.e., concave side, and that media expresses all 3 caveolins. Cav-1 staining in KO did not exceed staining seen in absence of primary antibody (NP). *B*: Western blots using Cav-3 antibody (*top*) and results from densitometric scanning of Cav-3 band (*bottom*). Proteins left on gel after transfer were stained with Coomassie brilliant blue, and sections around 42-kDa actin band are shown below blots as a control for protein loading. Protein expression differs between vessels from different vascular sites, explaining slightly different protein patterns; *n*, number of blots run. $^{**}P < 0.01$ and $^{***}P < 0.001$ vs. WT.

Experiments were carried out in a blinded manner, and genotypes were only revealed following complete analysis.

For plasma-volume determination, mice were allowed to stabilize for 20 min following surgery. Tracer amounts of ^{125}I-HSA (human serum albumin-I-125, RISA, 3 mg/ml, 5 MBq; Amersham Health) were administered in the right jugular vein. To reduce the amount of free iodine, the ^{125}I-HSA was filtered before administration by using Amicon YM-30 (Millipore, Bedford, MA). Immediately after the injection, the catheter was removed and the vein was ligated. To determine the amount of ^{125}I-HSA injected, the vial containing the tracer was counted for radioactivity before injection and was then compared with the amount left in the vial and in the equipment involved. The injected volume was kept at 50 ± 20 μl. Four 10-μl blood samples were collected at 5, 20, 40, and 60 min after injection. The catheter was filled with heparinized saline, which was temporarily removed during sampling. After the last blood sample was obtained, 80 μl blood was drawn for hematocrit measurement. Radioactivity measurements were performed in a gamma counter (Wizard 1480; LKP Wallac, Turku, Finland). The amount of radioactivity in plasma (cpm/ml) was plotted vs. time in a semilogarithmic diagram. The data was fitted by using an exponential regression function ($y = a \cdot e^{-bx}$), and the tracer concentration was extrapolated to *time 0*. Plasma volume was finally calculated by dividing the total amount of radioactivity injected into the mouse by the plasma tracer concentration at *time 0*.

Chemicals and reagents. Unless otherwise specified, chemicals and reagents were obtained from Sigma (St. Louis, MO).

Statistics. Mean values ± SE are shown. Student's *t*-test for unpaired data, or, in the case of multiple comparisons, ANOVA followed by Bonferroni's post hoc test was used to calculate statistical significance.

RESULTS

Caveolin expression in SMA, aorta, and portal vein. The distribution of Cav-1, -2, and -3 in SMAs was examined by using immunofluorescence. Cav-1 and -2 were readily detected both in the endothelium and in the media of SMAs from WT mice (Fig. 1*A*). The SMA media, but not the endothelium, stained positive for Cav-3 (Fig. 1*A*). In keeping with loss of Cav-1, no staining exceeding that with primary antibody omission control was seen in KO [Fig. 1*A*, *top right* vs. NP (no primary)]. Consistent with >90% breakdown of Cav-2 (5, 23), staining for this protein was largely absent in KO (Fig. 1*A*, *middle right*). Similar to previous findings in KO femoral artery (27), a reduced medial staining for Cav-3 was detected in KO SMAs (Fig. 1*A*, *bottom right*). To test whether Cav-3 expression in KO is reduced in other vascular preparations, we compared Cav-3 expression in SMAs, aorta, and portal vein by Western blotting (Fig. 1*B*). Cav-3 expression was reduced by 50–60% in all cases. Staining of nontransferred proteins on the gels with Coomassie blue is shown below the blots to demonstrate protein loading (Fig. 1*B*).

Ultrastructure of SMAs. Electron microscopic examination of SMAs from KO mice did not reveal any conspicuous morphological changes at low magnification, other than an apparent increase in media thickness, with an increased number of cell layers compared with WT (Fig. 2, *D* vs. *A*). Focal adhesions (dense bands), extracellular matrix, and overall cell morphology appeared similar at higher magnification (Fig. 2, *B* and *E*). Further increases in magnification revealed numerous caveolae in the smooth muscle cell plasma membrane in WT (Fig. 2*C*). Consistent with almost complete loss of caveolae in aortic and bladder smooth muscle (5, 31), caveolae appeared to be absent in the media of KO SMAs, as illustrated in Fig. 2*F*.

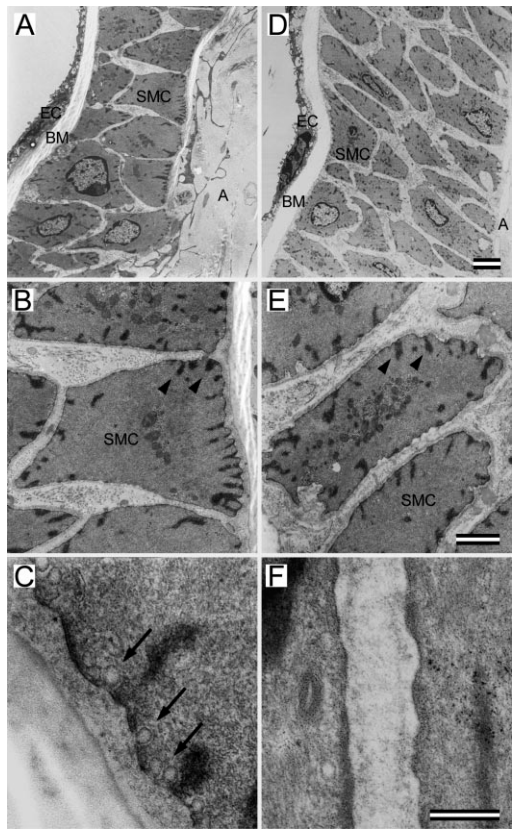

Fig. 2. Electron micrographs of SMAs from WT (*A*, *B*, and *C*) and KO (*D*, *E*, and *F*) mice. Scale bars = 2 μm (*A* and *D*), 1 μm (*B* and *E*), and 250 nm (*C* and *F*). *A* and *D*: endothelial cells (EC), basal membrane (BM), smooth muscle cells (SMC), and adventitia (A) are indicated. *B*, *C*, *E*, and *F*: SMC in media are shown. Arrowheads point to dense bands (focal adhesions) in membrane of individual cells. Caveolae, indicated by arrows, are clearly seen in WT at highest magnification (*C*).

Increased α_1-adrenergic contraction in KO SMAs but not in aorta. An increased media thickness in KO would be associated with increased arterial force development, which may, however, be masked by increased NO production. To eliminate NO production, arteries were denuded and the NOS inhibitor L-NAME (300 μM) was included. Cumulative concentration-response curves using the selective α_1-receptor agonist cirazoline revealed greater force in KO compared with WT at all concentrations exceeding 0.1 μM (Fig. 3*A*), with no change in potency (EC_{50} = 91 ± 11 nM in WT and 69 ± 9 nM in KO, $P > 0.05$). No difference in cirazoline-induced force was detected in the denuded aorta in the presence of L-NAME (Fig. 3*B*, EC_{50} = 150 ± 29 nM in WT and 183 ± 25 nM in KO).

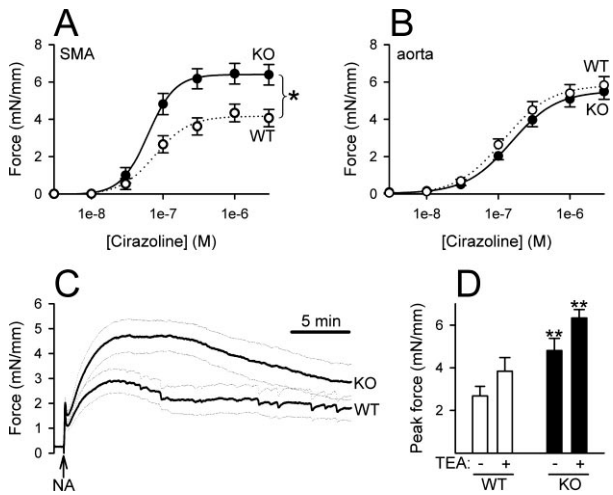

Fig. 3. *A* and *B*: concentration-response relationships for selective α_1-adrenergic agonist cirazoline in denuded SMAs ($n = 16$ preparations) and aorta ($n = 16$ preparations), respectively, in presence of N^{ω}-nitro-L-arginine methyl ester (L-NAME; 300 μM). $^*P < 0.05$ vs. WT for 4 highest concentrations. Data from each experiment were fitted by using a 4-parameter logistic function to yield EC_{50} values, which were not significantly different. Best fits of logistic function to average data are plotted. *C*: noradrenaline-induced (1 μM) contraction normalized to arterial cylinder length as a function of time in denuded SMAs from WT and KO mice in presence of L-NAME. Average traces from 10 preparations of each genotype ± SE (dotted lines) are shown. *D*: compiled data of peak force in response to noradrenaline in absence and presence of K^+-channel inhibitor tetraethylammonium (TEA; $n = 10$ and 8 preparations). $^{**}P < 0.01$ vs. WT.

To address whether increased contraction would also be seen using the physiological ligand on α_1-receptors, SMAs were stimulated with noradrenaline (1 μM, ~80% of E_{max}). Average force traces from 10 individual preparations are shown in Fig. 3*C*. The difference between KO and WT was maximal after 7–10 min stimulation and was less pronounced during early and late phases of contraction. Peak force was significantly greater in KO (Fig. 3*D*). The K^+-channel inhibitor tetraethylammonium (20 mM) was then added to optimize conditions for force generation. Noradrenaline-induced force was greater also following K^+-channel inhibition (Fig. 3*D*).

Arterial remodeling in Cav-1 KO mice. To assess arterial structure quantitatively, vascular sections were fixed and stained with hematoxylin and eosin or Masson's trichrome for morphometry (Fig. 4*A*). The analysis indicated increased media thickness and media area in SMAs (Fig. 4*B*). Trichrome staining did not indicate increased connective tissue deposits in KO compared with WT and did not reveal any obvious change

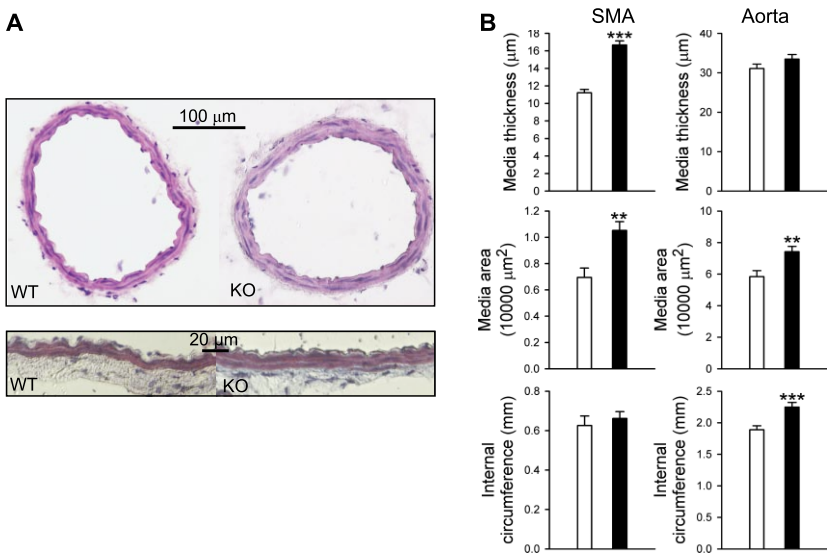

Fig. 4. *A*: hematoxylin and eosin- (*top*) and trichrome- (*bottom*) stained sections of SMAs from WT and KO, respectively. *B*: summarized data from morphometry; $n = 13–15$; $^{**}P < 0.01$ and $^{***}P < 0.001$ vs. WT.

in adventitial thickness (Fig. 4*A*). In the aorta, the internal circumference was increased, whereas the media thickness was unchanged (Fig. 4*B*). In SMAs, the internal circumference was not significantly different between KO and WT either in immersion-fixed (WT, $n = 12$; KO, $n = 8$) or perfusion-fixed (WT, $n = 3$; KO, $n = 5$) preparations, and there was no significant difference in circumference between these two fixation methods in either genotype. However, lumen dimensions are highly dependent on pressure and might be affected by fixation conditions. In Fig. 4, the pooled data are shown, but lumen dimensions were also determined in live arteries at defined pressure levels as described below and in Fig. 6.

SMAs were mounted in a pressure myograph, and vessel dimensions were determined by using a CCD camera and an edge-detection system (see METHODS). Measurements were made in the absence of extracellular Ca^{2+} to abolish arterial tone. Passive pressure-diameter relationships were determined as shown in Fig. 6*A*. At an intraluminal pressure of 95 mmHg, lumen diameter was not significantly different in KO (257 ± 9 μm) vs. WT (242 ± 12 μm; $n = 11$; $P > 0.05$). From the edge-detection system, wall thickness was estimated as 24 ± 2 μm in KO vs. 14 ± 1 μm in WT ($n = 12$; $P < 0.001$), and wall cross-sectional area was estimated as $2.2 \pm 0.2 \times 10^4$ μm^2 in KO vs. $1.2 \pm 0.1 \times 10^4$ μm^2 in WT ($n = 12$; $P < 0.001$). Importantly, the wall-to-lumen ratio was greater in KO (0.096 ± 0.006 vs. 0.063 ± 0.006; $n = 12$; $P < 0.001$). These measurements refer to the total wall thickness as determined by the CCD camera, so to get an estimate of the media-to-lumen ratio, the media areas, determined histologically (Fig. 4*A*), were used to calculate the expected media thickness at the pressure levels and diameters shown in Fig. 6*A*. At all pressure levels above 20 mmHg, the media-to-lumen ratio was higher in KO; e.g., at 95 mmHg it was 0.048 vs. 0.036.

To address whether the changes in arterial structure would translate into an altered L_0, circumference-tension relationships in endothelium-denuded SMAs were generated under isometric conditions by using the wire myograph. The relationship between internal circumference and active force on depolarization with high-K^+ solution (60 mM) was shifted to the right in KO compared with WT (Fig. 5*A*), as was the relationship between circumference and passive force (Fig. 5*B*). Determination of the optimum for force development in each experiment revealed a significant increase of L_0 in KO (Fig. 5*C*). Small arteries in KO mice thus have a hypertrophic muscle layer and exhibit signs of outward remodeling but have increased wall-to-lumen ratio.

Increased rate of thymidine incorporation in SMAs. To assess DNA synthesis independently of hemodynamic conditions in vivo, whole mesenteric arterial trees were subjected to organ culture, and thymidine incorporation was measured. Consistent with a thicker media, mesenteric artery trees weighed more in KO than in WT (4.2 ± 0.2 vs. 2.7 ± 0.1 mg; $P < 0.001$; $n = 7$ and 8) and contained more protein (0.24 ± 0.03 vs. 0.13 ± 0.01 mg; $P < 0.01$). Thymidine incorporation relative to protein content was increased in KO by 31 ± 14% ($P < 0.05$; $n = 6$), as assessed in organ culture.

Myogenic tone. To test properties of tone in KO compared with WT arteries in an integrated setting, experiments were run in the pressure myograph. In a first series of experiments, pressure was increased in steps from 20 to 120 mmHg to produce myogenic tone. Passive lumen diameter was significantly increased in KO compared with WT over the pressure range 20–50 mmHg (Fig. 6*A*). Active lumen diameter was significantly increased in KO over the entire pressure range (Fig. 6*B*). Consistent with earlier findings (1, 7), myogenic tone (%reduction in diameter on activation; see METHODS) was considerably lower in KO compared with WT SMAs (Fig. 6*C*). L-NAME increased myogenic tone in KO, but it was still significantly lower than in WT. No effect of L-NAME on myogenic tone was observed in WT.

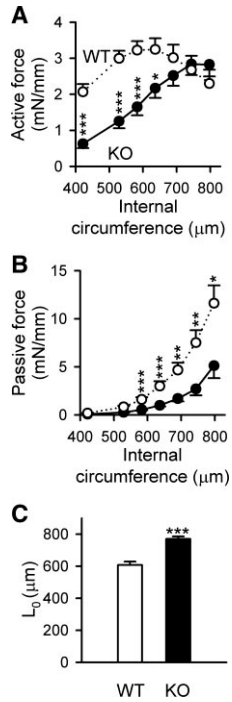

Fig. 5. Active (60 mM K^+, *A*) and passive (*B*) force in denuded SMAs from WT (○) and KO (●) mice as a function of circumference. Optimal circumference for active force (L_0) is shown in *C*; $n = 9$ animals for each genotype. *$P < 0.05$, **$P < 0.01$, and ***$P < 0.001$ vs. WT.

Flow-induced dilatation and combined tone. We next examined flow-induced dilatation at 95 mmHg and with the combination of α_1-agonist and pressure. Flow caused a rate-dependent reduction of myogenic tone in WT SMAs (Fig. 6*D*). In KO SMAs that had developed myogenic tone, flow-induced dilatation was absent (Fig. 6*D*). Treatment with L-NAME conferred on the KO arteries an ability to dilate in response to increased flow but did not affect flow-induced dilatation in WT (Fig. 6*E*). Moreover, flow-induced dilatation was not different in KO compared with WT following precontraction with the α_1-adrenergic agonist cirazoline (combined tone; Fig. 6*F*). Neither L-NAME nor indomethacin inhibited flow-mediated dilatation under combined tone, suggesting that dilatation was due to a mechanism independent of NOS and cyclooxygenase.

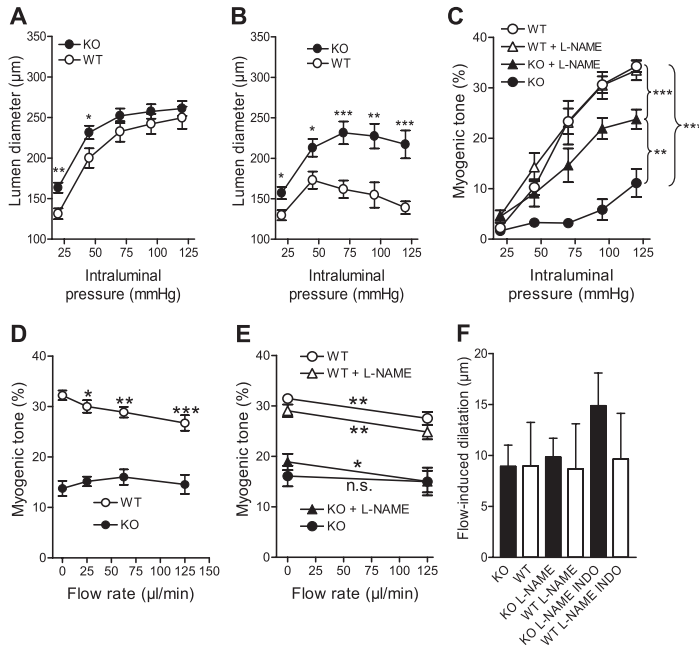

Fig. 6. Myogenic tone in SMAs was evaluated from passive vessel diameter in calcium-free solution (*A*) and active diameter in presence of calcium (*B*) and was expressed as %diameter reduction (myogenic tone; *C*). Myogenic tone was determined in absence and presence of L-NAME (300 μM) in WT and KO mice (*C*; n = 6–11). In SMAs that demonstrated spontaneous myogenic tone at 95 mmHg, increasing rates of intraluminal flow were applied and flow-mediated dilatation was evaluated (*D*). Note that different diameters result in different shear stresses in WT and KO at identical flow rates. Shear stress was ~50% lower in KO compared with WT. *E*: flow-induced dilatation was evaluated in presence and absence of L-NAME (300 μM; n = 5–7). Arteries that completely lacked myogenic tone were excluded from analysis in *D* and *E*, which conceals effect of L-NAME on myogenic tone shown in *C*. Flow-induced dilatation was evaluated in SMAs preconstricted with α_1-adrenergic agonist cirazoline (0.03 μM) following development of myogenic tone at 95 mmHg (*F*). Flow rates were adjusted to cause a shear stress of 25 dyn/cm^2. Flow was applied in absence of inhibitors, in presence of L-NAME (300 μM), and in presence of indomethacin (Indo; 10 μM), as indicated. In *F*, no comparisons of WT vs. KO were significant. $^*P < 0.05$, $^{**}P < 0.01$, and $^{***}P < 0.001$ vs. WT.

To illustrate differences between tone induced by pressure alone and by the combination of pressure and adrenergic stimulation (combined tone), data at 95 mmHg in Fig. 6, *C* and *F*, were replotted in Fig. 7. The difference in myogenic tone between KO and WT was greater than was the difference in combined tone (compare Fig. 7, *A* vs. *B*). This was seen both in the absence and presence of flow (not shown). Addition of L-NAME did not eliminate the difference in myogenic tone between WT and KO (Fig. 7*A*) but eliminated the difference between WT and KO during combined tone (Fig. 7*B*). The lower myogenic tone was therefore compensated by a relatively greater diameter change in response to adrenergic stimulation, so that the combined tone differed less or not at all.

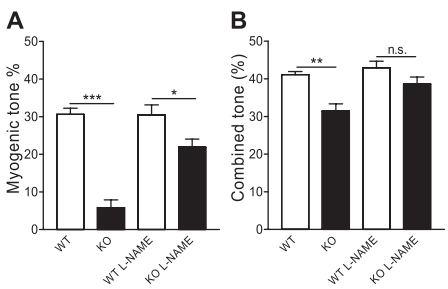

Fig. 7. Tone expressed as %diameter reduction on activation in SMAs at 95 mmHg (myogenic tone; *A*) and at 95 mmHg in presence of cirazoline (0.03 μM, combined tone; *B*) in presence and absence of L-NAME. n.s., not significant. $^*P < 0.05$, $^{**}P < 0.01$, and $^{***}P < 0.001$ vs. WT.

Plasma volume expansion. Anesthetized WT (n = 7) and KO (n = 8) mice were injected with tracer amounts of ^{125}I-HSA. The concentration of tracer in plasma decreased in an exponential manner for both WT and KO, with the correlation coefficients for the average curves being 0.96 and 0.95, respectively. The plasma volume was significantly increased in KO (6.0 ± 0.3 ml/100g body wt) compared with WT mice (5.2 ± 0.1 ml/100g body wt; $P < 0.05$). Hematocrit did not differ between genotypes (WT, 0.402 ± 0.006; KO, 0.405 ± 0.013; $P > 0.05$).

Blood pressure following NOS inhibition. Blood pressure and heart rate were recorded in WT and KO mice (Fig. 8*A*) in the presence and absence of L-NAME. Consistent with previous data (26), blood pressure was similar in WT and KO mice before L-NAME administration (Fig. 8*B*), whereas heart rate was slightly but significantly increased in KO in the present series (Fig. 8*C*). The relative increase in blood pressure on administration of L-NAME was 17 ± 3% in WT and 38 ± 6% in KO (n = 11 and 6, respectively; $P = 0.001$), illustrating the greater influence of NO on blood pressure in KO. Following L-NAME, blood pressure was significantly greater in KO compared with WT, with no difference in heart rate (Fig. 8, *B* and *C*). We also observed greater blood pressure variability in KO mice, as evident from the blood pressure records in Fig. 8*A*. These slow fluctuations disappeared following L-NAME administration.

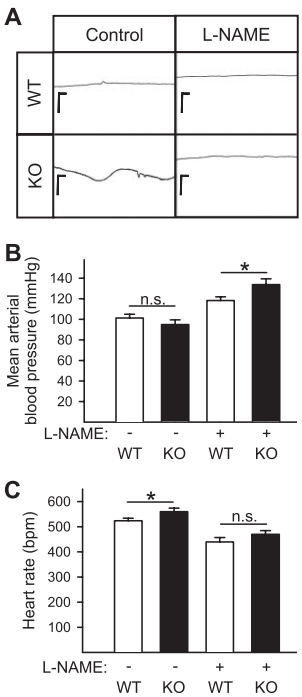

Fig. 8. *A*: representative records of mean arterial blood pressure in 1 WT and 1 KO mouse before and after administration of L-NAME. Calibration bars represent 1 min and 40 mmHg, respectively. Horizontal calibration bar is positioned at 80 mmHg, and bottom of each panel is at 0 mmHg. *B*: compiled mean arterial pressures. *C*: heart rate obtained by reducing filtering and increasing chart speed at regular intervals in experiment; $n = 6–11$ in all panels; n.s., not significant; $^*P < 0.05$ vs. WT.

DISCUSSION

The high basal NO production (5, 23, 32, 35), the major reduction of myogenic tone (1, 5, 7), and the age-dependent development of cardiac dysfunction (4, 32, 35) in Cav-1 KO mice would be expected to result in lowered systemic blood pressure. This has not been seen to occur in adult KO mice (26). The hypotheses that loss of Cav-1 is associated with arterial remodeling, increased α_1-adrenergic contraction, and plasma volume expansion were therefore tested. Consistent with the hypotheses, SMAs were remodeled in KO mice and α_1-adrenergic contraction was increased under isometric conditions. Moreover, a modest (14%) increase in plasma volume was detected. Mean arterial blood pressure was normal in KO mice compared with WT, as was also shown in a previous study (26). Following NOS inhibition, blood pressure was higher in KO than in WT, indicating the presence of blood pressure-elevating changes masked by increased NO-mediated dilatation.

Remodeling was present in the splanchnic circulation (present study) and possibly in the hind limb (20, 27). In contrast, the aorta exhibited an increase in circumference but not in media thickness or force development. Although the precise mechanisms of remodeling are debatable, some predictions can be made from the architectural reorganization. As pointed out by Folkow (8), an increased wall-to-lumen ratio is of advantage for controlling vascular diameter and resistance. Indeed, a 30% shortening of the outer muscle layer would increase resistance 7-fold by using the geometry in WT mesenteric arteries (media thickness, 11 μm; radius, 103 μm), whereas resistance would increase 11-fold in KO arteries (media thickness, 17 μm; radius, 103 μm), as calculated by using Poiseuille's law. Thus a more efficient control of vascular resistance conferred on small arteries by increased wall-to-lumen ratio may contribute to a greater blood pressure response to vasoconstrictor stimuli in KO than in WT.

We noted increased wet weight and protein contents in KO compared with WT SMAs and slightly higher rates of thymidine incorporation in organ culture. This is consistent with the negative regulatory role of Cav-1 in cellular growth and proliferation (10–13, 17, 23, 30). This effect may contribute to medial hypertrophy. However, other possible mechanisms may play a role. Arterial dilatation at unaltered blood pressure will lead to increased arterial wall tension, which is a powerful stimulus for growth signaling in smooth muscle (14). Aorta, in contrast to SMA, did not show significant media hypertrophy despite increased diameter in the KO. This may be related to the fact that the aorta is a conduit vessel essentially without resistance function and that elastic fibers rather than smooth muscle cells carry the major part of its wall tension.

Responsiveness to α_1-adrenergic agonists in denuded SMAs in the presence of L-NAME was increased in KO arteries. It was previously shown that α_1-receptor responses were increased in the denuded femoral artery from KO mice and that this difference was eliminated by inhibition of protein kinase C (27). This suggests that Cav-1 and caveole negatively influence signaling downstream of the α_1-receptor. Elimination of this effect in KO arteries would act in synergy with the increased media thickness. As seen in the present study, time courses of α_1-adrenergic contraction also differ between WT and KO, and contraction by high-K^+ solution was, if changed at all, reduced in KO. In endothelium-intact arteries, Drab et al. (5) found reduced responses to angiotensin II and endothelin-1 in Cav-1 KO but unchanged responses to α_1-receptor stimulation. This may be taken to indicate that an increased vasodilating drive from the endothelium is compensated by a specifically increased smooth muscle responsiveness to α_1-agonists. Further support for a specific role of caveolae in α_1-receptor signaling is the finding that chemical loading of the scaffolding domain peptide from Cav-1 into ferret aorta inhibited contraction induced by phenylephrine (15) but not high-K^+ solution. Finally, binding of radioactively labeled α_1-agonist to lipid raft fractions containing Cav-1 supports an association of α_1-receptors with caveolae in some instances (9, 19). Evidence against a role of caveolae in α_1-receptor signaling has, however, also been presented. We (6) and others (22) found that α_1-receptor responses resist disruption of caveolae by using cholesterol depletion. One possibility that would accommodate differences between different vascular beds is that caveolae dependence of α_1-signaling is dictated by the α_1-receptor isoform expressed. There are three α_1-adrenergic receptors, α_{1A}, α_{1B}, and α_{1D}, and their contribution to contraction may

vary between different arteries. No good pharmacological tools are, however, available to test that hypothesis.

Cav-3 expression was reduced in the absence of Cav-1 in several vascular preparations. This is consistent with data in the femoral artery (27) but differs from results in striated muscle (5). Because caveolae were absent, as seen by electron microscopy, it must be assumed that the contribution of Cav-3 to caveolae formation in the SMA media is minimal. Our ability to detect Cav-3 in venous smooth muscle, in which it is often undetectable, may relate to the use of very sensitive blotting reagents. The possible role played by Cav-3 in smooth muscle may be addressed by using Cav-3-deficient mice.

Myogenic tone stimulated by increased intraluminal pressure (the Bayliss effect) was reduced in SMAs from KO mice, which is in keeping with previous studies (1, 5, 7). Our data reveal that myogenic tone partly recovered after L-NAME. This indicates that increased basal NO release plays a considerable role in the impairment of this hemodynamic autoregulatory mechanism in SMAs. The impairment of myogenic tone remaining after L-NAME may involve reduced RhoA/Rho kinase activation, as suggested by Dubroca et al. (7), and functional activation of Ca^{2+}-activated K^+ channels, as proposed by Adebiyi et al. (1). Addition of L-NAME in the presence of α_1-agonist at 95 mmHg (combined tone) increased KO tone to the same level as that in identically treated WT arteries. This indicates a greater contribution to tone of α_1-adrenergic compared with myogenic mechanisms in KO vs. WT arteries in an integrated setting, such that the entire difference in tone between KO and WT is eliminated in the presence of L-NAME.

The endothelium responds acutely to shear stress by increasing eNOS activity and NO production through a process involving caveolae (25). Accordingly, flow-mediated dilatation in adrenergically stimulated carotid arteries, which in part depends on NO, was recently shown to be impaired in KO mice (33). In SMAs, we found that flow-induced dilatation of myogenic tone is reduced in KO mice. However, flow-induced dilatation recovered when eNOS was inhibited and tone was increased. Furthermore, no difference in flow-mediated dilatation was found when vessels were constricted by activation of α_1-adrenergic receptors and pressure. Thus the level of tone is an important determinant of the ability to dilate in response to flow, and this dilatation in the SMA seems to be largely independent of NO production, in accordance with earlier findings of NO-independent endothelium-mediated dilatation of resistance vessels in mice (3).

Plasma volumes and hematocrit values determined in the present study to calculate blood volume in a 25-g mouse yield 2.5 ml in KO vs. 2.2 ml in WT. This represents a 14% greater blood volume in the KO mice. Plasma volume expansion may be secondary to heart failure (16) and is expected to increase ventricular diastolic filling pressure, which indeed has been reported to be increased in KO (32). Importantly, increased ventricular filling would compensate reduced cardiac contractility and would thus improve cardiac output. Activation of the renin-angiotensin system and increased levels of vasopressin may mediate changes in plasma volume and contribute to blood pressure normalization, but to our knowledge concentrations of these mediators in plasma have not been determined in the Cav-1 KO mouse model.

Blood pressure was stated to be reduced in Cav-1 KO mice in one previous study (32), but no data were presented. Moreover, blood pressure was reported to be increased in the lung (35) in Cav-1 KO mice. The present study and our previous work (26) reveal no effect of Cav-1 ablation on mean systemic blood pressure. The effect of L-NAME, however, was doubled in KO vs. WT, indicating a much greater influence of NO on blood pressure. This likely reflects alleviated Cav-1 inhibition of NOS activity (4, 5, 18, 23, 35). Heart rate was slightly increased in the absence of L-NAME but not in its presence, suggesting baroreceptor reflex activation in the former situation.

In conclusion, the present study has shown that arterial remodeling and increased α_1-adrenergic contraction in KO mice compensate for a reduced myogenic tone in maintaining blood pressure. Moreover, enhanced NO release caused by loss of Cav-1 impairs myogenic reactivity and plays a greater role for blood pressure as revealed by L-NAME. Finally, KO mice have a greater plasma volume. It may be speculated that remodeling and plasma-volume expansion counterbalance increased NO-mediated dilatation and heart failure, resulting in a largely normal, albeit fluctuating, central blood pressure in the systemic circulation in the absence of Cav-1. However, a wide variety of caveolae-associated mechanisms involving additional cells and tissues may play a role, and blood pressure could be reduced earlier or later in life. Whether changes in arterial geometry and plasma volume are compensatory or reflect a primary regulatory role of Cav-1 is not presently known. Plasma volume expansion occurs in heart failure (16), which develops in KO mice (4, 32, 35). Vascular remodeling, on the other hand, may reflect the role of Cav-1 in regulation of growth and proliferation (10–13, 17, 23, 30).

ACKNOWLEDGMENTS

We thank Gunnel Roos for genotyping, Ina Nordström for help with the thymidine incorporation study, and Matthias Mörgelin for help with electron microscopy. We also thank Gustav Grände for assistance with plasma-volume determinations.

GRANTS

Supported by the Swedish Research Council [Grants 71X-14955 (K. Swärd), 71X-28 (P. Hellstrand), 04X-08285-17A (B. Rosengren)], by grants from Crafoord (R. Hallmann and K. Swärd), Åke Wiberg (K. Swärd), Magnus Bergvall (K. Swärd), and the Royal Physiographic Societies (R. Hallmann and K. Swärd), by the Heart-Lung Foundation (K. Swärd and P. Hellstrand), by Stiftelsen Konsul Thure Carlssons Minne (K. Swärd), and by a grant from the Torsten and Ragnar Söderberg Foundation to the Vascular Wall Program at Lund University. B. Rosengren was supported by a postdoctoral fellowship from the Norwegian Research Council (ES247409).

REFERENCES

1. **Adebiyi A, Zhao G, Cheranov SY, Ahmed A, Jaggar JH.** Caveolin-1 abolishment attenuates the myogenic response in murine cerebral arteries. *Am J Physiol Heart Circ Physiol* 292: H2556–H2557, 2007.
2. **Bergdahl A, Gomez MF, Dreja K, Xu SZ, Adner M, Beech DJ, Broman J, Hellstrand P, Swärd K.** Cholesterol depletion impairs vascular reactivity to endothelin-1 by reducing store-operated Ca^{2+} entry dependent on TRPC1. *Circ Res* 93: 839–847, 2003.
3. **Brandes RP, Schmitz-Winnenthal FH, Feletou M, Godecke A, Huang PL, Vanhoutte PM, Fleming I, Busse R.** An endothelium-derived hyperpolarizing factor distinct from NO and prostacyclin is a major endothelium-dependent vasodilator in resistance vessels of wild-type and endothelial NO synthase knockout mice. *Proc Natl Acad Sci USA* 97: 9747–9752, 2000.

4. **Cohen AW, Hnasko R, Schubert W, Lisanti MP.** Role of caveolae and caveolins in health and disease. *Physiol Rev* 84: 1341–1379, 2004.
5. **Drab M, Verkade P, Elger M, Kasper M, Löhn M, Lauterbach B, Menne J, Lindschau C, Mende F, Luft FC, Schedl A, Haller H, Kurzchalia TV.** Loss of caveolae, vascular dysfunction, and pulmonary defects in caveolin-1 gene-disrupted mice. *Science* 293: 2449–2452, 2001.
6. **Dreja K, Voldstedlund M, Vinten J, Tranum-Jensen J, Hellstrand P, Swärd K.** Cholesterol depletion disrupts caveolae and differentially impairs agonist-induced arterial contraction. *Arterioscler Thromb Vasc Biol* 22: 1267–1272, 2002.
7. **Dubroca C, Loyer X, Retailleau K, Loirand G, Pacaud P, Feron O, Balligand JL, Levy BI, Heymes C, Henrion D.** RhoA activation and interaction with caveolin-1 are critical for pressure-induced myogenic tone in rat mesenteric resistance arteries. *Cardiovasc Res* 73: 190–197, 2007.
8. **Folkow B.** Physiological aspects of primary hypertension. *Physiol Rev* 62: 347–504, 1982.
9. **Fujita T, Toya Y, Iwatsubo K, Onda T, Kimura K, Umemura S, Ishikawa Y.** Accumulation of molecules involved in alpha1-adrenergic signal within caveolae: caveolin expression and the development of cardiac hypertrophy. *Cardiovasc Res* 51: 709–716, 2001.
10. **Galbiati F, Volonte D, Liu J, Capozza F, Frank PG, Zhu L, Pestell RG, Lisanti MP.** Caveolin-1 negatively regulates cell cycle progression by inducing G(0)/G(1) arrest via p53/p21$^{Waf/Cip1}$ dependent mechanism. *Mol Biol Cell* 8: 2229–2244, 2001.
11. **Gosens R, Stelmack GL, Dueck G, McNeill KD, Yamasaki A, Gerthoffer WT, Unruh H, Gounni AS, Zaagsma J, Halayko AJ.** Role of caveolin-1 in p42/p44 MAP kinase activation and proliferation of human airway smooth muscle. *Am J Physiol Lung Cell Mol Physiol* 291: L523–L534, 2006.
12. **Hassan GS, Jasmin JF, Schubert W, Frank PG, Lisanti MP.** Caveolin-1 deficiency stimulates neointima formation during vascular injury. *Biochemistry* 43: 8312–8321, 2004.
13. **Hassan GS, Williams TM, Frank PG, Lisanti MP.** Caveolin-1-deficient aortic smooth muscle cells show cell autonomous abnormalities in proliferation, migration, and endothelin-based signal transduction. *Am J Physiol Heart Circ Physiol* 290: H2393–H2401, 2006.
14. **Hellstrand P, Albinsson S.** Stretch-dependent growth and differentiation in vascular smooth muscle: role of the actin cytoskeleton. *Can J Physiol Pharmacol* 83: 869–875, 2005.
15. **Je HD, Gallant C, Leavis PC, Morgan KG.** Caveolin-1 regulates contractility in differentiated vascular smooth muscle. *Am J Physiol Heart Circ Physiol* 286: H91–H98, 2004.
16. **Kalra PR, Anagnostopoulos C, Bolger AP, Coats AJ, Anker SD.** The regulation and measurement of plasma volume in heart failure. *J Am Coll Cardiol* 39: 1901–1908, 2002.
17. **Kim HP, Wang X, Nakao A, Kim SI, Murase N, Choi ME, Ryter SW, Choi AM.** Caveolin-1 expression by means of p38β mitogen-activated protein kinase mediates the antiproliferative effect of carbon monoxide. *Proc Natl Acad Sci USA* 102: 11319–11324, 2005.
18. **Michel JB, Feron O, Sacks D, Michel T.** Reciprocal regulation of endothelial nitric-oxide synthase by Ca^{2+}-calmodulin and caveolin. *J Biol Chem* 272: 15583–15586, 1997.
19. **Morris JB, Huynh H, Vasilevski O, Woodcock EA.** Alpha1-adrenergic receptor signaling is localized to caveolae in neonatal rat cardiomyocytes. *J Mol Cell Cardiol* 41: 17–25, 2006.
20. **Neidhold S, Eichhorn B, Kasper M, Ravens U, Kaumann AJ.** The function of alpha- and beta-adrenoceptors of the saphenous artery in caveolin-1 knockout and wild-type mice. *Br J Pharmacol* 150: 261–270, 2007.
21. **Ostrom RS, Insel PA.** The evolving role of lipid rafts and caveolae in G protein-coupled receptor signaling: implications for molecular pharmacology. *Br J Pharmacol* 143: 235–245, 2004.
22. **Potocnik SJ, Jenkins N, Murphy TV, Hill MA.** Membrane cholesterol depletion with beta-cyclodextrin impairs pressure-induced contraction and calcium signalling in isolated skeletal muscle arterioles. *J Vasc Res* 44: 292–302, 2007.
23. **Razani B, Engelman JA, Wang XB, Schubert W, Zhang XL, Marks CB, Macaluso F, Russell RG, Li M, Pestell RG, Di Vizio D, Hou H Jr, Kneitz B, Lagaud G, Christ GJ, Edelmann W, Lisanti MP.** Caveolin-1 null mice are viable but show evidence of hyperproliferative and vascular abnormalities. *J Biol Chem* 276: 38121–38138, 2001.
24. **Rizzo V, Sung A, Oh P, Schnitzer JE.** Rapid mechanotransduction in situ at the luminal cell surface of vascular endothelium and its caveolae. *J Biol Chem* 273: 26323–26329, 1998.
25. **Rizzo V, McIntosh DP, Oh P, Schnitzer JE.** In situ flow activates endothelial nitric oxide synthase in luminal caveolae of endothelium with rapid caveolin dissociation and calmodulin association. *J Biol Chem* 273: 34724–34729, 1998.
26. **Rosengren BI, Rippe A, Rippe C, Venturoli D, Swärd K, Rippe B.** Transvascular protein transport in mice lacking endothelial caveolae. *Am J Physiol Heart Circ Physiol* 291: H1371–H1377, 2006.
27. **Shakirova Y, Bonnevier J, Albinsson S, Adner M, Rippe B, Broman J, Arner A, Swärd K.** Increased Rho activation and PKC-mediated smooth muscle contractility in the absence of caveolin-1. *Am J Physiol Cell Physiol* 291: C1326–C1335, 2006.
28. **Shaul PW, Anderson RG.** Role of plasmalemmal caveolae in signal transduction. *Am J Physiol Lung Cell Mol Physiol* 275: L843–L851, 1998.
29. **Shaul PW, Smart EJ, Robinson LJ, German Z, Yuhanna IS, Ying Y, Anderson RG, Michel T.** Acylation targets endothelial nitric-oxide synthase to plasmalemmal caveolae. *J Biol Chem* 271: 6518–6522, 1996.
30. **Williams TM, Lee H, Cheung MW, Cohen AW, Razani B, Iyengar P, Scherer PE, Pestell RG, Lisanti MP.** Combined loss of INK4a and caveolin-1 synergistically enhances cell proliferation and oncogene-induced tumorigenesis: role of INK4a/CAV-1 in mammary epithelial cell hyperplasia. *J Biol Chem* 279: 24745–24756, 2004.
31. **Woodman SE, Cheung MW, Tarr M, North AC, Schubert W, Lagaud G, Marks CB, Russell RG, Hassan GS, Factor SM, Christ GJ, Lisanti MP.** Urogenital alterations in aged male caveolin-1 knockout mice. *J Urol* 171: 950–957, 2004.
32. **Wunderlich C, Schober K, Lange SA, Drab M, Braun-Dullaeus RC, Kasper M, Schwencke C, Schmeisser A, Strasser RH.** Disruption of caveolin-1 leads to enhanced nitrosative stress and severe systolic and diastolic heart failure. *Biochem Biophys Res Commun* 340: 702–708, 2006.
33. **Yu J, Bergaya S, Murata T, Alp IF, Bauer MP, Lin MI, Drab M, Kurzchalia TV, Stan RV, Sessa WC.** Direct evidence for the role of caveolin-1 and caveolae in mechanotransduction and remodeling of blood vessels. *J Clin Invest* 116: 1284–1291, 2006.
34. **Zhao YY, Liu Y, Stan RV, Fan L, Gu Y, Dalton N, Chu PH, Peterson K, Ross J Jr, Chien KR.** Defects in caveolin-1 cause dilated cardiomyopathy and pulmonary hypertension in knockout mice. *Proc Natl Acad Sci USA* 99: 11375–11380, 2002.

Paper III

European Journal of Pharmacology 602 (2009) 399–405

Contents lists available at ScienceDirect

European Journal of Pharmacology

journal homepage: www.elsevier.com/locate/ejphar

Pulmonary, Gastrointestinal and Urogenital Pharmacology

Impaired nerve-mediated relaxation of penile tissue from caveolin-1 deficient mice

Yulia Shakirova *, Petter Hedlund, Karl Swärd

Department of Experimental Medical Science, Lund University, Biomedical Centre, BMC D12, SE-221 84 Lund, Sweden

ARTICLE INFO

Article history:
Received 22 July 2008
Received in revised form 29 October 2008
Accepted 17 November 2008
Available online 25 November 2008

Index words:
Caveolae
Penile erection
Physiology
Nitric oxide
Phosphodiesterase
Guanylate cyclase

ABSTRACT

Caveolin-1-deficient mice are characterised by a high vascular NO production. Because NO-dependent smooth muscle relaxation is considered to play an important role in penile erection, it was hypothesized that the erectile function would be affected by genetic ablation of caveolae. This study assessed penile erectile mechanisms in caveolin-1 knockout (KO) mice *ex vivo*. Immunofluorescence confirmed caveolin-1 expression primarily in the endothelium surrounding the sinusoids of the corpus cavernosum, but also in smooth muscle cells of the sinusoidal bundles. In KO mice, caveolin-1 was absent, and the expression of the caveola-associated protein PTRF-Cavin was reduced. Nitric oxide synthase (endothelial and neuronal) and caveolin-3 levels were not affected, and staining of the neuronal marker PGP 9.5 did not disclose any apparent change in the density or pattern of innervation. Moreover, no apparent morphological differences were noted. Functionally, the force response following stimulation of α_1-adrenergic receptors, and the sensitivity to the Rho-kinase inhibitor Y27632, were unaltered, whereas relaxation of α_1-precontracted corpus cavernosum in response to electrical field stimulation and the muscarinic agonist carbachol were impaired. The nitric oxide donor sodium nitroprusside produced less relaxation in KO as compared to wild type corpus cavernosum. We conclude that nerve-mediated dilatation of the corpus cavernosum is impaired in the absence of caveolin-1, and that this is due in part to reduced sensitivity of the target tissue to NO. All in all our data support an important role of caveolin-1 in penile erection.

1. Introduction

Penile erection is a process dependent on the production of nitric oxide by neuronal and endothelial nitric oxide synthases (nNOS, eNOS) (Musicki and Burnett, 2006). In a classical paradigm, release of NO from nerve fibres triggers rapid influx of blood into the sinusoids of corpus cavernosum leading to increased shear stress, activation of the protein kinase Akt, and sustained production of NO by endothelial nitric oxide synthase (eNOS) (Andersson, 2001). NO subsequently relaxes smooth muscle in the corpus cavernosum through activation of soluble guanylyl cyclase (sGC) and protein kinase G. The major current treatment of impotence targets the breakdown of cyclic GMP by phosphodiesterase 5 (Feifer and Carrier, 2008).

Nitric oxide synthase is located in and regulated by plasma membrane organelles called caveolae (García-Cardeña et al., 1996; Michel et al., 1997; Shaul et al., 1996). These are 50–100 nm large Ω-shaped membrane invaginations enriched in cholesterol and sphingolipids. Caveolae are sensitive to cholesterol depletion and require the presence of the homologous proteins caveolin-1 or caveolin-3 (Cohen et al., 2004). Targeting of eNOS to caveolae has been shown to require acylation (Shaul et al., 1996), and the so-called scaffolding domain from caveolin-1 inhibits eNOS catalytic activity (Ju et al., 1997). In keeping with an inhibitory interaction between eNOS and caveolin-1, NO production is increased in mice lacking caveolin-1 (Razani et al., 2001; Drab et al., 2001; Zhao et al., 2002), resulting in ~3-fold increases in the NO metabolites nitrite and nitrate in plasma (Zhao et al., 2002; Wunderlich et al., 2006). Arterial and intestinal smooth muscle preparations from caveolin-1-deficient mice have also been shown to exhibit increased activation of contractile pathways, such as RhoA and protein kinase C (PKC) (Shakirova et al., 2006). Finally, caveolae have been proposed to play a role in fibrotic signaling (Tourkina et al., 2005; Wang et al., 2006).

Given that both NO-dependent regulation of vascular tone and contractile and fibrotic mechanisms may be modulated by caveolae, caveolae may play a role in erectile function. Indeed, trabecular smooth muscle-to-collagen ratio is decreased in aging, and this correlates with reduced expression of caveolin-1 (Bakircioglu et al., 2001). On the other hand, the beneficial effects of low fat diet and exercise on erectile function were associated with a limitation of the interaction between eNOS and caveolin-1 (Musicki et al., 2008). Erectile mechanisms have not been examined in caveolin-1-deficient mice, but urogenital phenotypes have been described, including changes in bladder function as well as distension of the seminal vesicles (Woodman et al., 2004).

In support of a role of caveolae in erection, it was found that pharmacological disruption of caveolae by cholesterol depletion impaired relaxation of the corpus cavernosum in response to exogenous NO and activators of sGC, but not in response to activation of cavernosal nerves (Linder et al., 2005). sGC and caveolin-1 were

* Corresponding author. Tel.: +46 46 2224575; fax: +46 46 222 4546.
E-mail address: Yulia.Shakirova@med.lu.se (Y. Shakirova).

0014-2999/$ – see front matter © 2008 Elsevier B.V. All rights reserved.
doi:10.1016/j.ejphar.2008.11.033

found to colocalise in the endothelium, suggesting that caveolae may be necessary for proper activation of sGC. However, cholesterol depletion is not specific for caveolae, but also affects membrane rafts, membrane fluidity, and membrane integrity. The goal of the present study was therefore to test if genetic ablation of caveolin-1 would result in a disturbance of erectile signalling in vitro.

2. Materials and methods

2.1. Caveolin-1-deficient mice

Caveolin-1-deficient (KO) mice were obtained from the Jackson Laboratory (Bar Harbor, Maine), backcrossed on the C57Bl6/J background, and genotyped as described by Razani et al. (2001). After six backcrosses, KO mice were maintained by homozygous breeding. Wild type (WT) C57Bl6/J mice, matched for age and sex, were obtained from Taconic (Ejby, Denmark). Mice were 16–22 weeks old. The local animal ethics committee in Lund/Malmö approved all experiments.

2.2. Tissue preparation

Mice were sacrificed by CO_2 asphyxation and erectile tissue was obtained as described (Hedlund et al., 2000). Dissected tissue was immediately placed in cold HEPES buffered Krebs solution (composition in mM: NaCl 135.5, KCl 5.9, $MgCl_2$ 1.2, glucose 11.6, HEPES 11.6, pH 7.4). Corpus cavernosum preparations (~0.3×0.3×3 mm) were dissected free through careful opening of tunica albuginea from its proximal extremity towards the penile shaft.

2.3. Western blotting

Western blotting was performed as described (Shakirova et al., 2006), with antibody dilutions as recommended by the manufacturers. Antibodies against caveolin-1 (clone 2297), caveolin-3 (clone 26), and eNOS (clone 3) were from BD Biosciences Pharmingen. The PTRF-Cavin antibody (ab48824) was from Abcam. iNOS and nNOS antibodies (sc-651, sc-648) were from Santa Cruz (Santa Cruz Biotechnology Inc, CA). The β-actin antibody (A5441) was from Sigma (Sigma Aldrich, Sweden). Protein concentration was determined using EZQ protein assay (R-33200, Molecular Probes, CA). Equal amounts of protein were loaded in all lanes. Optical densities×mm^2 of the bands of interest were normalized to the corresponding β-actin band on the same membrane.

2.4. Myograph experiments

Corpus cavernosum strips were mounted in a wire myograph (610 M, Danish MyoTechnology). Baths contained aerated HEPES buffered Krebs solution with 2.5 mM Ca^{2+}. A basal tension of 2.5 mN was applied. After equilibration for $^{1/2}$h, the solution was exchanged for high-K^+ solution, obtained by replacing 60 mM NaCl for KCl. For electrical field stimulation preparations were mounted as described (Hedlund et al., 2000). Strips were first stimulated with 0.3 μM 2-[(2-cyclopropylphenoxy)methyl]-4,5-dihydro-1H imidazole (cirazoline, ~80% of E_{max}, 0.99±0.13 mN, n=10 for WT, and 0.85±0.09 mN n=10 for KO, P>0.05). On top of the contractile plateau, preparations were electrically stimulated at increasing frequencies using platinum electrodes coupled to a Grass stimulator. Relaxation was elicited by

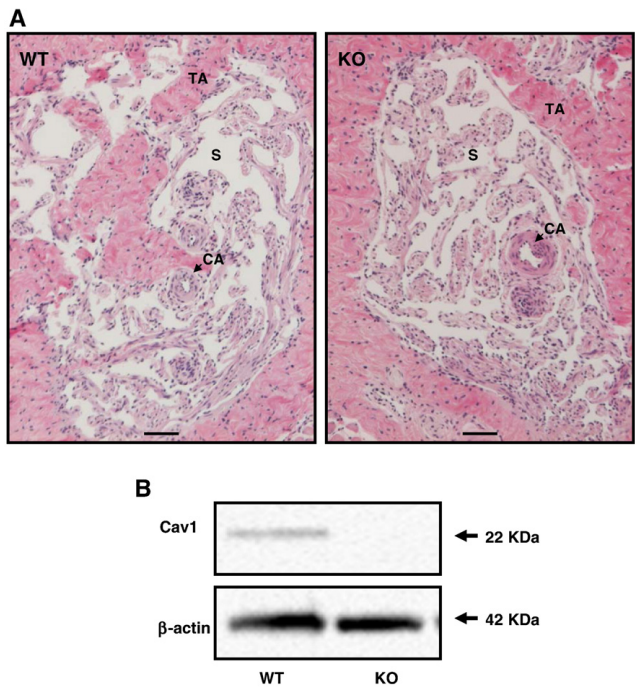

Fig. 1. Gross morphology of penile erectile tissue from wild type (WT) and caveolin-1 knockout (KO) mice. A shows hematoxylin and eosin stained sections (TA: tunica albuginea; S: sinusoidal space; CA: cavernous artery). Scale bars represent 100 μm. B shows Western blots of caveolin-1 using homogenates from WT and KO corporal strips. β-actin was used as a loading control.

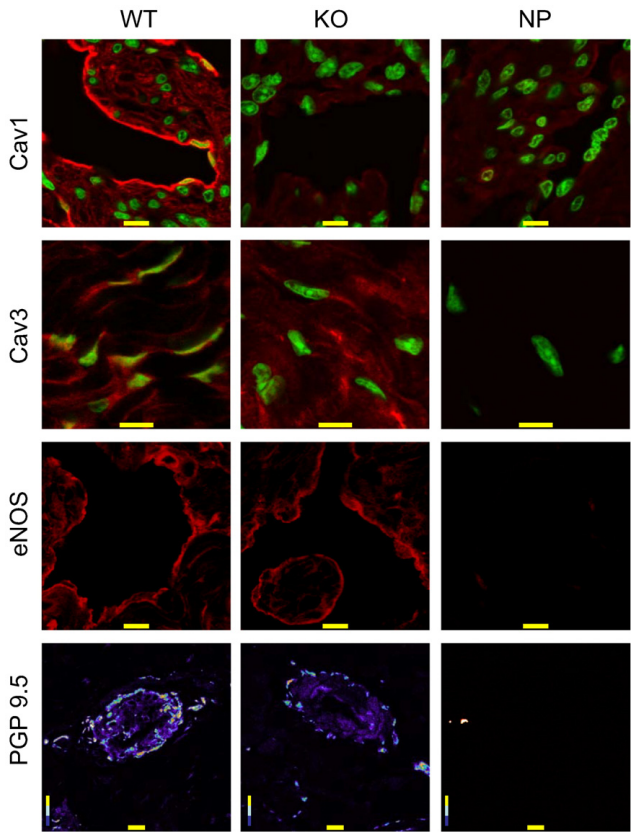

Fig. 2. Immunofluorescence staining for caveolin-1, caveolin-3, eNOS (all in red), PGP 9.5 (violet to yellow for increasing intensity), and nuclei (green) in WT and KO corpus cavernosum. The PGP 9.5 images are centered on branches of the central arteries. Images to the left represent staining in WT, middle images staining in KO, and right images primary antibody omission controls (NP: no primary). Scale bars represent 10 μm.

0.5 ms stimulation at 2 min intervals and stepwise increases in voltage (1, 2, 4, 8, 16, and 32 V).

2.5. Histology and immunofluorescence

Following relaxation in Ca^{2+}-free solution for 30 min, corpus cavernosum preparations were immersed in Histochoice (Amresco) overnight. After incubation in fixative, tissues were washed in 70% ethanol and maintained therein at 4 °C for 3 days, with three solution changes, until further processing. Following incubation in 96% (2 h) and 100% ethanol (1 h), 1:1 ethanol:xylene (30 min), and xylene (1 h), tissues were immersed in paraffin (2*1 h) and embedded. 10 μm sections were cut and deparaffinized.

For immunofluorescence, tissue sections were washed (2×30 min in PBS), permeabilized with 0.2% Triton-X-100 for 15 min, blocked with 2% bovine serum albumin in PBS for 2 h, and incubated with primary antibodies in the same solution overnight at 4 °C. Primary antibodies against caveolin-1 (clone 2297), and -3 (clone 26), (BD Biosciences/Pharmingen), eNOS (BD Biosciences / Pharmingen), and PGP 9.5 (RA95101, UltraClone Limited) were used, with dilutions as recommended by the manufacturer. After washing in PBS, sections were incubated either with Cy5-labeled anti-mouse IgG (65470, Jackson Immunoreserach Lab.Inc) or Alexa flour 488 goat anti-rabbit (A-11070, Molecular Probes) in PBS with 2% bovine serum albumin for 1 h at ambient temperature. Nuclei were stained with Sytox Green (S7020, Molecular Probes). All proteins were detected by monitoring Cy5 fluorescence upon excitation at 633 nm in a Zeiss LSM 510 confocal microscope. Sytox Green and PGP 9.5 fluorescence was monitored upon excitation at 488 nm. For gross morphology, sections were stained with hematoxylin and eosin (Merck, Darmstadt, Germany).

2.6. Chemicals

(+)-(R)-trans-4-(1-Aminoethyl)-N-(4-pyridyl) cyclohexanecarboxamide dihydrochloride, monohydrate (Y-27632) was from CalBiochem/EMD Biosciences. All other chemicals were of analytical grade or better and obtained from Sigma (Sigma Aldrich, Sweden).

2.7. Statistics

Mean values±S.E.M. are shown. Student's *t*-test for unpaired data was used to test for differences between groups. $P<0.05$ was considered significant. Significance is indicated by $^{*}P<0.05$, $^{**}P<0.01$, and $^{***}P<0.001$.

3. Results

3.1. Morphology and immunofluorescence

Hematoxylin and eosin stained sections of the corpus cavernosum from wild type (WT) and knock out (KO) mice did not reveal any apparent morphological differences (Fig. 1A). Western blots of strips dissected free from the tunica albuginea demonstrated expression of one caveolin-1 isoform in WT corpus cavernosum that was absent in the KO (Fig. 1B).

Immunofluorescence staining using a caveolin-1 antibody disclosed strong staining of WT corpus cavernosums, especially of endothelial cells surrounding sinusoids and dressing capillaries (Fig. 2). Fainter staining was seen in the cell membrane of cells inside the septa, which are likely smooth muscle cells, and in those cells, caveolin-1 appeared clustered along the membrane profiles. The caveolin-1 antibody did not label KO endothelial cells, and the clusters seen in the septal cells of the WT were absent. The faint staining remaining in the KO did not exceed that in primary antibody omission controls (Fig. 2). Caveolin-3 staining was restricted to the septal cells in WT, and the intensity of the caveolin-3 staining was unchanged in the KO. Immunoreactivity for endothelial nitric oxide synthase (eNOS) was detected primarily in endothelial cells of the sinusoids (Fig. 2). Staining for PGP 9.5, a neuronal marker, was seen around vascular structures, and had a similar intensity in WT and KO (Fig. 2).

3.2. Western blotting

The amounts of eNOS and nNOS were not different in WT and KO corpus cavernosum (Fig. 3A, B). The caveolin-3 protein level appeared to be reduced in the KO, but this difference was not significant (Fig. 3C). The level of PTRF-Cavin, a protein that plays a role in caveola-formation, was reduced in corpus cavernosums from caveolin-1-deficient mice (Fig. 3D). Inducible nitric oxide synthase was not detected in either WT or KO corpus cavernosum (not shown).

3.3. Contractile properties of the corpus cavernosum

The contractile response to 60 mM K^+ was not different in KO vs. WT corpus cavernosum (0.67 ± 0.1 vs. 0.65 ± 0.1 mN, n = 8 for WT and n = 7 for KO). Moreover, the response to the α_1-adrenergic agonist cirazoline was similar in WT and KO preparations (Fig. 4A). This was seen both in the presence and absence of the nitric oxide synthase blocker N_ω-nitro-L-arginine methyl ester (L-NAME, 100 μM).

To address the possibility that Rho-kinase activity is altered in corporal tissue from KO mice, sensitivity to Rho-kinase inhibitor Y27632 was tested. Corporal smooth muscle strips precontracted with 0.3 μM cirazoline were exposed to cumulatively increasing concentrations of Y27632 (Fig. 4B). The absolute magnitude of relaxation and the sensitivity to Rho-kinase inhibition was similar in KO and WT corpus cavernosum (Fig. 4B). 100 μM L-NAME did not affect this pattern.

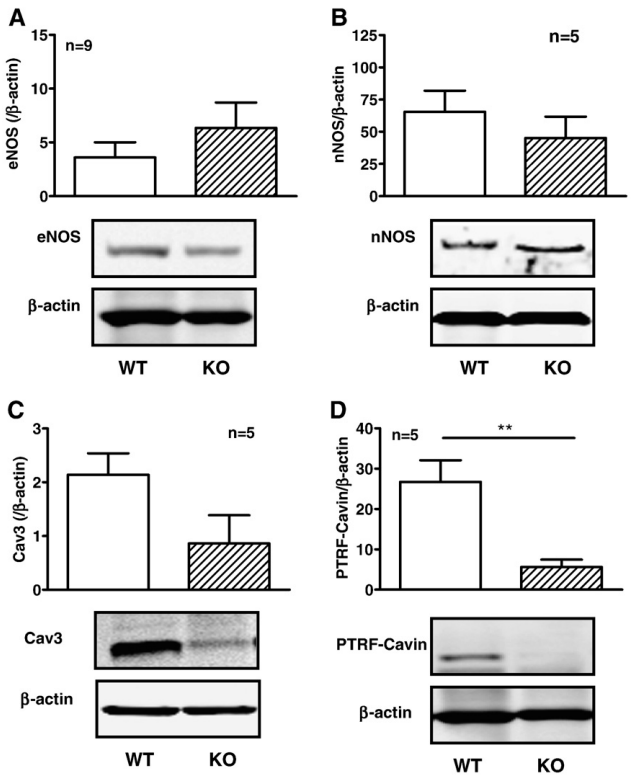

Fig. 3. Western blots using antibody against endothelial nitric oxide synthase (eNOS, A), neuronal NOS (nNOS, B), caveolin-3 (C), and PTRF-Cavin (D). The optical density × mm^2 of the band of interest was divided by that of β-actin (× 100). N-numbers in this and the following figures refer to the number of animals.

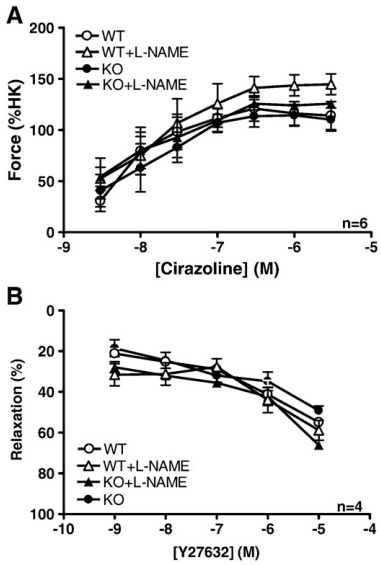

Fig. 4. Concentration response relationships for the α_1-adrenergic agonist cirazoline with or without L-NAME in corporal smooth muscle strips from WT and KO mice. Force was normalized to contraction by 60 mM K^+ (A). Concentration response relationship for the Rho-kinase inhibitor Y27632 following precontraction with 0.3 μM cirazoline (B).

3.4. Relaxation of the corpus cavernosum

EFS-induced relaxation was impaired in KO vs. WT corpus cavernosum (Fig. 5A, typical records are shown to the right). Relaxation was completely abolished by L-NAME in both WT and KO corpus cavernosum, and the difference between genotypes was eliminated (Fig. 5A).

Similar to EFS, the muscarinic agonist carbachol relaxed corpus cavernosum preparations in a dose-dependent manner. Muscarinic relaxation was significantly impaired in corpus cavernosum from KO mice. The difference between WT and KO was again eliminated by L-NAME (Fig. 5B).

Finally, the nitric oxide donor sodium-nitroprusside (SNP) was introduced in cumulatively increasing concentrations. Relaxation in response to SNP was impaired (Fig. 5C) in KO relative to WT preparations.

4. Discussion

The major finding of this study is that nerve-mediated relaxation of the corpus cavernosum is impaired in mice lacking caveolin-1. Because the amount of neuronal nitric oxide synthase and the appearance of neuronal structures were the same, impaired dilatation is likely not due to a difference in innervation. Relaxation in response to muscarinic stimulation, acting via endothelial nitric oxide synthase, was similarly impaired. This argues that NO, irrespective of its cellular source, causes less effective dilatation of the corpus cavernosum in the absence of caveolae. Accordingly, relaxation of the corpus cavernosum by the NO donor sodium nitroprusside was impaired. This is consistent with the idea that caveolae-dependent mechanisms downstream of NO generation are necessary for proper erectile function.

Relaxation induced by electrical field stimulation is a result of accumulation of cyclic GMP (Andersson, 2001). It has been proposed that soluble guanylyl cyclase requires association with caveolin-1 for erection in the rat (Linder et al., 2006), possibly because it needs to be in proximity with protein kinase G. Such a scenario may be consistent with impaired relaxation in response to an NO donor, but is not readily reconciled with the three-fold increase in cGMP seen in isolated smooth muscle cells from caveolin-1-deficient mice (Drab et al., 2001). Involvement of downstream protein effectors, such as protein kinase A and G may also be considered. cGMP-dependent kinase 1 plays an important role in relaxation of the corpus cavernosum (Hedlund et al., 2000). Protein kinase A and G have been found to colocalize with caveolin-1 in the aortic endothelium (Linder et al., 2005), and it cannot be ruled out that this is important for proper function in the cellular context of the corpus cavernosum. Impaired NO-mediated relaxation may also be caused by eNOS uncoupling. It was recently demonstrated that eNOS from caveolin-1-deficient mice generates more superoxide (Wunderlich et al., 2008). In fact, both the activity and expression of soluble guanylyl cyclase and the cGMP-dependent kinase I, are regulated in a redox-sensitive fashion (Schulz et al., 2008).

Increased endothelium-dependent relaxation of arteries from caveolin-1-deficeint mice has been demonstrated (e.g. Razani et al., 2001; Drab et al., 2001). This contrasts with the present findings, arguing that the role of caveolin-1 in regulation of NO signaling differs in corpus cavernosum compared to systemic arteries. Of note, El-Yazbi et al. (2005) reported that NO-dependent and EFS-induced dilatation of jejunal smooth muscle strips from caveolin-1-deficient mice was reduced, similar to our findings. Moreover, reduced relaxation in response to sodium nitroprusside, but not in response to direct activation of protein kinase G, was seen. Thus, in the ileum, the defect was localized at the level of soluble guanylyl cyclase.

Caveolin-1 staining was seen in both endothelium and in smooth muscle cells of the corpus cavernosum. Caveolin-3 staining was restricted to smooth muscle, but was fainter than in skeletal muscle occasionally present on the same glass. Caveolin-3 expression was unchanged in caveolin-1-deficient corpus cavernosum. The protein PTRF-Cavin, recently shown to be critical for caveola-formation (Hill et al., 2008), was reduced by ~80%. This is in keeping with a role of caveolin-1 in stabilizing PTRF-Cavin (Hill et al., 2008).

Reduced expression of caveolin-1 has been associated with increased collagen (Bakircioglu et al., 2001). Fibrosis may impair the erectile mechanism by restricting inflow of blood and reducing venous occlusion (Simopoulos et al., 2001). Gross morphology did not support any major fibrosis in the knockout. Fibrosis may not affect contractile dynamics *ex vivo*, but would compound erectile dysfunction *in vivo*. Another aspect not captured *ex vivo* is flow-mediated activation of eNOS, which is considered to be critical for upholding erection (Andersson, 2001). Flow-mediated signaling has been demonstrated to be impaired in caveolin-1-deficient mice (Albinsson et al., 2008; Yu et al., 2006) again arguing that erectile impairment may be more severe *in vivo*.

Vasoconstriction evoked by α_1-adrenergic stimulation maintains the penis in a flaccid state (Andersson, 2001). Increased arterial α_1-adrenergic contractility has been seen in caveolin-1-deficient mice (Shakirova et al., 2006; Albinsson et al., 2007; Neidhold et al., 2007). The response to cirazoline was not affected in KO corpus cavernosum. L-NAME did not significantly increase contractile force in either KO or WT, suggesting that basal NO production in the corpus cavernosum is low, which may be necessary to keep the penis flaccid.

RhoA/Rho-kinase signaling is believed to play a critical role in the corpus cavernosum (Chitaley et al., 2001; Park et al., 2006; Wang et al., 2002), and to be important for NO-mediated dilatation (Mills et al., 2002). No difference in sensitivity to Y27632 was detected in corpus cavernosum from KO when compared to WT controls, suggesting that impaired dilatation in the KO is independent of RhoA/Rho-kinase signaling in corporal tissue.

Taken together, this study has demonstrated a role of caveolin-1 in erectile function. Impaired nerve-mediated relaxation, and relaxation in response to both muscarinic stimulation and an NO-donor, suggests

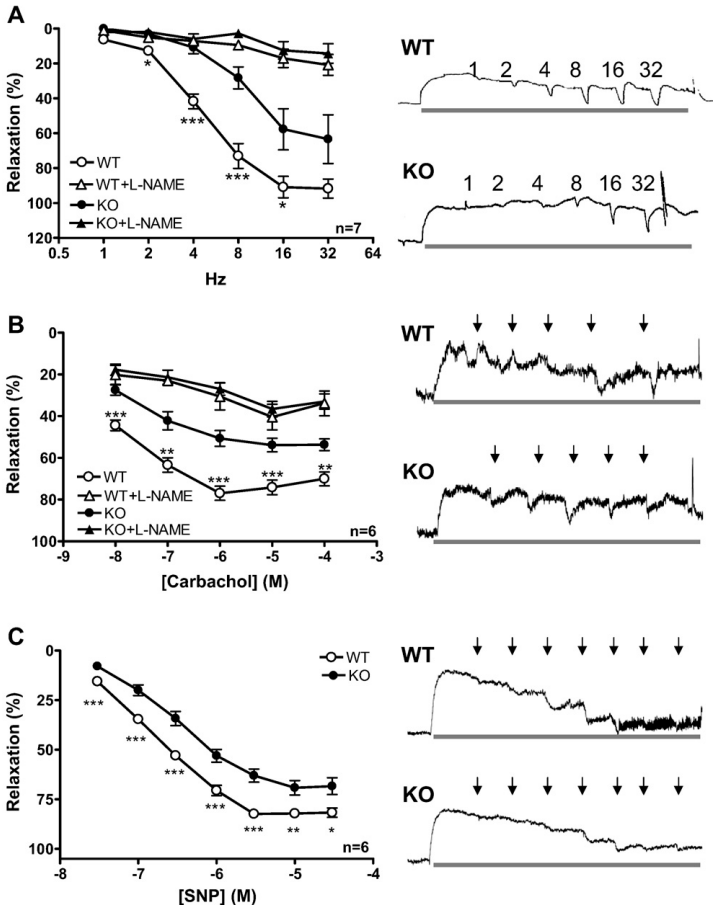

Fig. 5. A shows relaxation induced by electrical field stimulation in corporal strips precontracted with 0.3 μM cirazoline. Typical traces are shown to the right. B shows dose response relationships to muscarinic agonist carbachol after precontraction with 0.3 μM cirazoline. C shows relaxation by increasing concentrations of sodium nitrprusside (SNP) after precontraction with 0.3 μM cirazoline. WT: wild type; KO: knock out. *$P<0.05$, **$P<0.01$, and ***$P<0.001$ for WT vs. KO.

that the erectile mechanism is disturbed at or below the level of soluble guanylyl cyclase. The caveolin-1-deficient mouse may thus be considered a model for studying vasculogenic erectile dysfunction.

Acknowledgements

This study was supported by the Swedish Research Council, the Swedish Heart Lung Foundation, the Crafoord Foundation, the Royal Physiographic Society, the Thorsten and Ragnar Söderberg Foundation, the Thure Carlsson Foundation, and the Faculty of Medicine at Lund University. KS holds a senior scientist position at the Swedish Research Council.

References

Albinsson, S., Shakirova, Y., Rippe, A., Baumgarten, M., Rosengren, B.I., Rippem, C., Hallmann, R., Hellstrand, P., Rippe, B., Swärd, K., 2007. Arterial remodeling and plasma volume expansion in caveolin-1-deficient mice. Am. J. Physiol., Regul. Integr. Comp. Physiol. 293, R1222–R1231.

Albinsson, S., Nordström, I., Swärd, K., Hellstrand, P., 2008. Differential dependence of stretch and shear stress signaling on caveolin-1 in the vascular wall. Am. J. Physiol. Cell Physiol. 294, C271–C279.

Andersson, K.E., 2001. Pharmacology of penile erection. Pharmacol. Rev. 53, 417–450.

Bakircioglu, M.E., Sievert, K.D., Nunes, L., Lau, A., Lin, C.S., Lue, T.F., 2001. Decreased trabecular smooth muscle and caveolin-1 expression in the penile tissue of aged rats. J. Urol. 166, 734–738.

Chitaley, K., Wingard, C.J., Webb, R.C., Branam, H., Stopper, V.S., Lewis, R.W., Mills, T.M., 2001. Antagonism of Rho-kinase stimulates rat penile erection via a nitric oxide-independent pathway. Nat. Med. 7, 119–122.

Cohen, A.W., Hnasko, R., Schubert, W., Lisanti, M.P., 2004. Role of caveolae and caveolins in health and disease. Physiol. Rev. 84, 1341–1379.

Drab, M., Verkade, P., Elger, M., Kasper, M., Löhn, M., Lauterbach, B., Menne, J., Lindschau, C., Mende, F., Luft, F.C., Schedl, A., Haller, H., Kurzchalia, T.V., 2001. Loss of caveolae, vascular dysfunction, and pulmonary defects in caveolin-1 gene-disrupted mice. Science 293, 2449–2452.

El-Yazbi, A.F., Cho, W.J., Boddy, G., Daniel, E.E., 2005. Caveolin-1 gene knockout impairs nitrergic function in mouse small intestine. Br. J. Pharmacol. 145, 1017–1026.

Feifer, A., Carrier, S., 2008. Pharmacotherapy for erectile dysfunction. Expert Opin. Investig. Drugs. 17, 679–690.

García-Cardeña, G., Oh, P., Liu, J., Schnitzer, J.E., Sessa, W.C., 1996. Targeting of nitric oxide synthase to endothelial cell caveolae via palmitoylation: implications for nitric oxide signaling. Proc. Natl. Acad. Sci. U. S. A. 93, 6448–6453.

Hedlund, P., Aszodi, A., Pfeifer, A., Alm, P., Hofmann, F., Ahmad, M., Fässler, R., Andersson, K.E., 2000. Erectile dysfunction in cyclic GMP-dependent kinase I-deficient mice. Proc. Natl. Acad. Sci. U. S. A. 97, 2349–2354.

Hill, M.M., Bastiani, M., Luetterforst, R., Kirkham, M., Kirkham, A., Nixon, S.J., Walser, P., Abankwa, D., Oorschot, V.M., Martin, S., Hancock, J.F., Parton, R.G., 2008. PTRF-Cavin, a conserved cytoplasmic protein required for caveola formation and function. Cell 132, 113–124.

Ju, H., Zou, R., Venema, V.J., Venema, R.C., 1997. Direct interaction of endothelial nitric oxide synthase and caveolin-1 inhibits synthase activity. J. Biol. Chem. 272, 18522–18525.

Linder, A.E., McCluskey, L.P., Cole, K.R., Lanning, K.M., Webb, R.C., 2005. Dynamic association of nitric oxide downstream signaling molecules with endothelial caveolin-1 in rat aorta. J. Pharmacol. Exp. Ther. 314, 9–15.

Linder, A.E., Leite, R., Lauria, K., Mills, T.M., Webb, R.C., 2006. Penile erection requires association of soluble guanylyl cyclase with endothelial caveolin-1 in rat corpus cavernosum. Am. J. Physiol., Regul. Integr. Comp. Physiol. 290, R1302–R1308.

Michel, J.B., Feron, O., Sacks, D., Michel, T., 1997. Reciprocal regulation of endothelial nitric-oxide synthase by Ca^{2+}-calmodulin and caveolin. J. Biol. Chem. 272, 15583–15586.

Mills, T.M., Chitaley, K., Lewis, R.W., Webb, R.C., 2002. Nitric oxide inhibits RhoA/Rho-kinase signaling to cause penile erection. Eur. J. Pharmacol. 439, 173–174.

Musicki, B., Burnett, A.L., 2006. eNOS Function and dysfunction in the penis. Exp. Biol. Med. 231, 154–165.

Musicki, B., Liu, T., Strong, T., Jin, L., Laughlin, M.H., Turk, J.R., Burnett, A.L., 2008. Low-fat diet and exercise preserve eNOS regulation and endothelial function in the penis of early atherosclerotic pigs: a molecular analysis. J. Sex. Med. 5, 552–561.

Neidhold, S., Eichhorn, B., Kasper, M., Ravens, U., Kaumann, A.J., 2007. The function of alpha- and beta-adrenoceptors of the saphenous artery in caveolin-1 knockout and wild-type mice. Br. J. Pharmacol. 150, 261–270.

Park, K., Kim, S.W., Rhu, K.S., Paick, J.S., 2006. Chronic administration of an oral Rho kinase inhibitor prevents the development of vasculogenic erectile dysfunction in a rat model. J. Sex. Med. 3, 996–1003.

Razani, B., Engelman, J.A., Wang, X.B., Schubert, W., Zhang, X.L., Marks, C.B., Macaluso, F., Russell, R.G., Li, M., Pestell, R.G., Di Vizio, D., Hou Jr., H., Kneitz, B., Lagaud, G., Christ, G.J., Edelmann, W., Lisanti, M.P., 2001. Caveolin-1 null mice are viable but show evidence of hyperproliferative and vascular abnormalities. J. Biol. Chem. 276, 38121–38138.

Schulz, E., Jansen, T., Wenzel, P., Daiber, A., Münzel, T., 2008. Nitric oxide, tetrahydrobiopterin, oxidative stress, and endothelial dysfunction in hypertension. Antioxid. Redox. Signal. 10, 1115–1126.

Shakirova, Y., Bonnevier, J., Albinsson, S., Adner, M., Rippe, B., Broman, J., Arner, A., Swärd, K., 2006. Increased Rho activation and PKC-mediated smooth muscle contractility in the absence of caveolin-1. Am. J. Physiol. Cell Physiol. 291, C1326–1335.

Shaul, P.W., Smart, E.J., Robinson, L.J., German, Z., Yuhanna, I.S., Ying, Y., Anderson, R.G., Michel, T., 1996. Acylation targets endothelial nitric-oxide synthase to plasmalemmal caveolae. J. Biol. Chem. 271, 6518–6522.

Simopoulos, D.N., Gibbons, S.J., Malysz, J., Szurszewski, J.H., Farrugia, G., Ritman, E.L., Moreland, R.B., Nehra, A., 2001. Corporeal structural and vascular micro architecture with X-ray micro computerized tomography in normal and diabetic rabbits: histopathological correlation. J. Urol. 165, 1776–1782.

Tourkina, E., Gooz, P., Pannu, J., Bonner, M., Scholz, D., Hacker, S., Silver, R.M., Trojanowska, M., Hoffman, S., 2005. Opposing effects of protein kinase Calpha and protein kinase Cepsilon on collagen expression by human lung fibroblasts are mediated via MEK/ERK and caveolin-1 signaling. J. Biol. Chem. 280, 13879–13887.

Wang, H., Eto, M., Steers, W.D., Somlyo, A.P., Somlyo, A.V., 2002. RhoA-mediated Ca^{2+} sensitization in erectile function. J. Biol. Chem. 277, 30614–30621.

Wang, X.M., Zhang, Y., Kim, H.P., Zhou, Z., Feghali-Bostwick, C.A., Liu, F., Ifedigbo, E., Xu, X., Oury, T.D., Kaminski, N., Choi, A.M., 2006. Caveolin-1: a critical regulator of lung fibrosis in idiopathic pulmonary fibrosis. J. Exp. Med. 203, 2895–2906.

Woodman, S.E., Cheung, M.W., Tarr, M., North, A.C., Schubert, W., Lagaud, G., Marks, C.B., Russell, R.G., Hassan, G.S., Factor, S.M., Christ, G.J., Lisanti, M.P., 2004. Urogenital alterations in aged male caveolin-1 knockout mice. J. Urol. 171, 950–957.

Wunderlich, C., Schober, K., Lange, S.A., Drab, M., Braun–Dullaeus, R.C., Kasper, M., Schwencke, C., Schmeisser, A., Strasser, R.H., 2006. Disruption of caveolin-1 leads to enhanced nitrosative stress and severe systolic and diastolic heart failure. Biochem. Biophys. Res. Commun. 340, 702–708.

Wunderlich, C., Schmeisser, A., Heerwagen, C., Ebner, B., Schober, K., Braun-Dullaeus, R.C., Schwencke, C., Kasper, M., Morawietz, H., Strasser, R.H., 2008. Chronic NOS inhibition prevents adverse lung remodeling and pulmonary arterial hypertension in caveolin-1 knockout mice. Pulm. Pharmacol. Ther. 21, 507–515.

Yu, J., Bergaya, S., Murata, T., Alp, I.F., Bauer, M.P., Lin, M.I., Drab, M., Kurzchalia, T.V., Stan, R.V., Sessa, W.C., 2006. Direct evidence for the role of caveolin-1 and caveolae in mechanotransduction and remodeling of blood vessels. J. Clin. Invest. 116, 1284–1291.

Zhao, Y.Y., Liu, Y., Stan, R.V., Fan, L., Gu, Y., Dalton, N., Chu, P.H., Peterson, K., Ross Jr., J., Chien, K.R., 2002. Defects in caveolin-1 cause dilated cardiomyopathy and pulmonary hypertension in knockout mice. Proc. Natl. Acad. Sci. U. S. A. 99, 11375–11380.

Paper IV

European Journal of Pharmacology 634 (2010) 142–148

Contents lists available at ScienceDirect

European Journal of Pharmacology

journal homepage: www.elsevier.com/locate/ejphar

Pulmonary, Gastrointestinal and Urogenital Pharmacology

Human urinary bladder smooth muscle is dependent on membrane cholesterol for cholinergic activation

Yulia Shakirova [a,*], Michiko Mori [a], Mari Ekman [a], Jonas Erjefält [a], Bengt Uvelius [b], Karl Swärd [a]

[a] Department of Experimental Medical Science, Lund University, Biomedical Centre, BMC D12, SE-221 84 Lund, Sweden
[b] Department of Urology, Clinical Sciences, Lund University, SE-221 84 Lund, Sweden

ARTICLE INFO

Article history:
Received 16 July 2009
Received in revised form 9 December 2009
Accepted 9 February 2010
Available online 20 February 2010

Keywords:
Incontinence
Muscarinic receptor
Detrusor
Caveolae
Caveolin-1
Human

ABSTRACT

Voiding is mediated by muscarinic receptors in urinary bladder smooth muscle cells. Lipid rafts and caveolae are cholesterol enriched membrane domains that modulate the activity of G protein-coupled receptors and second messenger systems. Conflicting findings regarding sensitivity of muscarinic signalling to cholesterol desorption, which perturbs lipid rafts and caveolae, have been reported, and no study has used human urinary bladder. Here, the dependence of human bladder muscarinic receptor signalling on plasma membrane cholesterol was examined. Nerve-mediated contraction, elicited by electrical field stimulation of human bladder strips, was impaired by desorption of cholesterol using methyl-β-cyclodextrin, and the concentration–response curve for the muscarinic agonist carbachol was right-shifted. No effect of cholesterol desorption was observed in rat, and in mouse increased maximum contraction was seen. Expression of caveolin-1, $PLC_{\beta1}$ and M_3 muscarinic receptors did not differ between species in a manner that would explain the differential sensitivity to cholesterol desorption. In human bladder, threshold depolarisation eliminated the difference between cyclodextrin-treated and control preparations. Contraction elicited by depolarisation *per se* was not affected. M_3 muscarinic receptors appeared clustered along plasma membrane profiles as shown by immunohistochemical staining of human bladder, but no redistribution in association with cholesterol reduction was seen. Thus, muscarinic receptor-induced contraction of the urinary bladder exhibits species-specific differences in its sensitivity to cholesterol desorption suggesting differential roles of lipid rafts/caveolae in muscarinic receptor signalling between species.

1. Introduction

Lower urinary tract dysfunction (incontinence, overactive bladder) is a major pathology affecting the quality of life of millions of people, and with considerable economic impact (Levy and Muller, 2006; Milsom et al., 2000). The cholinergic nervous system plays a critical role in voiding through activation of muscarinic receptors in the bladder (Hegde, 2006). Muscarinic receptors in the urinary bladder are mainly represented by the muscarinic M_2 and M_3 receptor subtypes (Wang et al., 1995). Studies using knock-out mice have established a major role for muscarinic M_3 receptors (Matsui et al., 2002), which couple to Gq causing bladder contraction and voiding. Muscarinic M_2 receptors may prevent β-adrenergic formation of cyclic AMP, indirectly promoting bladder contraction (Ehlert et al., 2005), and this receptor subtype may assume a more prominent role in bladder pathology (Braverman et al., 1998).

Lipid rafts are dynamic aggregates of cholesterol and sphingolipids in the plasmalemma that are considered to play a role in signalling from G protein-coupled receptors (Simons and Toomre, 2000). Caveolae, a subcategory of lipid rafts, are 50 to 100 nm flask-shaped invaginations in the membrane (Cohen et al., 2004) and these organelles have been proposed to organize receptors and signalling intermediaries central to smooth muscle contraction (Bergdahl and Swärd, 2004). Caveolae are abundant in the detrusor (Gabella and Uvelius, 1990). Mice lacking caveolin-1 also lack caveolae in the bladder and exhibit several urological defects including decreased contractility on stimulation with carbachol (Lai et al., 2004, 2007; Woodman et al., 2004). Genetic ablation of caveolae was found to be associated with a 70% decrease in acetylcholine release from bladder nerve terminals (Lai et al., 2004).

Desorption of cholesterol from the cell membrane using cyclodextrins (Kilsdonk et al., 1995) causes reversible disassembly of caveolae (Dreja et al., 2002; Rothberg et al., 1992). Cholesterol lowering is not specific for caveolae and also affects lipid rafts and membrane fluidity. An advantage, however, over the genetically caveolae-ablated mice, is that compensation developing in response to life-long loss of caveolins is avoided. Moreover, cyclodextrins allow probing of the role of lipid rafts/caveolae in species other than the mouse, including humans.

A few studies on the role of caveolae for the function and localization of muscarinic receptors have accumulated. Feron et al. (1997) demonstrated that muscarinic M_2 receptors dynamically target rat cardiomyocyte

* Corresponding author. Tel.: +46 46 2224575; fax: +46 46 2113417.
E-mail address: Yulia.Shakirova@med.lu.se (Y. Shakirova).

0014-2999/$ – see front matter © 2010 Elsevier B.V. All rights reserved.
doi:10.1016/j.ejphar.2010.02.017

caveolae. Moreover, in guinea pig intestinal smooth muscle muscarinic M_2 receptors were demonstrated to co-localize with caveolae (Iino and Nojyo, 2006), but the consequences for signalling are uncertain as discrepant findings were reported in mouse and rat (El-Yazbi et al., 2008; Shakirova et al., 2006; Somara et al., 2007). M_3 muscarinic receptors were recently colocalized with caveolin-1 in canine airway smooth muscle, and disruption of caveolae impaired cholinergic Ca^{2+} signalling in both canine and human airway muscle cells (Gosens et al., 2007). Only one study has probed the role of caveolae in cholinergic bladder contraction in a species other than the mouse. Cristofaro et al. (2007) disrupted caveolae in rat bladder using cyclodextrin and found that cholinergic contractions were unchanged.

In view of the apparent controversy regarding the dependence of cholinergic signalling on rafts/caveolae we hypothesized that differences may exist between species. In the present study the sensitivity of human bladder cholinergic contraction to cholesterol desorption was examined and compared with that of rat and mouse bladders.

2. Materials and methods

2.1. Patients and animals

Human bladder tissue was obtained from patients undergoing radical cystectomy for treatment of localized bladder cancer. 25 patients, 20 male and 5 female, with ages ranging from 39 to 82 years (median 67) were selected on the basis of localization, size and spread of the bladder cancer. 16–22 week old C57Bl6/J mice were obtained from Taconic (Ejby, Denmark). Female Sprague–Dawley rats weighing 250 g were obtained from the same vendor. Human experiments were approved by the regional human ethics committee and all patients gave their written informed consent. The local animal ethics committee in Lund/Malmö approved all experiments involving animals.

2.2. Tissue preparation

Human bladder specimens were dissected from the ventral midportion of the excised bladder, and rapidly transported to the lab in ice-cold HEPES buffered Krebs (composition in mM: NaCl 135.5, KCl 5.9, $MgCl_2$ 1.2, glucose 11.6, HEPES 11.6, pH 7.4). Only healthy tissue far from the tumor was used for experimentation. Mice and rats were killed by CO_2 asphyxiation and the bladder was rapidly removed. Bladders were immediately placed in cold nominally Ca^{2+}-free HEPES buffered Krebs solution. Homogenous bundles of urinary bladder smooth muscle were carefully dissected free of fat and connective tissue and the urothelium was removed. Strips measuring 1 mm (width) × 0.2 mm (thickness) × 3 mm (length, mouse dimensions), 1 mm × 0.3 mm × 3 mm (rat), and 1 mm × 0.8 mm × 3 mm (human) were mounted horizontally using silk sutures.

2.3. Electrical field stimulation

Using silk sutures, strips were mounted on steel pins connected to a force transducer in 5 ml open organ baths with Krebs solution (composition in mM: NaCl 119, KCl 4.6, NaH_2PO_4 1.2, $NaHCO_3$ 15, $MgCl_2$ 1.2, glucose 5.5 and $CaCl_2$ 1.5), gassed with 95% O_2 and 5% CO_2 at 37 °C (pH 7.4). The passive tension was adjusted to 3 mN and preparations were allowed to equilibrate for 45 min. Strips were first activated with high K^+ solution (obtained by exchanging NaCl for KCl) twice (5 min each). The mean value of the initial peak responses was used as reference for normalization of subsequent force responses. Platinum electrodes were then mounted on both sides of the preparation. Strips were activated at two-minute intervals for 5-s periods at 20 Hz (pulse duration 0.5 ms) with increasing voltage to find the optimal stimulation voltage. This voltage was used during the remainder of the experiment. Cholesterol was removed by incubation for 40 min in 10 mM methyl-β-cyclodextrin (mβcd), (Dreja et al., 2002; Kilsdonk et al., 1995). Treatment with mβcd depletes roughly 20% of tissue cholesterol and leads to reversible disruption of caveolae (Dreja et al., 2002). Control and cyclodextrin-treated preparations were always run in parallel. Frequency–response curves were then determined by increasing the frequency in steps from 1 to 50 Hz (5 s stimuli at two-minute intervals). The experiments were terminated by high K^+ activation to ensure that force was not lost during the course of the experiments.

2.4. Myograph experiments

Smooth muscle strips were mounted in myographs (610 M, Danish MyoTechnology). Baths contained aerated HEPES buffered Krebs solution with 2.5 mM Ca^{2+}. A basal tension of 3 mN was applied as above. After equilibration for 30 min at 37 °C, the solution was changed to high K^+ solution, obtained by replacing 60 mM NaCl for KCl, for 7 min. Following relaxation cholesterol was extracted with cyclodextrin as above. Carbachol was added in a cumulative manner to final concentrations ranging between 10^{-8} and 3×10^{-5} M. Each concentration was maintained for 7 min. Force responses to agonists were expressed relative to mean high K^+ induced contraction. In Fig. 3D preparations were partially contracted using 25 mM K^+ following cholesterol desorption and washing. Carbachol was then added cumulatively during sustained contraction as above. The force caused by 25 mM K^+ did not differ between groups and was not subtracted from the carbachol-induced force in 3A.

2.5. Western blotting

Western blotting was performed as described (Shakirova et al., 2006), with antibody dilutions as recommended by the manufacturers. Antibodies against caveolin-1 (clone 2297), PTRF-cavin (Polymerase and Transcript Release Factor-cavin, a.k.a. cavin-1), and phospholipase $C_{\beta 1}$ ($PLC_{\beta 1}$) were from BD Biosciences Pharmingen. Anti-M_3 (H-210) was from Santa Cruz Biotechnology (Santa Cruz, CA). Protein concentration was determined using EZQ protein assay (R-33200, Molecular Probes, CA). Equal amounts of protein were loaded in all lanes. After transfer of proteins to nitrocellulose membranes, proteins remaining on the gel were stained with Coomassie brilliant blue. Blots and gels were analyzed in the Fluor-S™ MultiImager (BIO-RAD) using general background subtraction. Optical densities times the area (mm^2) of the bands of interest was normalized to total protein in the same lane on the gels. Sections of these gels, centered over actin, are shown below blots as controls for protein loading.

2.6. Immunohistochemistry

Following relaxation in Ca^{2+}-free solution for 30 min at room temperature, human urinary bladder preparations were fixed in Histochoice (Amresco, Solon, Ohio, USA) overnight and embedded in paraffin. M_2 and M_3 muscarinic receptors were visualized on 3 μm serial paraffin sections using an automated immunohistochemistry robot (Autostainer, DakoCytomation, Glostrup, Denmark) and the EnVision™ Detection System Peroxidase/DAB (K5007, Dako, Glostrup, Denmark). In preliminary tests two distinct antibodies against the M_3 receptor were evaluated (AB9217, Chemicon International, Inc., Millipore, Temecula, CA, USA, and GTX13063, GeneTex, Inc., Irvine, CA, USA). Both tested antibodies produced similar M_3 staining patterns but the GeneTex antibody was selected for the remainder of the study.

Briefly, sections were deparaffinized, rehydrated, and subjected to heat-induced antigen retrieval using a low pH citrate buffer (pH 6; only M_3) and a pressure cooker (2100 Retriever, Prestige Medical Ltd., Blackburn, England). Endogenous peroxidase activity was blocked with 0.3% hydrogen peroxide before incubation with rabbit polyclonal

antibodies against M_2 (1:300, AB9452, Chemicon International) or M_3 muscarinic receptors (1:100, GTX13063, GeneTex). The primary antibodies were detected with polymer-bound anti-rabbit secondary antibodies and horseradish peroxidase (HRP) (EnVision™, Dako). After counter staining with Mayer's haematoxylin cell nuclei appear blue whereas M_2 or M_3 immunoreactivity is identified by the brown HRP product. All slides were examined by bright field microscopy (Nikon E80i, Nikon, Tokyo, Japan). Negative controls were performed by omitting the primary antibody or using matched control sera.

2.7. Chemicals

All chemicals not specified above were of analytical grade or better and obtained from Sigma (Sigma Aldrich, Sweden).

2.8. Statistics

In the typical experiment an even number of preparations ranging from 4 to 12 from each patient or animal was mounted. Half of the preparations were treated with mβcd and the other half with vehicle. The means of the contractile responses of all control- and all mβcd-treated strips from each individual were then entered into graphs and statistical tests and considered to represent one observation. Means based on all subjects (±S.E.M.) are shown in the figures. The number of animals/human subjects are denoted by *h* (number of human subjects), *r* (number of rats), and *m* (number of mice). Student's *t*-test for paired or unpaired data, as appropriate, was used to test for differences between groups. $P<0.05$ was considered significant. One-way ANOVA followed by Bonferroni's multiple comparisons test was used for multiple comparisons. Significance is indicated by $^{*}P<0.05$, and $^{**}P<0.01$.

3. Results

3.1. EFS-induced contraction of human bladder strips following desorption of cholesterol

Electrical field stimulation (EFS), at frequencies ranging from 1 to 50 Hz, caused a frequency-dependent increase of contraction in human bladder strips. At frequencies exceeding 10 Hz EFS-induced contraction was impaired following reduction of cholesterol using methyl-β-cyclodextrin (mβcd, Fig. 1A). Threshold depolarisation with 25 mM K^+ eliminated the effect of cholesterol lowering and reduced the amplitude of EFS-induced contractions (Fig. 1B). Stimulation with K^+-high solution following either EFS protocol caused indistinguishable contraction in control and depleted preparations (Fig. 1C).

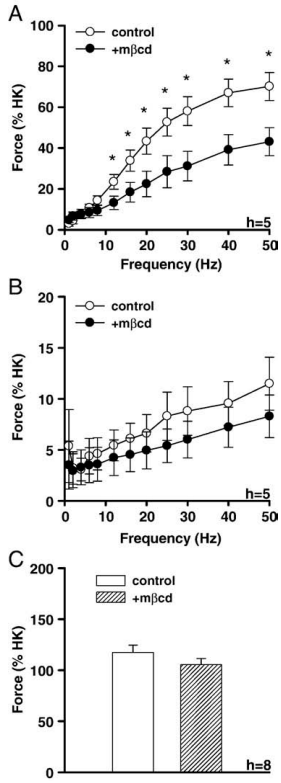

Fig. 1. (A) shows force elicited by electrical field stimulation (EFS), normalized to the mean of two reference high K^+ contractions (125 mM). Open symbols represent vehicle-treated control strips from human urinary bladder and filled symbols represent methyl-β-cyclodextrin-treated (mβcd, 10 mM, 40 min) strips from the same patients run in parallel. At frequencies between 10 and 50 Hz EFS-induced contraction was impaired following depletion of cholesterol ($P<0.05$). (B) shows an identical experiment to that in (A) except that all preparations were pre-contracted with 25 mM K^+ prior to EFS. (C) shows force elicited by 125 mM K^+ following vehicle/mβcd and EFS. Force is normalized to the mean of two reference high K^+ contractions (125 mM) prior to the depletion protocol. In this and the following figure *h* denotes the number of human subjects.

3.2. Effect of cholesterol desorption on carbachol contraction in urinary bladder from different species

Full concentration–response curves for the muscarinic receptor agonist carbachol were generated in human (Fig. 2A), rat (Fig. 2B) and mouse (Fig. 2C) bladder strips. In human bladder strips, contractile responses to carbachol were significantly suppressed between 0.03 and 3 μM following cholesterol reduction. Contractility at saturating concentrations of carbachol was however unaffected. Cholesterol reduction had no effect in rat bladder (Fig. 2B). In the mouse, cholesterol desorption increased force at the two highest carbachol concentrations (Fig. 2C), but did not right- or left-shift the curve.

3.3. Effect of depolarisation on cholinergic contraction following cholesterol desorption from human urinary bladder

Depolarisation with 25 mM K^+ completely eliminated the effect of cholesterol desorption on the concentration–response curve for carbachol in human urinary bladder (Fig. 3A), similar to the effect of threshold depolarisation on EFS-induced contraction (cf. Fig 1B). Moreover, the difference in the concentration–response relationships between control and cholesterol-depleted preparations appeared less pronounced in the presence of nifedipine (1 μM, Fig. 3B), but a significant difference was still seen at 0.3 μM. Contraction induced by depolarisation was not significantly affected by cholesterol desorption at any concentration of K^+ (Fig. 3C).

3.4. Effect of cholesterol desorption on purinergic contraction in human bladder

The peak response of human bladder strips on application of a single concentration of the purinergic agonist ATP (1 mM) was not affected by cholesterol desorption (26 ± 13% of HK for control vs. 25 ± 10% for mβcd, $h=4$).

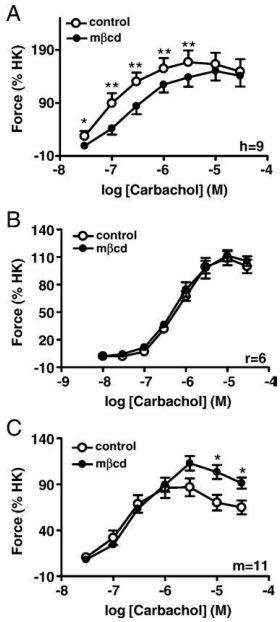

Fig. 2. Concentration–response relationships for the muscarinic receptor agonist carbachol in human (A), rat (B), and mouse (C) control (white symbols) and cholesterol-depleted (black symbols) urinary bladder strips. Force was normalized to the depolarisation-induced contraction (60 mM K^+, HK) elicited before the depletion protocol. *h*, *r*, and *m* refer to the number of humans, rats, and mice, respectively.

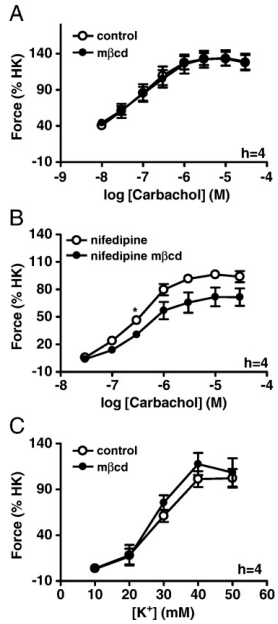

Fig. 3. (A) shows concentration–response relationships for carbachol in control (white circles) and mβcd-treated (black circles) human bladder strips following pre-treatment with 25 mM K^+. (B) shows concentration–response relationships for carbachol in human bladder in the presence of the L-type Ca^{2+}-channel blocker nifedipine (1 μM). (C) shows concentration–response relationships for K^+-high solution.

3.5. Expression of M_3, phospholipase $C_{\beta 1}$, caveolin-1 and PTRF-cavin

The expression of proteins involved in caveolae-formation and muscarinic receptor signalling was next compared between species using Western blotting. The expression of caveolin-1, PTRF-cavin, M_3, and phospholipase $C_{\beta 1}$ did not differ between human and rat bladder (Fig. 4A–D). Caveolin-1 appeared higher in rat than in mouse bladder, but this difference did not reach significance. $PLC_{\beta 1}$ was higher in mouse bladder compared to both human and rat bladders. Mouse urinary bladder also expressed more M_3 receptor protein in comparison to both human and rat bladders. PTRF-cavin levels did not differ between human, mouse, and rat urinary bladders.

3.6. Immunohistochemical demonstrations of M_2 and M_3 muscarinic receptors in human bladder tissue

Immunoreactivity for M_2 and M_3 muscarinic receptors was observed in the detrusor smooth muscle of human urinary bladder as demonstrated in Fig. 5A (M_2) and 5C (M_3). Desorption of cholesterol did not affect the pattern or intensity of the M_2 or M_3 immunoreactivity (compare 5B vs. 5A for M_2 and 5D vs. 5C for M_3). The staining for M_2 was homogenously distributed over the smooth muscle cells. In contrast, the M_3 immunoreactivity was clustered to distinct areas at or near the membrane suggesting compartmentalization of M_3 receptors on smooth muscle cells (Fig. 5E and F). A handful of such clusters per cell were seen in cross-sections at high magnification (Fig. 5F). Apart from positive staining in the detrusor smooth muscle, M_2 (Fig. 5G) and M_3 (Fig. 5H) muscarinic receptor immunoreactivity was also localized to the endothelium and vascular smooth muscle of blood vessels in the urinary bladder.

4. Discussion

In the present study species-specific differences in the sensitivity of muscarinic receptor signalling to cholesterol desorption are unveiled. It is well established that the reduction of plasma membrane cholesterol leads to disruption of lipid rafts and caveolae. This is found here to cause sizeable inhibition of cholinergic contraction in human, but not in mouse or rat urinary bladder. Differences in the ability of cyclodextrins to remove cholesterol and to ablate caveolae between species are possible. In rat bladder, a desorption-protocol similar to that used here was however found to affect serotonin, angiotensin II, and bradykinin contraction as well as the ultra structure of caveolae, despite leaving carbachol responses unaltered (Cristofaro et al., 2007). Thus, rat bladder muscarinic contraction does not resist cholesterol desorption because caveolae are insensitive to the effects of cyclodextrins. The effect of cholesterol desorption in human bladder does not represent a general impairment of contractility because cholesterol reduction did not affect purinergic contraction or contraction induced by membrane depolarisation. Moreover, threshold depolarisation eliminated the effect of cholesterol lowering, suggesting that the signalling mechanism targeted may be located downstream of receptor activation and involving membrane depolarisation.

This work is not the first to document differences between human and rodent bladder function. Recent work has demonstrated that relaxation by cathecholamines is dominated by β_3-adrenergic receptors in human bladder whereas β_2-adrenergic receptors dominate in the mouse (Wuest et al., 2009). Moreover, Ca^{2+} influx mechanisms were found to differ between mouse, pig, and human detrusor, with a smaller contribution of L-type Ca^{2+} channels in

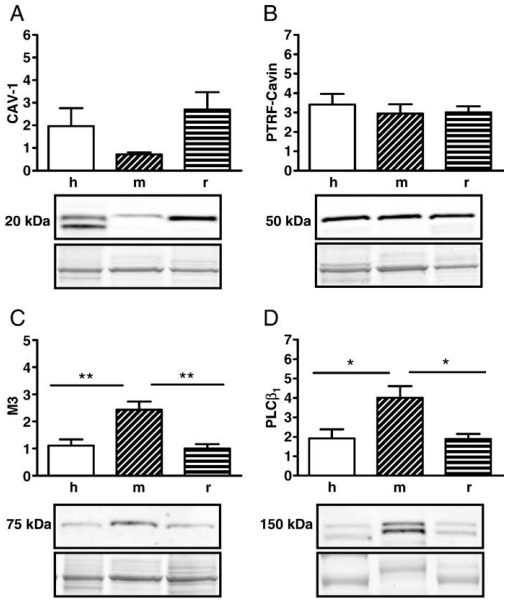

Fig. 4. The results of Western blotting for caveolin-1 (A), PTRF-cavin (B), M_3 (C), and phospholipase $C_{\beta 1}$ (D) are summarized as bar graphs for human, mouse, and rat urinary bladders. Expression was normalized to total protein on the Coomassie brilliant blue stained gel. Representative Western blots and excerpts from the stained gel, centered over actin, are shown below each bar graph. Positions of molecular weight markers are indicated to the left of the blots. *h*, *m*, and $r = 4$.

human as compared to pig and mouse (Wuest et al., 2007). The atropine resistant component of contractions elicited by electrical field stimulation is also considerably larger in mouse (50–75%) than in human (25%) bladder (Wuest et al., 2005). A different dependence of muscarinic receptors on membrane cholesterol, and thus presumably on rafts/caveolae, may now be added to this list of discrepancies between man and rodent detrusor function.

It is necessary to discuss what desorption of cholesterol vis à vis lifetime genetic ablation of caveolin tells us about the physiological function of caveolae in the bladder. While lowering of cholesterol causes clear-cut disassembly of caveolae (Dreja et al., 2002; Cristofaro et al., 2007; Rothberg et al., 1992) it also affects lipid rafts, which are planar assemblies of glycosphingolipids, cholesterol, and glycosylphosphatidylinositol-anchored proteins. Moreover, cyclodextrin treatment may affect rather specific interactions between e.g. receptors and cholesterol molecules as well as the fluidity of the membrane. Thus, cholesterol reduction cannot be equated with disruption of the caveolin-1 gene, and these interventions do indeed often result in opposite effects. For example, the activity of endothelial nitric oxide synthase (eNOS), which is a prototypical caveolae-associated enzyme, is inhibited by desorption of cholesterol (Darblade et al., 2001), but increased in caveolin-1-deficient mice (Drab et al., 2001; Razani et al., 2001; Zhao et al., 2002).

Findings in the mouse bladder seemingly replicate the situation with eNOS with regard to the opposing functions of cholesterol and caveolin-1. It has been reported that cholinergic contraction is impaired in caveolin-1-deficient mouse bladder (Lai et al., 2004; Woodman et al., 2004; Wuest et al., 2009), and that the gravity of this phenotype increases with age (Lai et al., 2007). As shown here, acute disruption of caveolae and lipid rafts actually has the opposite, albeit modest, effect in mouse bladder, i.e. it increases the efficacy of carbachol.

In order to better understand the differences in cholinergic sensitivity to reduction of cholesterol, the expression of proteins involved in formation of caveolae and in muscarinic signalling was examined. Differences in the expression of M_3 muscarinic receptors, and phospholipase $C_{\beta 1}$ were noted between mouse and rat, and occasionally human, bladder. It was recently discovered that PTRF-cavin (also known as cav-p60, PTRF, and cavin-1) plays a key role in formation of caveolae (Hill et al., 2008), and similar amounts of this protein were detected in all species. Importantly, all of the proteins examined appeared to be equally expressed in human and rat bladders. Thus different densities of caveolin-1, muscarinic M_3 receptors, or phospholipase $C_{\beta 1}$ are not likely to explain the differences in cholinergic sensitivity to cholesterol lowering between man and rat.

Our immunohistochemical staining supported subcellular compartmentalization of muscarinic M_3 but not M_2 receptors in human urinary bladder smooth muscle. The sarcolemma in most gastrointestinal and urogenital smooth muscle cells has a bipartite organization where longitudinal strands of membrane studded with caveolae are separated by so called dense bands. We have previously found that 7–15 such "caveolae domains" can be distinguished in cross-sectioned intestinal smooth muscle cells (Shakirova et al., 2006). This agrees roughly with the number of cross-sectional clusters of muscarinic M_3 receptors found here ($\approx$7). Our findings thus appear to be in accordance with the results of Gosens et al. (2007) who found muscarinic M_3 receptors to be clustered and to co-localize with caveolae domains in airway smooth muscle. The staining for muscarinic M_2 receptors, on the other hand, may at first glance appear to be at variance with the reported targeting of muscarinic M_2 receptors to caveolae in cardiomyocytes and intestinal smooth muscle (Feron et al., 1997; Iino and Nojyo, 2006). However, our tissues were fixed under non-stimulated and fully relaxed conditions precluding us from capturing any dynamic changes in localization.

Difficulties in raising specific antibodies against the family of G protein-coupled receptors have previously been recognized (Michel et al., 2009). Indeed, recent publications have raised concerns regarding the specificity of several commercially available anti-muscarinic receptor antibodies (Jositsch et al., 2009; Pradidarcheep et al., 2008, 2009). A number of hard criteria for acceptable specificity were set forth: i) absent staining in knock-out animals or after knock down, ii) increased staining in over-expressing cells lacking related receptor subtypes, and iii) a similar staining pattern using multiple antibodies against different receptor epitopes. Immunization peptides for pre-absorption control experiments were not available for the antibodies used in this study. One of the hard criteria above was however fulfilled, namely that the same pattern of immunoreactivity was produced by distinct antibodies against the same receptor.

In the human bladder our analysis allows us to generally localize the defect in muscarinic signalling that is caused by lowering of cholesterol. Because the response to depolarisation by K^+-high solution was unchanged, an effect on voltage gated Ca^{2+}-channels can be ruled out. It was found that threshold depolarisation eliminated the effect of mβcd treatment on both EFS-induced contractions and the concentration–response curve for carbachol. This would not occur if cholesterol reduction was acting at the receptor level and therefore favours a site of action located downstream of receptor activation and involving processes of membrane depolarisation. In support of this reasoning, introduction of the L-type Ca^{2+}-channel blocker nifidipine similarly appeared to reduce the effect of cholesterol desorption. Moreover, the cellular distribution of M_3 receptors was apparently not altered by cholesterol extraction. Thus, our findings appear to place the defect incurred by cholesterol desorption in human bladder at the level of

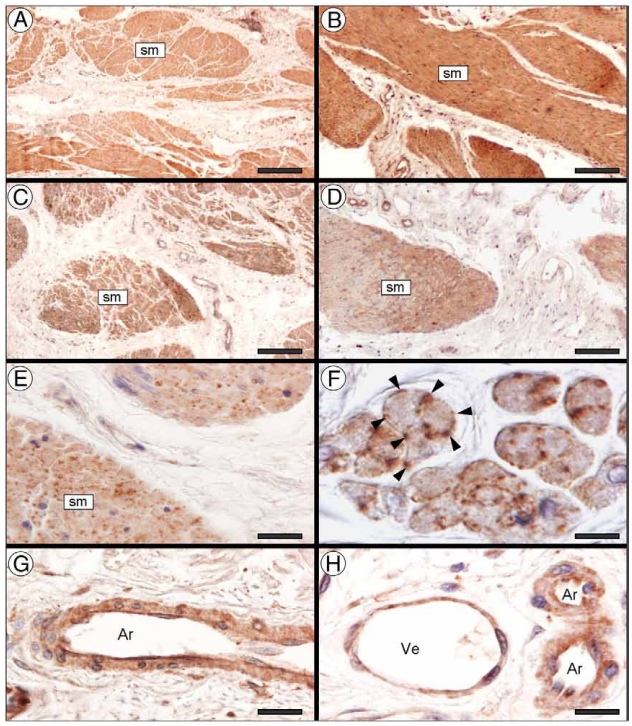

Fig. 5. Immunohistochemical labelling of muscarinic receptors in human bladder. The peroxidase activity of the secondary antibodies results in brown pigments and nuclei are stained blue. M_2 receptor in the human detrusor muscle (sm) (A) and in cholesterol-depleted detrusor (B). M_3 immunoreactivity in human detrusor (C) and in cholesterol-depleted urinary bladder (D). The distribution of M_3 was punctuated (E and F). A handful of such clusters per cell (arrowheads) were evident at higher magnification (F). Immunolocalization of M_2 (G) and M_3 (H) in arteries (Ar) and venules (Ve) of the urinary bladder. Scale bar: A, C = 100 μm; B, D = 50 μm; E, G, and H = 10 μm; F = 2.5 μm.

membrane depolarisation. This is consistent with the findings by Gosens et al. (2007). These authors depleted cholesterol from human airway smooth muscle cells and found that this impaired acetylcholine-mediated Ca^{2+} mobilization at intermediate agonist concentrations whereas neither the K_d nor B_{max} for muscarinic receptors was affected. Clearly, however, a contribution of effects involving e.g. transmitter release cannot be ruled out in our EFS experiments.

Taken together, the present study reveals that cholinergic contraction of the urinary bladder exhibits species-specific differences in its sensitivity to cholesterol desorption. Pinpointing the exact mechanism of action in human bladder will require further study, but the present data do suggest differential or even opposing roles of lipid rafts/caveolae in muscarinic signalling between species. Thus, attempts to target raft/caveolae-associated signalling mechanism in the urinary bladder for therapeutic benefit in man on the basis of results obtained in rodents may be unwarranted.

Acknowledgements

This work was supported by grants from the Swedish Research Council (K2009-65X-4955-01-3), ALF, the Crafoord Foundation, the Royal Physiographic Society, Lars Hierta's Foundation, Greta and Johan Kock's Foundation, and the Faculty of Medicine at Lund University. KS is a Senior Researcher at the Swedish Research Council.

References

Bergdahl, A., Swärd, K., 2004. Caveolae-associated signalling in smooth muscle. Can. J. Physiol. Pharmacol. 82, 289–299.
Braverman, A.S., Luthin, G.R., Ruggieri, M.R., 1998. M_2 muscarinic receptor contributes to contraction of the denervated rat urinary bladder. Am. J. Physiol. 275, R1654–R1660.
Cohen, A.W., Hnasko, R., Schubert, W., Lisanti, M.P., 2004. Role of caveolae and caveolins in health and disease. Physiol. Rev. 84, 1341–1379.
Cristofaro, V., Peters, C.A., Yalla, S.V., Sullivan, M.P., 2007. Smooth muscle caveolae differentially regulate specific agonist induced bladder contractions. Neurourol. Urodyn. 26, 71–80.
Darblade, B., Caillaud, D., Poirot, M., Fouque, M., Thiers, J.C., Rami, J., Bayard, F., Arnal, J.F., 2001. Alteration of plasmalemmal caveolae mimics endothelial dysfunction observed in atheromatous rabbit aorta. Cardiovasc. Res. 50, 566–576.
Drab, M., Verkade, P., Elger, M., Kasper, M., Lohn, M., Lauterbach, B., Menne, J., Lindschau, C., Mende, F., Luft, F.C., Schedl, A., Haller, H., Kurzchalia, T.V., 2001. Loss of caveolae, vascular dysfunction, and pulmonary defects in caveolin-1 gene-disrupted mice. Science 293, 2449–2452.
Dreja, K., Voldstedlund, M., Vinten, J., Tranum-Jensen, J., Hellstrand, P., Swärd, K., 2002. Cholesterol depletion disrupts caveolae and differentially impairs agonist-induced arterial contraction. Arterioscler. Thromb. Vasc. Biol. 22, 1267–1272.
Ehlert, F.J., Griffin, M.T., Abe, D.M., Vo, T.H., Taketo, M.M., Manabe, T., Matsui, M., 2005. The M_2 muscarinic receptor mediates contraction through indirect mechanisms in mouse urinary bladder. J. Pharmacol. Exp. Ther. 313, 368–378.
El-Yazbi, A.F., Cho, W.J., Schulz, R., Daniel, E.E., 2008. Calcium extrusion by plasma membrane calcium pump is impaired in caveolin-1 knockout mouse small intestine. Eur. J. Pharmacol. 591, 80–87.
Feron, O., Smith, T.W., Michel, T., Kelly, R.A., 1997. Dynamic targeting of the agonist-stimulated M2 muscarinic acetylcholine receptor to caveolae in cardiac myocytes. J. Biol. Chem. 272, 17744–17748.
Gabella, G., Uvelius, B., 1990. Urinary bladder of rat: fine structure of normal and hypertrophic musculature. Cell Tissue Res. 262, 67–79.

Gosens, R., Stelmack, G.L., Dueck, G., Mutawe, M.M., Hinton, M., McNeill, K.D., Paulson, A., Dakshinamurti, S., Gerthoffer, W.T., Thliveris, J.A., Unruh, H., Zaagsma, J., Halayko, A.J., 2007. Caveolae facilitate muscarinic receptor-mediated intracellular Ca2+ mobilization and contraction in airway smooth muscle. Am. J. Physiol. Lung. Cell. Mol. Physiol. 293, 1406–1418.

Hegde, S.S., 2006. Muscarinic receptors in the bladder: from basic research to therapeutics. Br. J. Pharmacol. 147 (2), S80–S87.

Hill, M.M., Bastiani, M., Luetterforst, R., Kirkham, M., Kirkham, A., Nixon, S.J., Walser, P., Abankwa, D., Oorschot, V.M., Martin, S., Hancock, J.F., Parton, R.G., 2008. PTRF-Cavin, a conserved cytoplasmic protein required for caveola formation and function. Cell 132, 113–124.

Iino, S., Nojyo, Y., 2006. Muscarinic M(2) acetylcholine receptor distribution in the guinea-pig gastrointestinal tract. Neuroscience 138, 549–559.

Jositsch, G., Papadakis, T., Haberberger, R.V., Wolff, M., Wess, J., Kummer, W., 2009. Suitability of muscarinic acetylcholine receptor antibodies for immunohistochemistry evaluated on tissue sections of receptor gene-deficient mice. Naunyn Schmiedebergs Arch. Pharmacol. 379, 389–395.

Kilsdonk, E.P., Yancey, P.G., Stoudt, G.W., Bangerter, F.W., Johnson, W.J., Phillips, M.C., Rothblat, G.H., 1995. Cellular cholesterol efflux mediated by cyclodextrins. J. Biol. Chem. 270, 17250–17256.

Lai, H.H., Boone, T.B., Yang, G., Smith, C.P., Kiss, S., Thompson, T.C., Somogyi, G.T., 2004. Loss of caveolin-1 expression is associated with disruption of muscarinic cholinergic activities in the urinary bladder. Neurochem. Int. 45, 1185–1193.

Lai, H.H., Boone, T.B., Thompson, T.C., Smith, C.P., Somogyi, G.T., 2007. Using caveolin-1 knockout mouse to study impaired detrusor contractility and disrupted muscarinic activity in the aging bladder. Urology 69, 407–411.

Levy, R., Muller, N., 2006. Urinary incontinence: economic burden and new choices in pharmaceutical treatment. Adv. Ther. 23, 556–573.

Matsui, M., Motomura, D., Fujikawa, T., Jiang, J., Takahashi, S., Manabe, T., Taketo, M.M., 2002. Mice lacking M_2 and M_3 muscarinic acetylcholine receptors are devoid of cholinergic smooth muscle contractions but still viable. J. Neurosci. 22, 10627–10632.

Michel, M.C., Wieland, T., Tsujimoto, G., 2009. How reliable are G-protein-coupled receptor antibodies? Naunyn Schmiedebergs Arch. Pharmacol. 379, 385–388.

Milsom, I., Stewart, W., Thüroff, J., 2000. The prevalence of overactive bladder. Am. J. Manag. Care 6, 565–573.

Pradidarcheep, W., Labruyere, W.T., Dabhoiwala, N.F., Lamers, W.H., 2008. Lack of specificity of commercially available antisera: better specifications needed. J. Histochem. Cytochem. 56, 1099–1111.

Pradidarcheep, W., Stallen, J., Labruyere, W.T., Dabhoiwala, N.F., Michel, M.C., Lamers, W.H., 2009. Lack of specificity of commercially available antisera against muscarinergic and adrenergic receptors. Naunyn Schmiedebergs Arch. Pharmacol. 379, 397–402.

Razani, B., Engelman, J.A., Wang, X.B., Schubert, W., Zhang, X.L., Marks, C.B., Macaluso, F., Russell, R.G., Li, M., Pestell, R.C., Di Vizio, D., Hou Jr., H., Kneitz, B., Lagaud, G., Christ, G.J., Edelmann, W., Lisanti, M.P., 2001. Caveolin-1 null mice are viable but show evidence of hyperproliferative and vascular abnormalities. J. Biol. Chem. 276, 38121–38138.

Rothberg, K.G., Heuser, J.E., Donzell, W.C., Ying, Y.S., Glenney, J.R., Anderson, R.G., 1992. Caveolin, a protein component of caveolae membrane coats. Cell 68, 673–682.

Shakirova, Y., Bonnevier, J., Albinsson, S., Adner, M., Rippe, B., Broman, J., Arner, A., Swärd, K., 2006. Increased Rho activation and PKC-mediated smooth muscle contractility in the absence of caveolin-1. Am. J. Physiol. Cell Physiol. 291, 1326–1335.

Simons, K., Toomre, D., 2000. Lipid rafts and signal transduction. Nat.Rev. Mol. Cell. Biol. 1, 31–39.

Somara, S., Gilmont, R.R., Martens, J.R., Bitar, K.N., 2007. Ectopic expression of caveolin-1 restores physiological contractile response of aged colonic smooth muscle. Am. J. Physiol. Gastrointest. Liver Physiol. 293, 240–249.

Wang, P., Luthin, G.R., Ruggieri, M.R., 1995. Muscarinic acetylcholine receptor subtypes mediating urinary bladder contractility and coupling to GTP binding proteins. J. Pharmacol. Exp. Ther. 273, 959–966.

Woodman, S.E., Cheung, M.W., Tarr, M., North, A.C., Schubert, W., Lagaud, G., Marks, C. B., Russell, R.G., Hassan, G.S., Factor, S.M., Christ, G.J., Lisanti, M.P., 2004. Urogenital alterations in aged male caveolin-1 knockout mice. J. Urol. 17, 1950–1957.

Wuest, M., Hecht, J., Christ, T., Braeter, M., Schoeberl, C., Hakenberg, O.W., Wirth, M.P., Ravens, U., 2005. Pharmacodynamics of propiverine and three of its main metabolites on detrusor contraction. Br. J. Pharmacol. 145, 608–619.

Wuest, M., Hiller, N., Braeter, M., Hakenberg, O.W., Wirth, M.P., Ravens, U., 2007. Contribution of Ca2+ influx to carbachol-induced detrusor contraction is different in human urinary bladder compared to pig and mouse. Eur. J. Pharmacol. 565, 180–189.

Wuest, M., Eichhorn, B., Grimm, M.O., Wirth, M.P., Ravens, U., Kaumann, A.J., 2009. Catecholamines relax detrusor through beta 2-adrenoceptors in mouse and beta 3-adrenoceptors in man. J. Pharmacol. Exp. Ther. 328, 213–222.

Zhao, Y.Y., Liu, Y., Stan, R.V., Fan, L., Gu, Y., Dalton, N., Chu, P.H., Peterson, K., Ross Jr., J., Chien, K.R., 2002. Defects in caveolin-1 cause dilated cardiomyopathy and pulmonary hypertension in knockout mice. Proc. Natl. Acad. Sci. U S A. 99, 11375–11380.

Paper V

ARTICLE IN PRESS
EJP-66859; No of Pages 7
European Journal of Pharmacology xxx (2010) xxx–xxx
Contents lists available at ScienceDirect
European Journal of Pharmacology
journal homepage: www.elsevier.com/locate/ejphar

Pulmonary, Gastrointestinal and Urogenital Pharmacology

Biochemical and functional correlates of an increased membrane density of caveolae in hypertrophic rat urinary bladder

Yulia Shakirova [a], Karl Swärd [a], Bengt Uvelius [b], Mari Ekman [a,*]

[a] Department of Experimental Medical Science, Lund University, Biomedical Centre, BMC D12, SE-221 84 Lund, Sweden
[b] Department of Urology, Clinical Sciences, Lund University, SE-221 84 Lund, Sweden

ARTICLE INFO

Article history:
Received 8 June 2010
Received in revised form 5 August 2010
Accepted 7 September 2010
Available online xxxx

Keywords:
Overactive bladder syndrome
Detrusor
Caveolae
Caveolin-1
Cavin-1

ABSTRACT

Organ hypertrophy is often found to be associated with changes in the expression of caveolins and altered density of caveolae in the membrane. A plethora of signalling intermediaries are associated with caveolae and loss of caveolae has profound effects on contractility of the urinary bladder. We hypothesized that smooth muscle hypertrophy caused by bladder outflow obstruction (BOO) might lead to an altered caveola density with consequences for contractile regulation. Rat BOO for 6 weeks caused a 2.56-fold increase in the number of smooth muscle caveolae per μm membrane. No changes in the expression of caveolin-1 or cavin-1, normalized to β-actin were seen, but membrane area per unit muscle volume dropped to 0.346. Hypertrophy was associated with altered contraction in response to carbachol. The effect on contraction of cholesterol desorption, which disrupts lipid rafts and caveolae, was however not changed. Contraction in response to bradykinin resisted mβcd in control destrusor, but was inhibited by it after 6 weeks of obstruction. It is concluded that rat detrusor hypertrophy leads to an increased number of caveolae per unit membrane area. This change is due to a reduction of membrane area per volume muscle and it does not play a role for cholinergic activation, but promotes contraction in response to bradykinin after long-term obstruction.

1. Introduction

The urinary bladder undergoes hypertrophy after outlet obstruction (BOO). Initially, the hypertrophy is compensatory and maximum micturition pressure increases to overcome the obstruction (Malmgren et al., 1987). Short-term BOO (Mattiasson and Uvelius, 1982; Saito et al., 1993) right-shifts the length–tension relationship and increases contractility in response to carbachol and ATP. Some agonist responses, such as that of bradykinin (Sjuve et al., 2000), increase out of proportion with the expansion of muscle cross-sectional area, indicating that changes also involve cellular signaling mechanisms. The shift of the length tension curve decreases the ability to produce pressure at low volume (Mattiasson and Uvelius, 1982), and leads to a residual volume. Long-term obstruction causes decompensation, associated with impaired contractility and a progressively increasing residual volume (Saito et al., 1993; Chang et al., 2009). Functional alterations in detrusor hypertrophy are associated with ultra structural changes, involving e.g. the sarcoplasmic reticulum, mitochondria and the plasma membrane (Gabella and Uvelius, 1990; Scott et al., 2004).

Caveolae are invaginations in the plasmalemma that play a role in signaling (Cohen et al., 2004). Caveolins (1–3) and cavins (1–4) are essential for the formation of caveolae (Cohen et al., 2004; Hill et al., 2008; Hansen et al., 2009; Bastiani et al., 2009). Genetic ablation of caveolin-1 leads to loss of caveolae in the male mouse detrusor (Woodman et al., 2004) and impairs force generation in response to cholinergic activation (Lai et al., 2007, 2004; Woodman et al., 2004) and KCl (Woodman et al., 2004; Wuest et al. 2009). Thus, caveolae play an essential role in activation of the mouse urinary bladder.

Hypertrophy is associated with changes in caveolae numbers. Cardiomyocyte hypertrophy increases the expression of caveolin-3 and the membrane density of caveolae (Goto et al., 1990; Kikuchi et al., 2005; Zeidan et al., 2008; Lu et al., 2009). Pulmonary arterial hypertension increases expression of caveolin-1 and the number of caveolae per μm membrane in smooth muscle (Patel et al., 2007). In contrast, BOO was recently found to reduce caveola density, but no morphometry was made (Polyák et al., 2009), and functional consequences were not examined. Importantly, the work generated so far on caveolae in association with hypertrophy was made prior to the realization that cavins play a role in caveola biogenesis (Hill et al., 2008; Hansen et al., 2009; Bastiani et al., 2009). Thus, information is lacking for a complete understanding of how caveolae change in relation to hypertrophy.

The aims of the present study were to examine how the density of caveolae changes in bladder hypertrophy, how this relates to the expression of caveolin-1 and cavin-1, and whether an altered density has contractile consequences. We created infravesical outflow obstruction in the rat (Gabella and Uvelius, 1990) and made a morphometric quantification of caveolae. The expression of caveolin-1 and cavin-1 was

* Corresponding author. Tel.: +46 46 2227795; fax: +46 46 2113417.
E-mail address: Mari.Ekman@med.lu.se (M. Ekman).

0014-2999/$ – see front matter © 2010 Elsevier B.V. All rights reserved.
doi:10.1016/j.ejphar.2010.09.050

determined, and the correlation between our structural and biochemical findings and bladder contractility was examined. Expression of M_3 muscarinic receptors and phopholipase $C_{\beta 1}$ was determined in view of the putative dependence of M_3 receptor signaling on caveolae.

2. Materials and methods

2.1. Animals and surgery

Female Sprague–Dawley rats weighing about 200 g were anesthetized by i.m. injection of ketamine (Ketalar®, Parke-Davis, Barcelona, Spain) 100 mg/kg, and xylazin (Rompun®, Bayer AG, Leverkusen, Germany) 15 mg/kg. The lower abdomen was opened and a standardized urethral obstruction was induced by placing a 1 mm metal rod along the urethra, and then tying a ligature with 4-0 Prolene®. The rod was then pulled out and the ligature left in situ. The abdominal wall was sutured in two layers with Dexon stitches. Unoperated littermates were used as controls. All obstructed rats had individually assigned controls, but control groups were combined in the final analysis. The local animal ethics committee in Lund/Malmö approved all procedures.

2.2. Tissue preparation

Operated animals and their controls were killed with increasing atmospheric CO_2 10 days or 6 weeks following surgery. The abdomen and thoracic cavity were rapidly opened and the bladder was cut at the bladder neck. Preparations for Western blotting, immunofluorescence staining, and mechanical experiments were dissected from the ventral mid-portion of the excised bladder in pre-cooled HEPES buffered Krebs solution (composition in mM: NaCl 135.5, KCl 5.9, $MgCl_2$ 1.2, glucose 11.6, HEPES 11.6, pH 7.4). For mechanical experiments and Western blotting the urothelium was removed by gentle dissection.

2.3. Electron microscopy

After 6 weeks controls and obstructed rats were killed by cervical dislocation and the bladders were dissected and weighed. The bladders were then cannulated and filled with 1 ml saline per 100 mg weight. The bladders were then transferred to 5% glutaraldehyde in 100 mM cacodulate buffer (pH 7.4) at room temperature (see Gabella and Uvelius, 1990). Segments of the mid-ventral portion of the bladder were cut and post-fixed in 1% osmium tetroxide for 1–2 h, block-stained with uranyl acetate, dehydrated and embedded in Araldite. Semi-thin sections were examined by phase contrast microscopy, and muscle bundles were chosen and cut transversely for electron microscopy (EM). The relative area of smooth muscle in the muscular layer was quantitated by placing a dotted transparent sheath on the micrographs (magnification 4700) and counting the number of dots over the bundles and dividing with the total number of dots over the micrograph. The relative smooth muscle membrane length per unit muscle cross-sectional area was measured by placing a sheath with parallel lines on the micrographs, and counting the number of intersections with cell membranes. At least 10 plates were used for each specimen. By dividing the mean numbers for the obstructed bladders with the corresponding from the controls, an estimate of cell membrane length per unit muscle area (which corresponds to muscle cell membrane area per unit muscle volume) was obtained.

At high magnification (×56,400) the maximum transverse caveola diameter was estimated by measurements on caveolae with a visible opening to the extracellular space. At least 10 such caveolae were measured in each specimen. The number of caveolae per unit cell membrane length was also determined. 66–281 μm of cell membrane length, containing 74–729 caveolae was used for these estimates in each specimen.

2.4. Western blotting

Western blotting was performed as described previously (Shakirova et al., 2006), with antibody dilutions as recommended. Antibodies against caveolin-1 (clone 2297) and PTRF-cavin (now referred to as cavin-1, see Bastiani et al., 2009 for the current cavin nomenclature) were from BD Biosciences Pharmingen. Anti-phospholipase $C_{\beta 1}$ ($PLC_{\beta 1}$) was from BD Biosciences, Pharmingen, and anti-M_3 (H-210) was from Santa Cruz Biotechnology (Santa Cruz, CA). Anti-β-actin (A-5441) was from Sigma (Sigma Aldrich, Sweden). The EZQ protein assay (R-33200, Molecular Probes, CA) was used to determine total protein in the bladder homogenates. Equal amounts of protein (30 μg) were loaded in all lanes. After transfer, proteins remaining on the gel were stained with Coomassie brilliant blue to allow for normalization to total actin. For data presented in the figures, optical densities times the area (mm^2) of the bands of interest was normalized to β-actin in the same lane and subsequently to the corresponding mean of the unobstructed controls.

2.5. Immunohistochemistry

Urinary bladders were filled with saline as above and fixed in Histochoice (Amresco, Solon, Ohio USA) overnight. Following fixation, preparations were washed three times in 70% ethanol. Following ascending ethanols (96%, 2 h, and 100%, 1 h), bladders were incubated in 1:1 ethanol:xylene (30 min) and xylene (1 h). Preparations were then embedded in paraffin. 10 μm sections were cut and deparaffinized, followed by washing (2×30 min in PBS), permeabilization (0.2% Triton X-100 for 15 min), and blocking (2% bovine serum albumin in PBS for 2 h). A polyclonal caveolin-1 antibody (610060 from BD Biosciences Pharmingen) was diluted (1:125) in PBS with albumin and sections were incubated overnight at 4 °C. Cy5-labeled anti-mouse IgG was used as secondary probe. Nuclei were stained with Sytox Green (1:3000, Molecular Probes). Fluorescence was captured using a Zeiss LSM 510 confocal microscope and identical settings for all specimens.

To quantify intracellular versus sarcolemma-associated caveolin-1 we measured fluorescence intensity in regions of interest inside cross-sectioned cell profiles (without nuclei) and on their cell membrane. The average intracellular fluorescence was then divided by the fluorescence in the membrane. The ratio thus obtained should reflect the intracellular to membrane distribution of caveolin-1 immunoreactivity.

2.6. Myograph experiments and cholesterol depletion

Detrusor strips were mounted horizontally using silk sutures in myograph (610 M, Danish MyoTechnology) chambers containing aerated HEPES buffered Krebs solution with 2.5 mM Ca^{2+}. Following slow stretching to a basal tension equivalent to L_0 (as determined in pilot experiments) and subsequent equilibration for 30 min at 37 °C, the solution was changed to high-K^+ solution, obtained by replacing 60 mM NaCl with KCl. Carbachol was added in a cumulative manner. Bradykinin was applied at a single concentration (1 μM). For chemical disruption of caveolae, half of the preparations were incubated for 40 min in 10 mM mβcd, dissolved directly in the HEPES-buffered Krebs solution, at 37 °C following the initial reference contraction with 60 mM K^+. Control preparations were maintained in the HEPES buffered Krebs during this period. Following experimentation the length was measured in the myograph chamber using the dissection microscope and an ocular with a calibrated length scale. The preparations were then cut just inside the silk sutures and weighed following gentle blotting on a filter paper. Stress (force per cross-sectional area) was calculated by multiplying force in mN with length in mm and density (assumed to be 1.06) and dividing with weight in mg.

Please cite this article as: Shakirova, Y., et al., Biochemical and functional correlates of an increased membrane density of caveolae in hypertrophic rat urinary bladder, Eur. J. Pharmacol. (2010), doi:10.1016/j.ejphar.2010.09.050

2.7. Chemicals

All chemicals were obtained from Sigma (Sigma Aldrich, Sweden).

2.8. Statistics

Mean values ± S.E.M. are shown. N-values refer to number of animals and are given in the figure legends and text. Student's t-test (two-tailed) for unpaired data was used to test for differences between groups. One way ANOVA followed by the Holm–Sidak post-hoc test was used for multiple comparisons. Statistical testing of differences in potency (EC_{50}) in Fig. 4B was performed on log transformed EC_{50} values (in μM). $P<0.05$ was considered significant. In the figures * indicates $P<0.05$, ** indicates $P<0.01$ and *** indicates $P<0.001$.

3. Results

3.1. Bladder weight after outlet obstruction

Control bladders weighed 82 ± 3 mg (n = 24). After 10 days and 6 weeks of obstruction, respectively, bladders weighed 238 ± 38 mg (n = 14, $P<0.01$ compared to controls) and 484 ± 132 mg (n = 8, $P<0.001$ compared to controls, $P<0.01$ compared to 10 days).

3.2. Morphometry of control and hypertrophic detrusor using electron microscopy

In addition to organ hypertrophy, bladder outlet obstruction for 6 weeks caused sizeable enlargement of smooth muscle cells (Fig. 1A and B). Caveolae were readily identified in the sarcolemma of detrusor smooth muscle cells in control rat bladders (Fig. 1C) and in bladders subjected to 6 weeks of outflow obstruction (Fig. 1D). In control bladder smooth muscle cells 1.30 ± 0.11 (n = 4 bladders) caveolae profiles per μm muscle cell membrane were seen. After 6 weeks of obstruction 3.33 ± 0.56 caveolae per μm membrane were seen (n = 4 bladders, $P<0.05$), corresponding to a 2.56-fold increase in comparison to control bladders. So called caveolae rosettes (inset in 1D) were occasionally seen in hypertrophic cells. Such rosettes were never seen in control bladder smooth muscle. The equatorial diameter of caveolae with visible openings was 78 ± 2 nm in the 4 control bladders, and 77 ± 3 nm in the 4 obstructed bladders. Thus, bladder hypertrophy increases the membrane density of caveolae in detrusor smooth muscle without changing their size or overall appearance.

To estimate membrane area, the number of membrane intersections with a grid superimposed on the electron micrographs was counted. The number of intersections amounted to 22.8 ± 4.7 per 100 μm^2 in cross-sectioned muscle bundles of the control bladders, and to 7.9 ± 0.7 per 100 μm^2 after 6 weeks of obstruction ($P<0.05$). The ratio between the mean value for the obstructed and the mean value for the controls was 0.346. This represents an estimate of the cell membrane length per unit muscle wall cross-sectional area in the obstructed group relative to that of the control group.

3.3. Expression of caveolin-1 and cavin-1 in hypertrophic detrusor

We assessed the expression of caveolin-1 and cavin-1, two proteins that are critical for formation of caveolae, by Western blotting (Fig. 2A, top two panels). We focused on caveolin-1 and cavin-1 rather than caveolins 2–3 or cavin-2, which may also be limiting for biogenesis of caveolae, because (i) caveolin-2 cannot give rise to caveolae independently of caveolin-1 (ii) caveolin-3 does not play a quantitatively

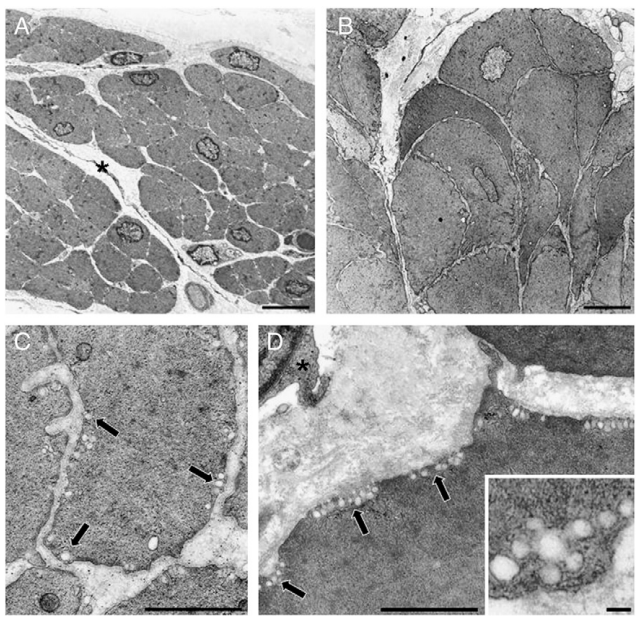

Fig. 1. Electron micrographs of smooth muscle cells in control and hypertrophic rat urinary bladder (A–D). A and B show cross-sectioned smooth muscle cells from control and hypertrophic rat bladder, respectively, at the same low (×2794) magnification. Asterisks indicate fibroblasts (A, D). C (control) and D (hypertrophic) show bladder smooth muscle cells at the same high (×28702) magnification. Examples of caveolae are highlighted with arrows in C and D. Scale bars represent 5 μm (A and B), 1 μm (C, D), and 100 nm (inset in D) n = 4 animals.

Please cite this article as: Shakirova, Y., et al., Biochemical and functional correlates of an increased membrane density of caveolae in hypertrophic rat urinary bladder, Eur. J. Pharmacol. (2010), doi:10.1016/j.ejphar.2010.09.050

important role for formation of caveolae in the urinary bladder (Woodman et al., 2004), and (iii) no antibodies against cavin-2 were available to us. Great care was taken to remove the mucosa and connective tissue before homogenates were made. No significant change in the expression of either caveolin-1 or cavin-1 at 10 days or 6 weeks of obstruction was noted, but a borderline significant increase of the cavin-1 to caveolin-1 ratio was seen at six weeks (1.07 ± 0.11 in controls compared to 2.01 ± 0.43 at 6 weeks, $P = 0.051$, $n = 8$). Three normalisation procedures were used: total protein, the actin band on the stained gel, β-actin on the same membrane; the latter is shown at the bottom of 2A and was used in the bar graphs for normalisation. Thus, the membrane density of caveolae increases in hypertrophic detrusor without a change in the contents of key caveolae proteins.

We also blotted for M_3 muscarinic receptors (Fig. 2A and B) and phospholipase $C_{\beta 1}$ ($PLC_{\beta 1}$; Fig. 2A) in view of the putative role of caveolae in signalling from M_3 receptors via phospholipase C in the bladder. M_3 receptor expression was increased at 6 weeks (Fig. 2A and B). $PLC_{\beta 1}$ expression was similarly increased at 6 weeks of obstruction (Fig. 2A).

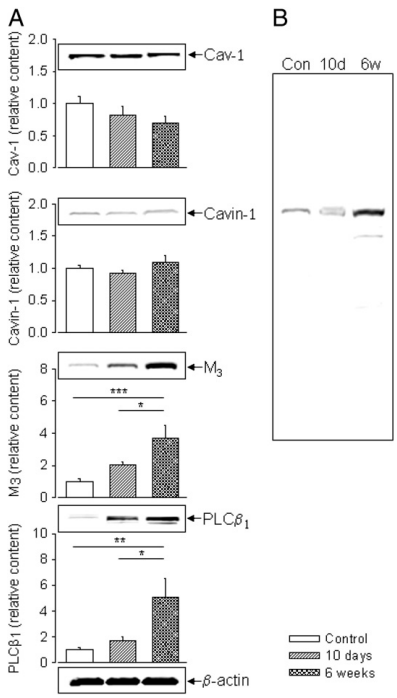

Fig. 2. Quantification of caveolin-1 (Cav-1), Cavin-1, M_3 muscarinic receptors, and phospholipase $C_{\beta 1}$ ($PLC_{\beta 1}$) in control bladders and in bladders subjected to 10 days and 6 weeks of outflow obstruction by Western blotting (A). Below the individual blots are bar graphs with compiled data (except in the case of β-actin). The optical density times the area (mm^2) of the band of interest was normalized first to β-actin in the same lane (bottom), to compensate for loading, and then to the corresponding mean value from the unobstructed controls, to get comparable values for the different proteins. The resulting values are referred to as relative content on the ordinate. $n = 8$ animals throughout. B shows full lanes with the M_3 receptor antibody using control bladder homogenate and homogenates from bladders obstructed for 10 days and 6 weeks, respectively. The identity of the lower M_3 band discernible at 6 weeks is not known, but it may represent a differentially glycosylated species or a protelolysis product.

3.4. Staining of caveolin-1 in control and hypertrophic detrusor

We next addressed whether bladder hypertrophy was associated with an altered subcellular distribution of caveolin-1 not detectable by Western blotting. Caveolin-1 was visualized by immunofluorescence in cross-sectioned detrusor smooth muscle cells. Nuclei were counterstained with Sytox green (Fig. 3A). Plotting caveolin-1 fluorescence along a vector bisecting the cells gave two membrane-associated fluorescence peaks (Fig. 3B). Little caveolin-1 was intracellular in control detrusor ($13 \pm 1\%$, $n = 10$ cells and 3 animals: fluorescence in the cytosol divided by the total fluorescence over the cell). Membrane targeting of caveolin-1 appeared to increase in hypertrophy, as reflected by a reduction of cytosolic to membrane fluorescence ratio (Fig. 3C).

3.5. Correlation between membrane density of caveolae and contractility

Caveolae play a role in mouse bladder cholinergic contractility as demonstrated using caveolin-1 knockout mice (Lai et al., 2007, 2004; Woodman et al., 2004). We therefore examined stress in response to the muscarinic agonist carbachol in obstructed and control rat bladder strips. As shown in Fig. 4A, stress was increased at the highest concentrations of carbachol after 10 days of obstruction. After 6 weeks of obstruction, on the other hand, stress was reduced at intermediate concentrations of carbachol. The potency was reduced at 10 days and at 6 weeks (Fig. 4B) as reflected by an increase of the EC_{50} value from

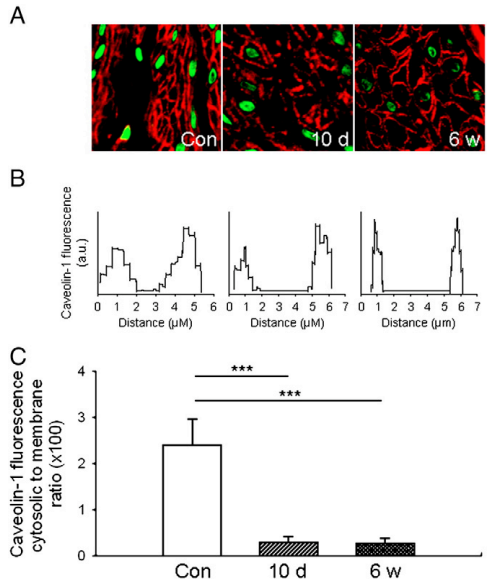

Fig. 3. A shows immunofluorescence staining of caveolin-1 (red) in control urinary bladder (Con), in bladder obstructed for 10 days (10 d), and in bladder obstructed for 6 weeks (6 w). Nuclei were counterstained with Sytox green. B shows fluorescence along vectors bisecting cells from control (left), 10 day obstructed (middle), and 6 week obstructed (right) bladders. The two fluorescence peaks are separated by a distance that corresponds with cell size as measured by electron microscopy, indicating that caveolin-1 resides primarily in the membrane. A.u.: arbitrary units. C shows summarized data on the intracellular to membrane-associated caveolin-1 fluorescence. $n = 3$ animals throughout. 30 cells from at least 3 glasses were evaluated in each animal.

Please cite this article as: Shakirova, Y., et al., Biochemical and functional correlates of an increased membrane density of caveolae in hypertrophic rat urinary bladder, Eur. J. Pharmacol. (2010), doi:10.1016/j.ejphar.2010.09.050

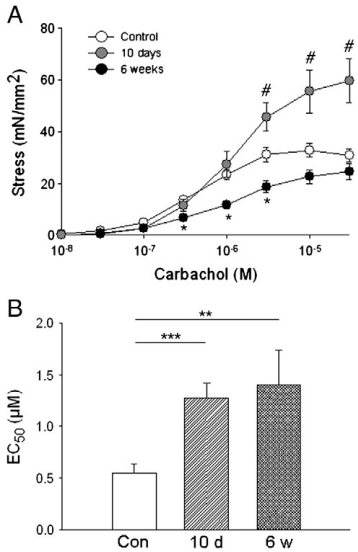

Fig. 4. A shows stress (force per cross-sectional area) in response to stimulation with the muscarinic agonist carbachol in control bladders (white circles), and in bladders obstructed for 10 days (gray circles) and 6 weeks (black circles), respectively. *Indicates $P<0.05$ vs. control bladders and bladders obstructed for 10 days. # indicates $P<0.05$ vs. control bladders and bladders obstructed for 6 weeks. B shows the potency (expressed as EC_{50}, i.e. the concentration causing half maximal activation) of carbachol as a function of obstruction (control bladders: white bar; 10 days of obstruction: grey bar; 6 weeks of obstruction: black bar). n = 20 control bladders, 11 bladders obstructed for 10 days, and 11 bladders obstructed for 6 weeks. **Indicates $P<0.01$ vs. control bladders, ***Indicates $P<0.001$ vs. control bladders.

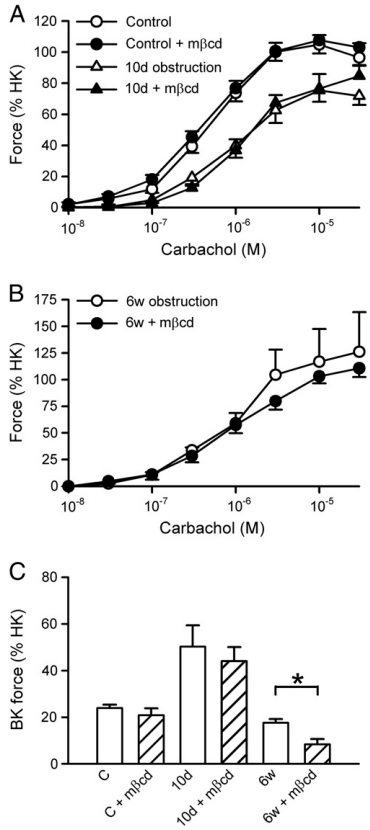

Fig. 5. Concentration–response relations for the muscarinic receptor agonist carbachol with and without pre-treatment with 10 mM methyl-β-cyclodextrin (mβcd, 10 mM) which reduces cholesterol and disrupts lipid raft and caveolae (A, B). Mβcd was applied for 40 min following the initial contraction with 60 mM K^+ (HK). Control bladders (±mβcd) and bladders obstructed for 10 days (±mβcd) are shown in A (n = 6–12). Bladders obstructed for 6 weeks (±mβcd) were plotted separately in B for clarity (n = 6). C shows contraction in response to a single concentration of bradykinin (1 μM, ±mβcd) in control bladders and after 10 days and 6 weeks of obstruction (n = 4–12).

0.55 ± 0.09 μM in controls to 1.27 ± 0.15 μM after 10 days, and 1.40 ± 0.33 μM after 6 weeks.

To probe any apparent correlations between caveola density and contractility more rigorously, we next examined the effects of methyl-β-cyclodextrin (mβcd). This substance binds to and removes cholesterol from the cell membrane (Kilsdonk et al., 1995) leading to reversible disruption of lipid rafts and caveolae (Dreja et al., 2002; Rothberg et al., 1992; Simons and Toomre, 2000). We predicted that contractility should be more sensitive to mβcd in hypertrophic detrusor if hypertrophy was associated with altered dependence of contraction on caveolae. Force was normalized to depolarisation-induced contraction. The dose-dependent contraction elicited by carbachol was resistant to mβcd irrespective of condition (control and 10 day hypertrophic detrusor detrusor in Fig. 5A, and 6 week hypertrophic detrusor in Fig. 5B). Bradykinin contraction, on the other hand, was insensitive to cholesterol desorption in control bladder and after 10 days of obstruction, but significant inhibition was seen at 6 weeks (Fig. 5C).

In Fig. 6A and B we have normalized content (i.e. the data in Fig. 2) to relative membrane area (10 day membrane area from Scott et al. 2004, 6 weeks: present study). The estimated membrane caveolin-1 content increases 2-fold and the estimated membrane cavin-1 content increases 3-fold at 6 weeks of hypertrophy (Fig. 6A). M_3 and $PLC_{\beta 1}$ change modestly at 10 days, and then increases considerably at 6 weeks (10–15-fold, Fig. 6B). In Fig. 6C the carbachol-induced contractions in Fig. 4 were normalized to the HK responses in the same strips rather than being expressed as stress. Relative carbachol contraction falls 10 days after obstruction (Fig. 6C). This occurs without any associated reduction of caveolin-1, M_3, or $PLC_{\beta 1}$ (6A, B). Thereafter a recovery of relative force in response to carbachol is seen at 6 weeks. Thus, increases in M_3 and $PLC_{\beta 1}$ (and caveolae) between 10 days and 6 weeks coincide with a recovery of carbachol-induced contraction.

4. Discussion

The present study establishes that long-term detrusor outlet obstruction in the rat leads to an increased number of caveolae per unit membrane area in smooth muscle cells. This finding is consistent with the literature on caveolae in hypertrophic cardiomyocytes (Goto et al., 1990; Kikuchi et al., 2005; Zeidan et al., 2008; Lu et al., 2009) and also with the demonstration that caveola density increases in hypertrophic pulmonary arterial smooth muscle in idiopathic pulmonary hypertension (Patel et al., 2007). The increased density of caveolae in the hypertrophic rat detrusor was however not associated with altered expression of caveolin-1 or cavin-1 (normalized to total protein, β-actin, or total actin) and did not affect contractility in response to carbachol as suggested by

Please cite this article as: Shakirova, Y., et al., Biochemical and functional correlates of an increased membrane density of caveolae in hypertrophic rat urinary bladder, Eur. J. Pharmacol. (2010), doi:10.1016/j.ejphar.2010.09.050

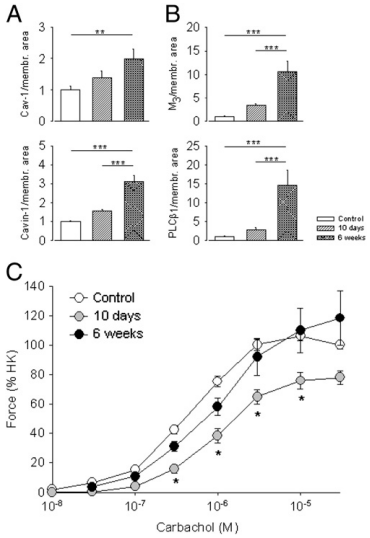

Fig. 6. Bar graphs in A shows caveolin-1 (Cav-1) and cavin-1, expression relative to membrane area rather than β-actin. Data are from Fig. 2 but now expressed per unit membrane area. The membrane area per unit muscle volume at 6 weeks was measured here by electron microscopy. The membrane area per volume muscle at 10 days of obstruction (0.66) was obtained from Scott et al. (2004). B shows M_3 and $PLC_{\beta 1}$ expression relative to membrane area. C shows concentration–response relationships for carbachol in control bladder strips and in bladder strips obtained after 10 days and 6 weeks of obstruction. The data in C is from Fig. 4, but normalized here to the HK-response in the same preparations rather than being expressed as stress. *Indicates $P<0.05$ vs. controls and 6 week obstructed bladders.

the chemical disruption of the caveola structure. The increased density of caveolae in bladders obstructed for 6 weeks did however facilitate bradykinin-induced contraction.

Staining for caveolin-1 was largely restricted to smooth muscle bundles in control and hypertrophic detrusor. Thus, changes in caveolin-1 expression in other cells than smooth muscle cells can be ruled out as an explanation for the discrepancy between caveolin-1 protein expression and caveola density. Altered distribution of caveolin-1 within the smooth muscle cells may also be ruled out because little caveolin-1 (~13% of total) was present intracellularly in controls. The mechanism behind the modestly reduced cytosolic to membrane ratio for caveolin-1 in the hypertrophic cells is not known. Because cavin-1 affects the cellular distribution of caveolin-1 (Hill et al., 2008) it is conceivable that an increased cavin-1 to caveolin-1 ratio may be responsible. However, even if the intracellular to plasma membrane ratio of caveolin-1 dropped in hypertrophy, this would at best (i.e. if all cytosolic caveolin-1 in control detrusor gave rise to caveolae in a 1:1 relationship after hypertrophy) lead to a 1.15-fold increase in caveola density (increased 2.56-fold).

Other explanations for an increased density of caveolae with unaltered caveolin-1 expression include sizeable increases of caveolin-3 or cavin-2 expression, both of which may contribute to biogenesis of caveolae (Cohen et al., 2004; Hansen et al., 2009). Alternatively, targeting of cavins to the membrane could increase. We have not measured expression of caveolin-3 or cavin-2, or membrane targeting of cavins, but, as discussed in the later part, a drop in membrane area per volume muscle fully accounts for the increase in membrane caveola density that we observe in hypertrophic bladder.

The membrane length per unit muscle area dropped to 0.345 after 6 weeks of hypertrophy (i.e. by 65%). Correspondingly, a 34% reduction after 10 days of obstruction has been reported (Scott et al., 2004). Caveolin-1 content per muscle protein was not significantly changed in the obstructed bladders at either 10 days or 6 weeks, and ≥87% was in the membrane in all conditions. Thus, the same amount of caveolin is distributed over a smaller membrane area in hypertrophy; i.e. the membrane density of caveolin-1 is increased in the detrusor muscle cells in obstructed bladders. For caveola density to increase 2.56-fold (as measured here) we predict that caveolin-1 content per unit protein should be 0.88 ($0.346 \times 2.56 = 0.88$). The difference between the measured (0.75, by Western blotting) and predicted (0.88) caveolin-1 expression at 6 weeks is within the margins of error of our measurements.

A recent study has to be reinterpreted in light of the considerations brought up here. Polyák et al. (2009) examined the expression of caveolin-1 and -3 in hypertrophic rabbit detrusor and found reduced expression of both proteins relative to controls. They also performed electron microscopy and reached the conclusion that hypertrophic detrusor had a reduced number of caveolae. This was however not backed up by quantitative morphometry. As shown here, the density of membrane caveolae does not correlate with expression of caveolin-1 unless correction is made for membrane area per volume tissue. Indeed, a 50% reduction of caveolin-1 expression relative to α-actin (Polyák et al., 2009) should be associated with an increased number of caveolae per unit smooth muscle membrane area. This is assuming that cavin-1 expression remains largely unchanged (this study), and that the membrane area per volume muscle drops below 50% (as measured here at 6 weeks). The slightly greater reduction of caveolin-1 in the study by Polyák et al., 2009 may relate to differences in the severity of obstruction, the different time-points studied, or that a different species was used.

To rigorously test whether an altered density of caveolae had an impact on contractility, we examined the effects of chemical ablation of caveolae. The sensitivity of carbachol contraction to chemical disruption of caveolae did not change with hypertrophy. On the other hand, the bradykinin response resisted cholesterol depletion in controls and at 10 days, but at 6 weeks bradykinin-induced contraction was inhibited by cholesterol depletion. We note that receptors for bradykinin were among the first G protein-coupled receptors to be suggested to associate with caveolae in a dynamic manner (de Weerd and Leeb-Lundberg, 1997). On the whole however, the finding that rat bladder muscarinic contraction was resistant to mβcd irrespective of caveola density supports the idea that caveolae play a minor role for acute cholinergic activation of the rat bladder. Similar conclusions were reached in our parallel work comparing mouse, rat and human bladder (Shakirova et al., 2010) where we also found that cholinergic activation of human bladder shows a much higher sensitivity to cholesterol desorption than does rat bladder. That study, and the present work, therefore indicates that the rat is not an ideal model to study the impact of hypertrophy-induced changes in caveola density on muscarinic activation.

A functionally relevant finding in relation to hypertrophy is that the potency for carbachol dropped while the membrane density of M_3 receptors and phospholipases $C_{\beta 1}$ increased. It has previously been speculated (Scott et al., 2004) that the increase in cell volume that occurs as a consequence of hypertrophy buffers changes in the intracellular Ca^{2+} concentration. Evidently, cell size is also expected to affect diffusion distances. Moreover, recent work has demonstrated impaired Ca^{2+}-sensitization via protein kinase Cα in severely obstructed bladders (Chang et al., 2009). We therefore speculate that the up-regulation of M_3 receptors and phospholipases $C_{\beta 1}$ partly compensates for an impairment of downstream activation mechanisms and that decompensation follows when such compensatory mechanisms have been exhausted.

In summary, rat detrusor hypertrophy due to outflow obstruction leads to an increased density of membrane caveolae. This is not associated with increased caveolin-1 or cavin-1 expression, but rather concomitant with a reduced membrane area relative to cell volume, a

Please cite this article as: Shakirova, Y., et al., Biochemical and functional correlates of an increased membrane density of caveolae in hypertrophic rat urinary bladder, Eur. J. Pharmacol. (2010), doi:10.1016/j.ejphar.2010.09.050

fact that needs to be considered in studies on changes in the membrane caveola density in association with hypertrophy. The increased membrane density of caveolae has no major effect on the sensitivity of muscarinic contraction to cholesterol desorption in the Sprague–Dawley rat, but facilitates contraction by bradykinin. Hypertrophy-induced changes in caveola density or caveolin/cavin expression may play a greater role for detrusor contraction in obstruction models in other species.

Acknowledgements

This work was supported by grants from the Swedish Research Council (K2009-65X-4955-01-3), the Crafoord Foundation, the Royal Physiographic Society, Lars Hierta's Foundation, Greta and Johan Kock's Foundation (all to KS), Governmental funding of Clinical Research within the National Health Service (BU), and the Faculty of Medicine at Lund University (KS). KS holds a senior scientist position at the Swedish Research Council.

References

Bastiani, M., Liu, L., Hill, M.M., Jedrychowski, M.P., Nixon, S.J., Lo, H.P., Abankwa, D., Luetterforst, R., Fernandez-Rojo, M., Breen, M.R., Gygi, S.P., Vinten, J., Walser, P.J., North, K.N., Hancock, J.F., Pilch, P.F., Parton, R.G., 2009. MURC/Cavin-4 and cavin family members form tissue-specific caveolar complexes. J. Cell Biol. 185, 1259–1273.

Chang, S., Hypolite, J.A., Mohanan, S., Zderic, S.A., Wein, A.J., Chacko, S., 2009. Alteration of the PKC-mediated signaling pathway for smooth muscle contraction in obstruction-induced hypertrophy of the urinary bladder. Lab. Invest. 89, 823–832.

Cohen, A.W., Hnasko, R., Schubert, W., Lisanti, M.P., 2004. Role of caveolae and caveolins in health and disease. Physiol. Rev. 84, 1341–1379.

de Weerd, W.F., Leeb-Lundberg, L.M., 1997. Bradykinin sequesters B2 bradykinin receptors and the receptor-coupled Galpha subunits Galphaq and Galphai in caveolae in DDT1 MF-2 smooth muscle cells. J. Biol. Chem. 272, 17858–17866.

Dreja, K., Voldstedlund, M., Vinten, J., Tranum-Jensen, J., Hellstrand, P., Swärd, K., 2002. Cholesterol depletion disrupts caveolae and differentially impairs agonist-induced arterial contraction. Arterioscler. Thromb. Vasc. Biol. 22, 1267–1272.

Gabella, G., Uvelius, B., 1990. Urinary bladder of rat: fine structure of normal and hypertrophic musculature. Cell Tissue Res. 262, 67–79.

Goto, Y., Yoshikane, H., Honda, M., Morioka, S., Yamori, Y., Moriyama, K., 1990. Three-dimensional observation on sarcoplasmic reticulum and caveolae in myocardium of spontaneously hypertensive rats. J. Submicrosc. Cytol. Pathol. 22, 535–542.

Hansen, C.G., Bright, N.A., Howard, G., Nichols, B.J., 2009. SDPR induces membrane curvature and functions in the formation of caveolae. Nat. Cell Biol. 11, 807–814.

Hill, M.M., Bastiani, M., Luetterforst, R., Kirkham, M., Kirkham, A., Nixon, S.J., Walser, P., Abankwa, D., Oorschot, V.M., Martin, S., Hancock, J.F., Parton, R.G., 2008. PTRF-Cavin, a conserved cytoplasmic protein required for caveola formation and function. Cell 132, 113–124.

Kikuchi, T., Oka, N., Koga, A., Miyazaki, H., Ohmura, H., Imaizumi, T., 2005. Behavior of caveolae and caveolin-3 during the development of myocyte hypertrophy. J. Cardiovasc. Pharmacol. 45, 204–210.

Kilsdonk, E.P., Yancey, P.G., Stoudt, G.W., Bangerter, F.W., Johnson, W.J., Phillips, M.C., Rothblat, G.H., 1995. Cellular cholesterol efflux mediated by cyclodextrins. J. Biol. Chem. 270, 17250–17256.

Lai, H.H., Boone, T.B., Yang, G., Smith, C.P., Kiss, S., Thompson, T.C., Somogyi, G.T., 2004. Loss of caveolin-1 expression is associated with disruption of muscarinic cholinergic activities in the urinary bladder. Neurochem. Int. 45, 1185–1193.

Lai, H.H., Boone, T.B., Thompson, T.C., Smith, C.P., Somogyi, G.T., 2007. Using caveolin-1 knockout mouse to study impaired detrusor contractility and disrupted muscarinic activity in the aging bladder. Urology 69, 407–411.

Lu, Y.M., Han, F., Shioda, N., Moriguchi, S., Shirasaki, Y., Qin, Z.H., Fukunaga, K., 2009. Phenylephrine-induced cardiomyocyte injury is triggered by superoxide generation through uncoupled endothelial nitric-oxide synthase and ameliorated by 3-[2-[4-(3-chloro-2-methylphenyl)-1-piperazinyl]ethyl]-5,6-dimethoxyindazole (DY-9836), a novel calmodulin antagonist. Mol. Pharmacol. 75, 101–112.

Malmgren, A., Sjögren, C., Uvelius, B., Mattiasson, A., Andersson, K.E., Andersson, P.O., 1987. Cystometrical evaluation of bladder instability in rats with infravesical outflow obstruction. J. Urol. 137, 1291–1294.

Mattiasson, A., Uvelius, B., 1982. Changes in contractile properties in hypertrophic rat urinary bladder. J. Urol. 128, 1340–1342.

Patel, H.H., Zhang, S., Murray, F., Suda, R.Y., Head, B.P., Yokoyama, U., Swaney, J.S., Niesman, I.R., Schermuly, R.T., Pullamsetti, S.S., Thistlethwaite, P.A., Miyanohara, A., Farquhar, M.G., Yuan, J.X., Insel, P.A., 2007. Increased smooth muscle cell expression of caveolin-1 and caveolae contribute to the pathophysiology of idiopathic pulmonary arterial hypertension. FASEB J. 21, 2970–2979.

Polyák, E., Boopathi, E., Mohanan, S., Deng, M., Zderic, S.A., Wein, A.J., Chacko, S., 2009. Alterations in caveolin expression and ultrastructure after bladder smooth muscle hypertrophy. J. Urol. 182, 2497–24503.

Rothberg, K.G., Heuser, J.E., Donzell, W.C., Ying, Y.S., Glenney, J.R., Anderson, R.G., 1992. Caveolin, a protein component of caveolae membrane coats. Cell 68, 673–682.

Saito, M., Wein, A.J., Levin, R.M., 1993. Effect of partial outlet obstruction on contractility: comparison between severe and mild obstruction. Neurourol. Urodyn. 12, 573–583.

Scott, R.S., Uvelius, B., Arner, A., 2004. Changes in intracellular calcium concentration and P2X1 receptor expression in hypertrophic rat urinary bladder smooth muscle. Neurourol. Urodyn. 23, 361–366.

Shakirova, Y., Bonnevier, J., Albinsson, S., Adner, M., Rippe, B., Broman, J., Arner, A., Swärd, K., 2006. Increased Rho activation and PKC-mediated smooth muscle contractility in the absence of caveolin-1. Am. J. Physiol. Cell Physiol. 291, 1326–1335.

Shakirova, Y., Mori, M., Ekman, M., Erjefält, J., Uvelius, B., Swärd, K., 2010. Human urinary bladder smooth muscle in dependent on membrane cholesterol for cholinergic activation. Eur. J. Pharmacol. 634, 142–148.

Simons, K., Toomre, D., 2000. Lipid rafts and signal transduction. Nat. Rev. Mol. Cell Biol. 1, 31–39.

Sjuve, R., Boels, P.J., Uvelius, B., Arner, A., 2000. Up-regulation of bradykinin response in rat and human bladder smooth muscle. J. Urol. 164, 1757–1763.

Woodman, S.E., Cheung, M.W., Tarr, M., North, A.C., Schubert, W., Lagaud, G., Marks, C.B., Russell, R.G., Hassan, G.S., Factor, S.M., Christ, G.J., Lisanti, M.P., 2004. Urogenital alterations in aged male caveolin-1 knockout mice. J. Urol. 17, 1950–1957.

Wuest, M., Eichhorn, B., Grimm, M.O., Wirth, M.P., Ravens, U., Kaumann, A.J., 2009. Catecholamines relax detrusor through beta 2-adrenoceptors in mouse and beta 3-adrenoceptors in man. J. Pharmacol. Exp. Ther. 328, 213–222.

Zeidan, A., Javadov, S., Chakrabarti, S., Karmazyn, M., 2008. Leptin-induced cardiomyocyte hypertrophy involves selective caveolae and RhoA/ROCK-dependent p38 MAPK translocation to nuclei. Cardiovasc. Res. 77, 64–72.

Please cite this article as: Shakirova, Y., et al., Biochemical and functional correlates of an increased membrane density of caveolae in hypertrophic rat urinary bladder, Eur. J. Pharmacol. (2010), doi:10.1016/j.ejphar.2010.09.050